Politecnico di Torino

Master's degree Course in Civil Engineering

Master's Degree Thesis

Analysis of existing tunnel Italian guidelines: segmental lining and fire induced damages

Supervisors:

Prof. Marco Barla

Dr. Alessandra Insana

Candidate:

Ali Abdallah

2026

Abstract

The Italian Guidelines for existing tunnels focus on structural safety, tunnel performance, durability, defect causes, inspections, and proper maintenance of tunnel structures. They provide a framework for identifying and classifying defects, evaluating their impact on structural performance, and managing risk over time. Among the different tunnel types addressed by these guidelines, segmental lining tunnels represent an important case due to their widespread use in modern underground infrastructure. Because of construction stages, rock–structure interaction, and long-term environmental exposure, segmental tunnel linings are prone to different forms of damage. These defects can develop during different phases of the tunnel life cycle, from segment production in the precast plant to transportation, on-site installation, and long-term operation.

One of the parts of this thesis addresses inspection activities in tunnel linings. Inspection activities allow the detection of early signs of deterioration, the evaluation of their extent and severity, including visual inspections based on the previous studies, approaches, artificial intelligence methods for automated defect detection, and non-destructive testing techniques applied to tunnel linings. In relation to inspection, the thesis also examines defects affecting new segmental tunnel linings. The study analyses defects reported in different guidelines and technical references, evaluating which defects are considered in these documents and, through their comparison, identifying additional defects related to segmental linings and proposing their inclusion in existing guidelines.

A second part of the thesis deals with the effects of severe accidental events on tunnel structures**.** Tunnel fires represent extreme conditions that can significantly affect the structural behavior of tunnels. In this context, numerical analysis provides a useful tool for investigating the response of tunnel linings subjected to fire damage. By simulating defects that may affect the tunnel structure due to fire, numerical modelling allows the evaluation of deformation patterns, plastic zone development, and stress redistribution. The aim is to investigate how fire-induced damage influences the behavior of the tunnel ground system under different rock mass conditions and tunnel depths.

إلى أمي وأبي،

اللذين كانا دائمًا مصدر الحب والدعم والقوة،

واللذين بفضلهما وصلت إلى هذه المرحلة من حياتي

وإلى أخي،

الذي كان سندًا لي ورفيقًا في كل الأوقات.

أهديكم هذا العمل

تعبيرًا عن امتناني ومحبتي الكبيرة لكم.

Contents

List of tables

List of Figures

Chapter 1

1. Introduction

The Italian Guidelines for tunnel safety and management establish inspection criteria, defect classification methods, and evaluations of defects. Within this framework, segmental lining tunnels may develop various defects throughout their service life, affecting both their durability and structural performance. These defects can originate during the manufacturing of precast segments, transportation to site, installation processes, or long-term operational conditions. While some defects remain minor and mainly aesthetic, others can influence the structural behaviour of the lining and its interaction with the surrounding ground. For this reason, the correct identification and evaluation of defects represent a fundamental step in ensuring the safety and serviceability of segmental lining tunnels.

The identification of defects relies primarily on inspection activities. Through systematic inspections, it is possible to detect early signs of deterioration, determine their causes, and evaluate their potential impact on tunnel stability. Over time, inspection techniques have evolved from conventional visual observations to more advanced approaches that include automated image analysis and non-destructive testing methods. Visual inspections remain essential for identifying surface anomalies and general conditions of the lining, while artificial intelligence techniques offer the possibility of faster and more consistent defect detection. In addition, non-destructive testing methods allow the investigation of internal or hidden damage that cannot be observed directly. Integrating multiple inspection methods provides a more reliable and comprehensive assessment of tunnel lining conditions.

In parallel with inspection activities, a clear classification of defects is necessary to distinguish between minor imperfections and structurally significant damage. Different guidelines and

research studies propose various classification systems based on the characteristics, causes, and severity of defects observed in tunnel linings. By comparing different classification approaches, it becomes possible to establish a more comprehensive framework for defect identification and assessment.

Although many defects develop gradually over time, tunnels also are subjected to extreme events that can significantly alter their structural behaviour. Tunnel fires represent one of the most critical scenarios, as high temperatures can lead to cracking, spalling, and weakening of both the lining and the surrounding rock mass. In severe cases, fire damage may result in the loss of structural support in localized areas of the tunnel lining. Understanding how tunnels respond to such conditions is essential for evaluating their stability and ensuring adequate safety measures.

Numerical modelling provides an effective tool for analysing the structural response of tunnels subjected to extreme conditions. By simulating specific damage scenarios, such as the loss of support at the tunnel crown due to fire, it is possible to evaluate deformation patterns, plastic zone development, and stress redistribution within the lining and surrounding ground. The behaviour of the tunnel is strongly influenced by the quality of the rock mass and the depth of overburden, which determines the level of confinement and overall stability of the system.

This Thesis combines a review of tunnel inspection techniques and defect classifications offered by different guidelines with a numerical investigation carried out by using a finite-element software. Different rock mass qualities and tunnel depths are considered to evaluate their influence on tunnel stability following crown removal. Additional analyses are performed to determine the threshold conditions for failure initiation between poor and moderate rock mass qualities. Through this approach, the work aims to give a brief overview of a limit rock mass model of certain mechanical properties at which safety conditions can be respected upon tunnel crown damage due to fire.

1.1 Thesis structure

This thesis is organized into five main chapters, each addressing a specific aspect of the study.

Chapter 1 presents the introduction, and the overall structure of the Thesis.

Chapter 2 reviews inspection and evaluation methods for segmental lining tunnels. The chapter examines conventional visual inspection techniques, recent developments in artificial intelligence for automated defect detection, and the application of non-destructive testing methods for identifying hidden or internal defects within tunnel linings.

Chapter 3 focuses on defects affecting segmental lining tunnels and their classification. Different types of damages are analyzed according to research studies and existing guidelines, with particular attention to technological and structural defects. A comparison between various defect catalogues is also presented in order to highlight similarities, differences, and implications for condition assessment.

Chapter 4 presents the numerical investigation of fire-induced damage in conventional tunnels. The structural response of the tunnel is analyzed through RS2 modelling by simulating crown removal under different rock mass qualities and overburden depths. Results are evaluated in terms of deformation, plastic zone development, and shear strain. Additional analyses are conducted to identify the conditions at which failure initiates between poor and moderate rock mass qualities, supported by a theoretical assessment based on the Hoek–Brown failure criterion.

Chapter 5 presents the final conclusions of the thesis, summarizing the main final findings

Chapter 2

Inspection and evaluation methods of segmental lining tunnels

2.1 Introduction

The performance of segmental tunnel linings depends on the ability to monitor their condition and identify any signs of deterioration. Damage may occur at different stages, from segment production to tunnel operation, and it is essential to provide early recognition to ensure structural reliability.

This chapter presents the main inspection and evaluation approaches used for segmental tunnel linings. First, the inspection procedures and quality control measures defined by the SIG (Società Italiana Gallerie) Working Group are described, including traceability systems and acceptance criteria applied during production, transportation, and installation phases. Then, recent developments in artificial intelligence are examined, focusing on the use of image-based systems and convolutional neural networks for automated defect detection and classification. Finally, non-destructive testing methods (NDT) are presented, including ground penetrating radar, ultrasonic techniques, and tomography, which allow the investigation of internal defects and hidden damage.

2.2 Inspection techniques and quality control

The SIG Working Group 2 report (2019) provides a detailed classification of defects affecting segmental tunnel linings and discusses their possible causes. In this section, the inspection procedures and observations described in the guideline are examined.

The life cycle of precast concrete segmental rings depends on careful logistical planning, ensuring safe transportation and installation while following the lining process requirements. Additionally, regular maintenance is necessary to guarantee adequate performance throughout the tunnel's lifespan, providing valuable insights into segmental ring linings for long, deep tunnels (Marini, 2023).

Inspection procedures are carried out including each stage of segments lifecycle from manufacturing production stage, transportation stage and installation checks, service life implementing periodic inspection and maintenance (Figure 1) (Chiriotti, 2019).

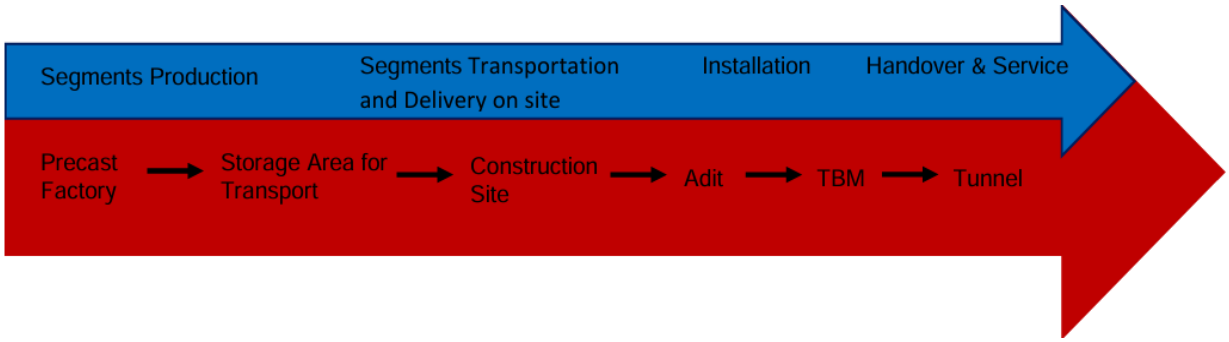

Figure 1 Phases of the segment life (SIG WG2, 2019)

Several parties are involved in the quality control of precast segments across all stages from production to installation and final handover. During the production phase, the segment manufacturer supervises fabrication according to the quality plan, while the main contractor ensures compliance with project specifications and may coordinate with an independent inspection agency for third-party verification on behalf of the project owner.

In the transportation and delivery phase, the manufacturer, transport company, and main contractor coordinate to manage logistics, documentation, and inspections. During the installation phase, the

tunnelling subcontractor (or the Main Contractor, if no subcontractor is present) installs the segments using a tunnel boring machine (TBM), under the supervision of the main contractor's Quality Assurance team, ensuring all quality and safety requirements are met.

Finally, in the handover and service phase, the Main Contractor delivers all quality records to the Project Owner, who verifies compliance and performance. An independent consultant or supervising authority may also assist in this final validation.

The quality control involves 3 detailed fundamental operations starting from traceability and data record, inspections, acceptance and/or repairs, transportation and delivery on site. Each segment undergoes these activities at every phase of its life and cannot be moved to the next stage of the process until all the quality criteria are fulfilled according to Figure 2.

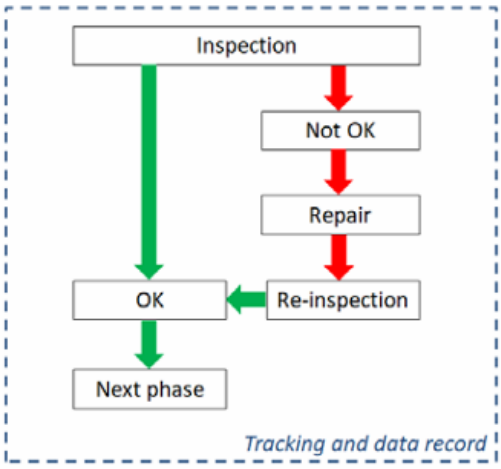

Figure 2 Segment Quality Acceptance Process (SIG WG2, 2019)

Traceability and data recording are based on a database compiled by the manufacturer for each segment, identified through a barcode that can be scanned when needed, and should be present from manufacturing process until the end of the handover and service phase. During production phase the database should contain segment information including production date, production ring number, segment unique identification number ID that shows the entire history of the segment, Reinforcement ID and type, mould ID and type, start-end date of casting, segment drawings, check list (inspections) to compile after moulding and for final acceptance for each segment and general materials specifications and quantities.

To ensure effective traceability and long-term data record management during transportation and delivery on site, it is essential to maintain a systematic database of all segment deliveries and related documentation. This includes the shipping request, shipping list, and loading pack, which should be accurately shared among the Manufacturer, Main Contractor, and Transport Company. Each segment must be tracked using a unique reference number, ensuring alignment with historical production and delivery data. As shown in Figure 3 ,this structured approach supports quality control, accountability, and efficient logistics across all stages from production to installation.

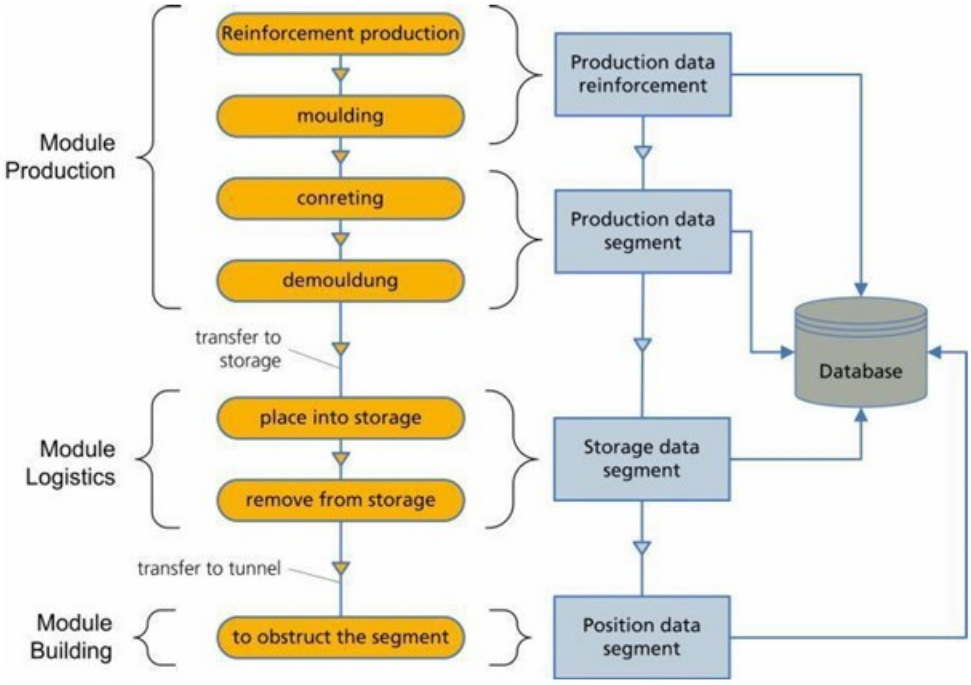

Figure 3 Database structure (SIG WG2, 2019)

As TBM advances, segments are transported from the site yard to the tunnel and loaded onto service vehicles. Before reaching the TBM, each segment is inspected and tracked by Subcontractor or Main Contractor personnel, with data logged into their systems. Final checks are done near the erector before installation. The Ring Building must be supervised to ensure proper alignment and avoid future damage. Daily Ring Erection Reports document TBM progress,

segment IDs, key positions, and any detected defects, are submitted to the technical teams for continues database updates.

After completing the ring building phase and finishing a tunnel stretch, a final inspection is performed before the tunnel is handed over to the project owner to verify that all segments have been properly recorded in the system, with complete data from production to installation (including IDs, damages, inspections, and repairs). Any missing information is added, and once finalized, the database is shared among all parties involved.

Going for the second and third operational step, inspections, acceptance and/or repairs to be compiled after demoulding and in a dedicated pre-storage area, the segments are inspected for damages, followed by categorization of damages as follow: minor defects for no action to be taken, major defects, or non-conformities that require special concept or rejection of the segment. This special concept consists of identification and mitigation of the non-conformity, definition of causes, and then applying the required corrective actions.

As part of the broader quality control procedure, further systematic inspections are performed before transport and upon arrival on site. These inspections are carried out by responsible quality control inspectors and documented through signed checklists. Based on predefined Close Out Criteria, segments are categorized as accepted, marked for repair, or rejected. Accepted segments are cleared for transport and use, while those requiring repairs are stored separately until re-evaluated.

Rejected segments, depending on project allowances, may be reused for non-structural applications or replaced entirely. Upon site delivery, further inspection is performed to verify conditions after handling and unloading, ensuring no damage occurred during transportation.

To streamline the inspection outcomes, a “traffic light” system shown in Figure 4 is applied. This system visually classifies segment status: green for accepted, yellow for repairable, red for rejected, and gray for segments placed under Non-Conformance Reports (NCRs). NCRs are issued for segments that do not meet repairable criteria but may be restored through an approved non-standard solution, subject to designer and project owner approval.

Related segments remain quarantined until the NCR conditions are resolved. This structured process ensures that only segments meeting all quality and safety standards are transported into the tunnel lining, supporting both construction safety and operational performance.

Segment Classification Upon Defect Evaluation	Defect Location	Defect Description
Pass - No Repairs Necessary	Extrados	**Broken Edges** ***(outside gasket groove)*** : Depth < 5 mm; Edge Affected Length ≤100mm;
		Surface Breakouts Depth < 5 mm; Diameter ≤20mm;
		Cracks Cracks widths ≤0.2 mm without impact on the structural integrity of the segment and Not through going cracks;
	Radial	**Broken Edges** ***(outside gasket groove and contact surface):*** Depth < 5 mm; Edge Affected Length ≤100mm; Affected Width ≤30mm;
	Intrados	**Broken Edges** Depth < 5 mm; Edge Affected Length ≤100mm; Affected Width ≤30mm;
		Surface Breakouts ***(patch repairs)*** Depth < 5 mm; Diameter ≤20mm;
		Cracks Cracks widths ≤0.2 mm without impact on the structural integrity of the segment and Not through going cracks;
Repair Is Required - Segment Acceptable Upon Accepted Repair	Extrados	**Broken Edges** ***(distance from gasket groove ≥ 10mm):*** Depth>5mm, and Max. up to No Visible Rebars; Edge Affected Length ≤200mm;
		Surface Breakouts ***(patch repairs)*** Depth>5mm, and Max. up to No Visible Rebars; Diameter ≤200mm;
	Radial	**Broken Edges** ***(distance from gasket groove ≥10mm and Contact Surface Not Affected):*** Depth>5mm, and Max. up to No Visible Rebars; Edge Affected Length ≤150mm;
	Intrados	**Broken Edges** ***(Contact Surface Not affected):*** Depth>5mm, and Max. up to No Visible Rebars; Edge Affected Length ≤150mm;
		Surface Breakouts ***(patch repairs):*** Depth>5mm, and Max. up to No Visible Rebars; Diameter ≤200mm;
Segment in Quarantine - NCR Repair	Extrados	**Broken Edges** ***(gasket groove Not Affected or minor defects which can be repaired):*** Depth up to No Visible Rebars; Edge Affected Length ≤500mm;
		Surface Breakouts ***(patch repairs):*** Depth>5mm, and Max. up to No Visible Rebars; Diameter ≤500mm;
		Cracks Crack width >0.2mm, without impact on the structural integrity of the segment and Not through going cracks;
	Radial	**Broken Edges** ***(distance from gasket groove ≥10mm); (Affected Contact Surface - Minor defects):*** Depth>5mm, and Max. up to No Visible Rebars; Edge Affected Length ≤100mm;
	Intrados	**Broken Edges** ***(Affected Contact Surface - Minor defects):*** Depth>5mm, and Max. up to No Visible Rebars; Edge Affected Length ≤150mm
		Surface Breakouts ***(patch repairs)*** Depth>5mm, and Max. up to No Visible Rebars; Diameter ≤500mm
		Cracks Crack width >0.2mm, without impact on the structural integrity of the segment and Not through going cracks;
Segment Rejected	Extrados	**Broken Edges** ***(gasket groove damaged - Major defects which can Not be repaired and/or Visible Rebars):***
		Surface breakouts Damaged Visible Rebars;
		Cracks Cracks widths >0.2 mm with impact on the structural integrity of the segment or through going cracks;
	Radial	**Broken Edges** ***(gasket groove damaged - Major defects which can Not be repaired and/or Visible Rebars and/or Affected Contact Surface - Major defects):***
	Intrados	**Broken Edges** Damaged Visible Rebars;
		Surface Breakouts Damaged Visible Rebars;
		Cracks Cracks widths >0.2 mm with impact on the structural integrity of the segment or through going cracks;

Figure 4 Transportation and delivery on site - traffic light table (SIG WG2, 2019)

Before installation, segments undergo the same acceptance process: they can be accepted, marked for repair, or rejected based on the Close Out Criteria. Only fully accepted rings are allowed for installation. Once a ring is built, segments can no longer be rejected. If major damage is found, special repair or mitigation measures must be applied to ensure tunnel safety.

The inspections, acceptance, and repairs for handover process begins with an internal inspection conducted by both the subcontractor/main contractor and an independent project owner inspector, where a ring condition report is filled to document any damages. Following this, a joint inspection is held to agree on necessary repairs, with updates made to the ring condition reports, carried out by the subcontractor/main contractor, with detailed records of the materials and methods used. The invert is then inspected, cleaned, and repaired if necessary. After completing these repairs, a final joint inspection ensures that all issues are resolved. If any remaining damages are found, they are repaired before the final acceptance. Once the tunnel meets all quality standards, the subcontractor/main contractor submits a final inspection report, and the tunnel is handed over to the project owner for further construction activities.

2.3 Inspection of segmental lining defects using artificial intelligence

Artificial Intelligence has begun to play a larger role in the inspection of the tunnel linings in recent years, particularly in mechanized tunnelling where precision is crucial. Recent research highlights a growing shift toward automated and semi-automated tunnel inspection systems as high-resolution imaging technologies become more widely available in infrastructure monitoring (Sjölander et al., 2023). Inspections are also becoming quicker, more accurate, and less reliant on human judgement thanks to these technologies. Nevertheless, the performance of automated inspection systems can be influenced by environmental conditions such as lighting variations, moisture, dust, and occlusions, which remain important challenges in practical tunnel environments (Yeum & Dyke, 2015). Numerous studies have investigated ways to automate AI inspections process, frequently with the aid of machine learning and image recognition tools. The potential of convolutional neural networks (CNNs) to identify and categorize flaws in precast tunnel segments is examined in one such study by Valentini and Faini (2024). Similar deep learning approaches have also been explored for crack detection and surface defect recognition in concrete structures, where convolutional neural networks have demonstrated strong performance in image-based damage identification (Zhang et al., 2016). Traditionally, checking these segments for defects has been done manually, a process that is not only time consuming but also vulnerable to inconsistencies and human error. To overcome this, the authors explore the use of artificial intelligence (AI), particularly CNNs, to automate the detection and classification of defects. A key

part of their approach involves applying a well-defined classification system that groups segment defects into seven main classes like cracks, blowholes, honeycombing, and edge damage with 23 detailed subcategories. By training models on large datasets of segment images and using techniques like data augmentation, AI systems can learn to spot and categorize issues such as cracks, voids, and edge damage with accuracy, more consistency and reliability. Recent research also shows that attention-based deep learning architectures can further improve defect detection performance by enabling the model to focus on the most informative regions of an image (Guo et al., 2021).

Before delivering solutions, artificial intelligence (AI) systems go through several processing phases. AI relies on algorithms and data to learn, reason, and solve problems. In tunnel inspection systems, this process is generally described as a workflow including data acquisition, image preprocessing, model inference, and post-processing for defect localization and measurement (Cha et al., 2017).

When solving any problem via AI, the first step involves understanding the issue by cognitively recognizing text, images, tables, videos and voice to extract the necessary related information. This information moreover needs to be gathered, through processing logical algorithms by systems, and this phase is called Reasoning. After information being gathered in the reasoning phase, now it is being learnt by machine learning techniques which analyse the data as input data to generate accurate outputs. Last step, which is to have more accurate data processed, is the human-machine interaction which includes using Natural Language Processing (NLP) technologies.

Artificial Neural Networks (ANNs) is mainly inspired by human biological neural networks. It consists of interconnected neurons in which data is processed. In this approach, neural networks are organized in interlinked different layers in which communication is occurring among them by a mathematical logic function for each single neuron.

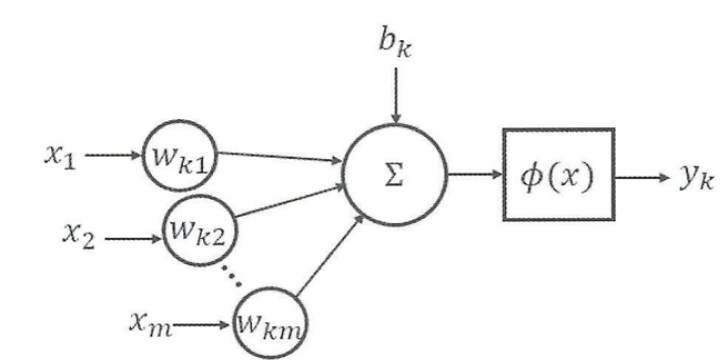

Figure 5 Artificial neuron diagram (Valentini and Faini, 2024)

ANNs consists of inputs x_{ki} which comes from previous layer and a single output y_k. The output of the single neuron K can be driven by a specific calculation which involves certain parameters. These parameters include an activation non-linear function Ø that controls the activation of the neuron, weights w_{ki} that are fitted in the learning process phase to determine the importance of the incoming inputs from previous layers, and a bias b_k to offset the result.

$$(y_k = \phi(b_k + \sum_{i=1}^{m}(w_{ki} \cdot x_i)) \qquad (2.1)$$

After defining the neural network architecture, the model must be trained. The training process consists of feeding the network with input data for which the correct outputs are already known. This procedure is repeated iteratively until the model achieves satisfactory accuracy when tested on previously unseen data. Through this process, the network adjusts its internal weight values in order to minimize the error and best approximate the desired output

CNNs, which are developed for image recognition and visualization, are arguably the most robust systems for image-based defect detection in tunnel segments. CNNs apply a series of filters to an image to access the important features in the image such as edges, texture and geometric figure. The identification of such important features allows for the identification of surface defects such as cracks and asymmetries in precast concrete segments. One feature of CNNs is their ability to learn variations in spatial hierarchies in images, which make them a good choice for systematic inspection tasks. Combining CNNs with other neural network types could increase the detection efficacy and diversity of the model, especially with more complicated or diverse inspection datasets.

To develop an AI-based system for defect recognition in tunnel segmental linings, a clear and structured process was followed by the authors of the paper. The first step involved identifying and categorizing the types of defects (see Table 1). Once the defect types were defined, the development moved to the technical setup. This included selecting an appropriate vision system in terms of hardware and user interface and building a model capable of detecting and classifying the predefined defects. The model was trained specifically for anomaly detection to recognize images that deviated from standard or defect-free normal segments images.

Table 1 Types of defects (Valentini and Faini, 2024)

Class	Defect Type	Description
A	Blowholes, air pockets	Surface defects caused by trapped air during concrete pouring and setting
B	Edge damage, chipping	Damage to edges or surfaces due to impact or abrasion
C	Cracking	Cracks resulting from shrinkage, thermal expansion, or stress factors
D	Honeycombing	Voids within the concrete mass due to poor compaction
E	Missing near gaskets	Absence of necessary inserts, leading to functional issues
F	Defects near gaskets	Irregularities or damages around gasket or joints
G	Wavy surface	Non uniform or undulating surface texture

The training process began with the collection of a large dataset consisting of 10,000 defective and 10,000 non-defective images. These images were carefully annotated and divided into training, validation, and test sets. Pre-processing steps were applied to prepare the images for analysis which included resizing and normalizing the images for uniformity, as well as applying data augmentation techniques such as rotation, translation, and brightness adjustments to improve the model's robustness against visual variation. Proper preprocessing is particularly important when dealing with high-resolution inspection images, where small defects may otherwise be lost during scaling or compression processes (Zhang et al., 2016).

The chosen network architecture was VGG16, part of the Visual Geometry Group family, which is well suited for visual recognition tasks. This training process used a backpropagation algorithm combined with gradient descent, and the model's performance was optimized using categorical cross entropy as the loss function.

To enhance interpretability, an attention mechanism was integrated which allowed the model to focus on the most relevant parts of the image and produce an intermediate output indicating the likelihood of defect presence. The final model output was a probability matrix representing the presence or absence of defects across the image as illustrated in Figure 6. This map uses parts of the neural network that are trained to differentiate between defective and non-defective items, employing a simple yes-or-no method. These advanced visual tools make it possible to not only detect defects but also estimate their size and spread allowing for an easier and smarter process results, allowing for more efficient decision making.

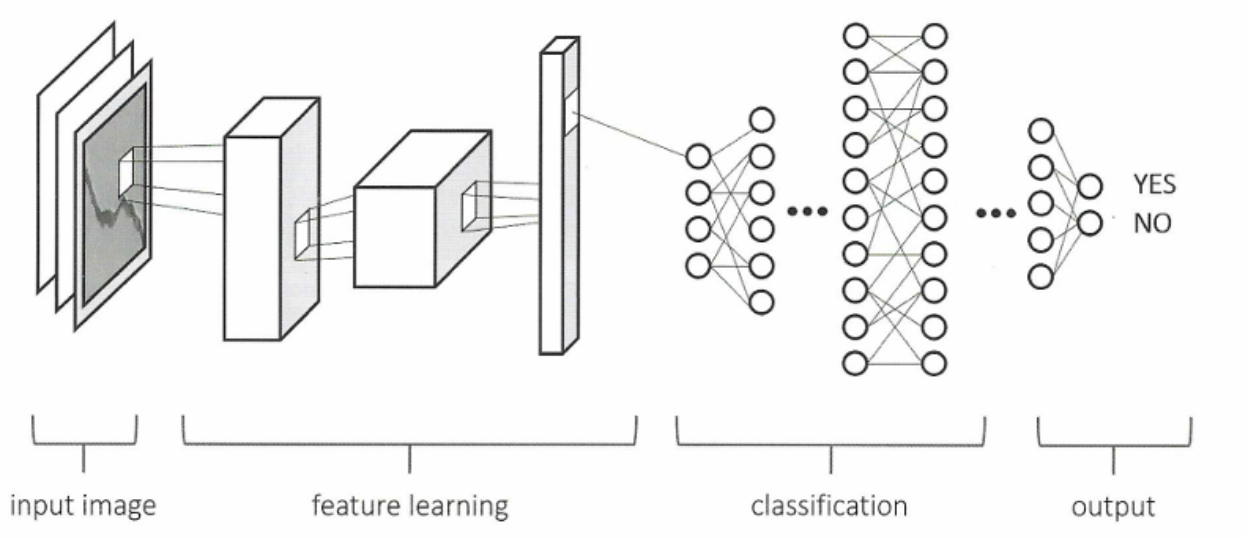

Figure 6 Neural network process for image classification and anomaly detection (Valentini and Faini, 2024)

After training, the model's performance was evaluated using accuracy, precision, recall, and F1 score. The F1-score is the harmonic mean of precision and recall, which gives a balanced measure of a model's ability to correctly identify positive cases while avoiding false ones. In computer vision studies, these evaluation metrics are commonly used together to assess the reliability of

defect detection systems and to compare the performance of different deep learning architectures (Guo et al., 2021).

These metrics helped assess how well the model detected defects accuracy showed overall correctness, precision focused on reducing false alarms, and its ability to catch all real defects by combining both precision and recall. The model was gradually refined by adjusting factors like the number of layers and learning rate, improving its ability to detect even subtle surface defects on segmental linings

The final model was tested on over 10,000 images and showed strong results in detecting various defects. A useful feature was the probability map, which highlighted accurately areas most likely to have issues. As shown in Figure 7, this feature helps in focusing attention on potential problem zones, making inspection faster and more consistent.

Figure 7 Expected anomalies in concrete segment defects (Valentini and Faini, 2024)

In the process of identifying defects, a neural network creates a probability map that shows where defects are likely to be in a picture. Figure 8 illustrates these using shades of red, where lighter red means a higher chance of defects. This map is then combined with the original photo of the object to help experts and automated systems to concentrate on areas that might have defects, speeding up the inspection process.

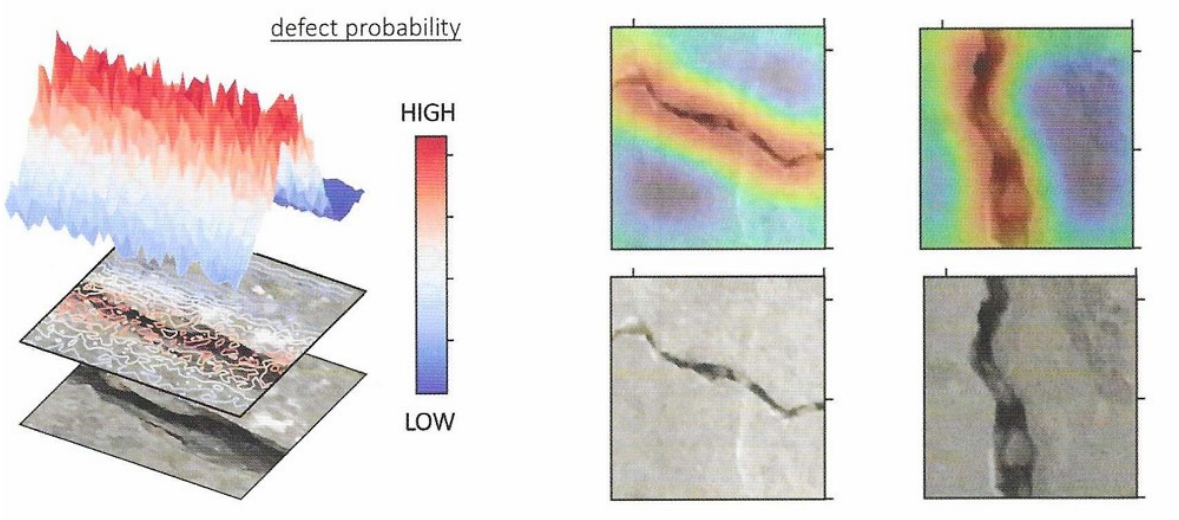

Figure 8 Anomaly detection probability distribution output (Valentini and Faini, 2024)

Based on the binary (yes/no) neural network prediction, a mission vision algorithm is applied to accurately identify the real defect boundary and locate cracks, as clearly shown in Figure 9a. In addition, when no defect is detected, the system generates an output image indicating the absence of defects, as illustrated in Figure 9b.

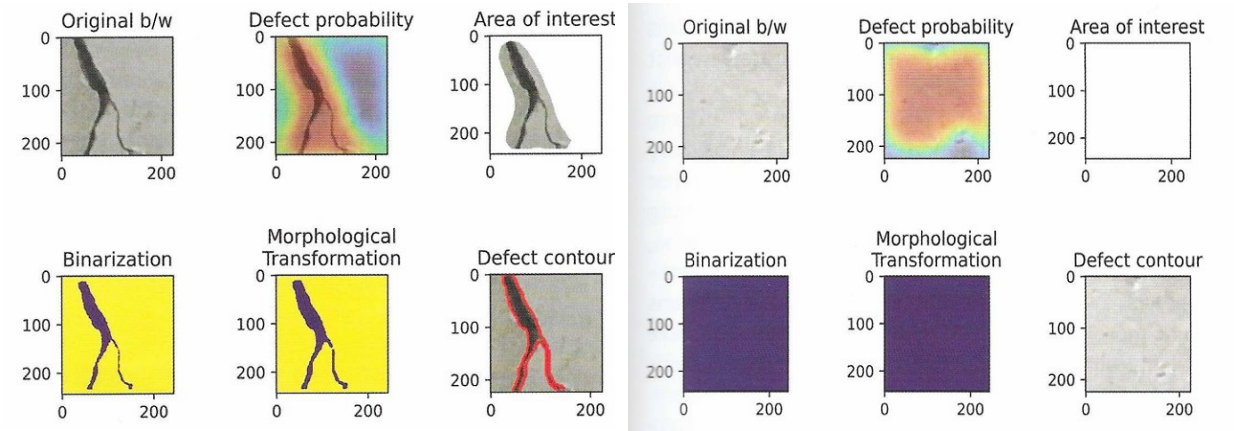

(a) (b)

Figure 9 a) Image classification and anomaly detection detail, b) same process but for no defect anomaly results (Valentini and Faini, 2024)

The algorithm applies some colour enhancement and image processing increasing image contrast using (CLAHE) a Contrast Limited Adaptive Histogram Equalization and finally it is now easily

to extract the main area of concern. The algorithm itself also can locate the threshold of the image and checking for prediction if higher or lower than that threshold using the set of pixels.

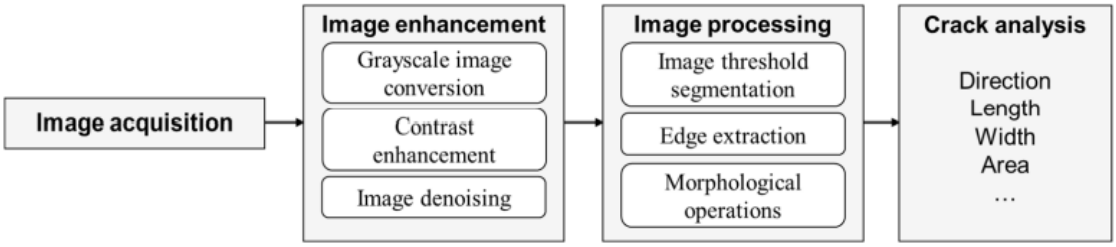

Figure 10 Flowchart of conventional image processing (Jiang et al., 2023)

The area of interest then is transformed into a grayscale image to move from 3D matrix to 1D matrix binary image with few enhancements to be able to simply say if the image has a defect or not. That happens by defining new threshold values that say for each area if true-1 meaning it has a defect and false=0 meaning it doesn't.

To clean up the image and make sure the defects are properly outlined, morphological transformations are used. These operations use a small matrix called a kernel that moves across the image, adjusting pixel values based on their neighbors. Erosion removes noise by shrinking white areas (defects), while in the opposite dilation expands them to fill gaps. When combined, opening (erosion followed by dilation) eliminates small white noise, and closing (dilation followed by erosion) fills tiny holes in defects. These techniques are especially useful for highlighting clear edges and improving defect outlines. However, classical image-processing techniques such as thresholding and morphological filtering are often sensitive to lighting variations and image noise, which has motivated the growing adoption of deep learning methods for infrastructure inspection (Yeum & Dyke, 2015). When an image has no edges, meaning it's uniformly 0s or 1s, these transformations have no effect, indicating the image is already smooth and clean.

The final step in detecting defects in precast concrete segments is identifying their boundaries. Since the image has already been converted to black and white (binary), the computer can now easily spot the edges which outline the shape of the defects. Once the defect is outlined, its size

can be measured in real units if the camera specs are known, but accuracy depends heavily on image framing and lighting conditions. If the camera isn't positioned well or lighting is poor, defects can be hidden or distorted, so proper setup and even lighting are crucial for reliable detection.

AI can be used not just during production, but also to monitor precast segments during various construction phases like transport, handling and installation. It can detect damage caused by handling and ensure proper placement during TBM installation. This full-cycle monitoring helps maintain quality, improves safety, and reduces costs making tunnel construction more efficient from start to finish.

Improving AI in defect detection will involve better cameras, lighting, and multi angle views for clearer images. In addition to standardized setups and training under varied conditions that will make systems more reliable, AI can boost inspection accuracy and support safer tunnel construction with the right tools, staff training, and updates. Despite the rapid progress of AI-based inspection systems, challenges remain regarding the generalization of trained models across different tunnel projects and imaging conditions (Sjölander et al., 2023)

2.4 Non-destructive testing techniques for tunnel lining inspection

Non-Destructive Testing (NDT) methods are one of the methods to inspect structural related defects, such as cracks, voids, delamination, and areas of material deterioration, without physically damaging the tunnel structure (Grosse & Ohtsu, 2008). These techniques are effective for new tunnels since the early detection of defects can prevent expensive maintenance, prolong the service life, and prevent future failure (Beck & Yuan, 2005). NDT delivers detailed and accurate information on the lining's internal condition so that engineers can make informed decisions on good data (Grosse & Ohtsu, 2008).

Ground-penetrating radar (GPR), ultrasonic pulse velocity (UPV), impact-echo, and infrared thermography are a few of the most popular NDT techniques utilized in tunnel inspection. They all offer advantages in inspecting different forms of structural defects, which can assist in offering

a complete and environmentally friendly inspection strategy for the tunnel lining throughout its lifespan (Grosse & Ohtsu, 2008).

GPR detects underground structures by propagating high frequency electromagnetic (EM) waves through materials. In GPR, an electromagnetic pulse is transmitted into the structure, and when it encounters interfaces between materials with different dielectric properties (like concrete, voids, or water filled cracks) part of the wave energy is reflected to the receiver. By analyzing the characteristics of the reflected echoes including travel time, amplitude, phase velocity, and attenuation with frequency, GPR can figure out the presence, depth, and type of subsurface anomalies and then after processing, it constructs a 2D image.

Figure 10a illustrates the GPR device, consisting of antennas for transmitting and receiving electromagnetic waves, a radar control unit with the function of processing GPR data, and other auxiliary structures. Figure 10 shows the basic principle of GPR for crack detection (Jiang et al., 2023).

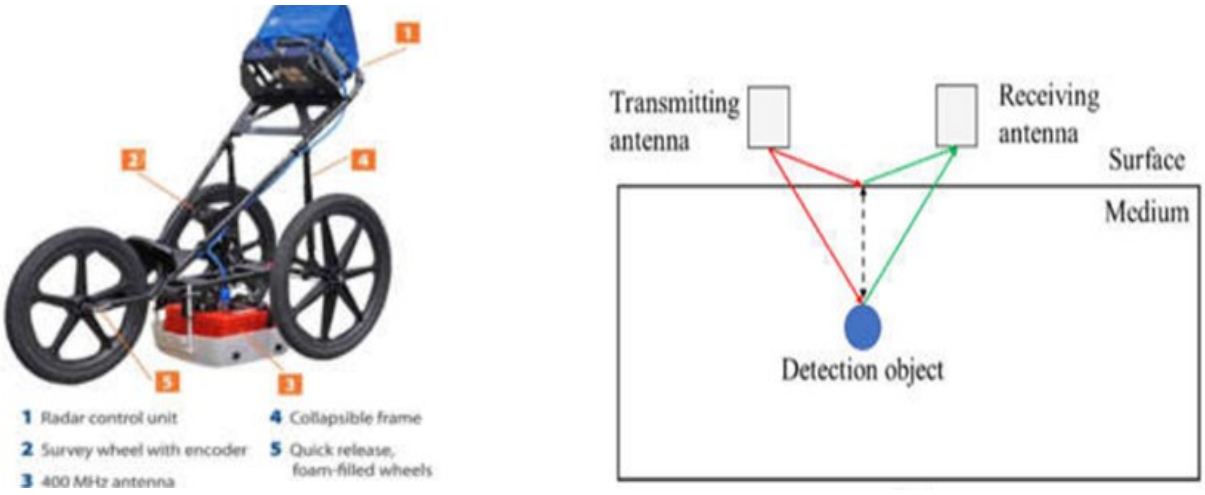

(a) (b)

Figure 10a) GPR radar GSSI SIR 3000(Jiang et al., 2023), Figure 10b) GPR Principle (Jiang et al., 2023)

In concrete structure applications, GPR equipment generally operates between 10–5000 MHz for different applications. A lower frequency increases the penetration capability of EM waves to detect deeper waves but require larger equipment, and a higher frequency increases the resolution. In practice, there is a trade-off between detection depth and accuracy (Peng et al., 2021).

GPR is used also to detect deeper defects like defects in the grouting section behind the segment in real time after grouting and after complete solidification through a finite difference time-domain numerical simulation and making it 3D to have real time monitoring. The test showed that 7 days were the perfect timing to detect the quality of grouting as well as important information about grout defects which are considered critical for a healthy complete ring structure including depth, cracks, voids and cavities.

In addition to the grout, researchers were able to detect the surrounding rock after the tunnel lining was completed, detecting loose rocks around tunnels by using ground-coupled GPR. However, boulders were detected using a 1.5 GHz antenna, and 2.6 GHz was used for the more precise detection of small and medium-sized rocks (Peng et al., 2021).

Another NDT method is sonic and ultrasonic techniques, for detection of defects for unilaterally accessible concrete structures such as thick concrete tunnel lining This method include various techniques like impact-echo technique, time-of-flight diffraction (TOFD), impulse response technique, ultrasonic tomography technique.

The Time-of-Flight Diffraction (TOFD) method is effective in identifying the diffraction of ultrasonic waves at the edges of cracks, which allows the determination of their location and size as illustrated in Figure 11, when the transmitter emits an ultrasonic pulse, part of the wave is diffracted by the crack tips.

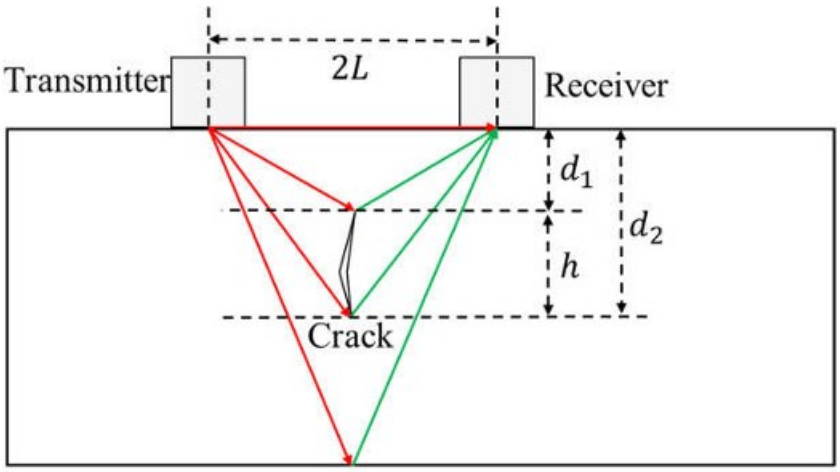

Figure 11 TOFD principle (Jiang et al., 2023)

This diffracted signal is captured by the receiver, and its arrival time is recorded. Using this data, and knowing the speed of signal (c), half length (L) between the transmitter and the receiver, travel time of the ultrasound beam (Δt), the depth (d) and dimensions of the crack (h) can be calculated using the following equation.

$$d = \sqrt{(\frac{c \cdot \Delta t}{2})^2 - L^2} \qquad (2.2)$$
$$h = d_2 - d_1$$

Another NDT method for crack detection is Surface Wave Transmission (SWT). This technique uses Rayleigh surface waves and estimates crack depth by analyzing the transmission of waves across a surface-breaking crack. Researchers have developed air-coupled SWT sensors to allow non-contact testing as shown in Figure 12, making the method faster and more practical. Numerical simulations particularly those based on the Finite Element Method (FEM) have been used to model wave behavior and validate experimental results, showing strong agreement with theoretical predictions. Although most studies have been conducted on specimens with artificial notches, SWT shows promising potential for tunnel lining inspections, especially when combined with other NDT techniques.

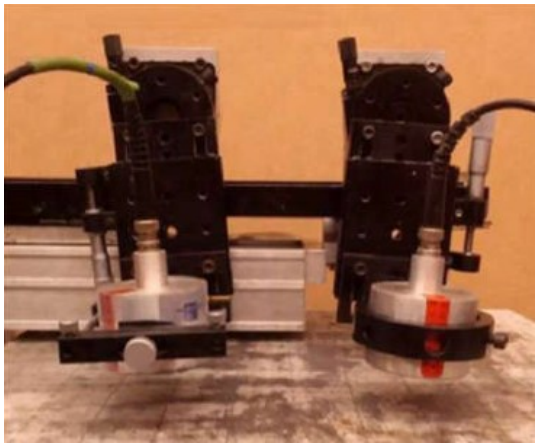

Figure 12 non-contact air-coupled ultrasonic sensors (Jiang et al., 2023)

Another intuitive NDT method for crack detection is tomography, which reconstructs internal images of concrete structures using sensor data. Electrical tomography techniques such as Electrical Resistivity Tomography (ERT), Electrical Capacitance Tomography (ECT), and Electrical Magnetic Tomography (EMT) can visualize crack positions by measuring changes in electrical properties.

To improve detection coverage and accuracy, modern systems often integrate multiple sensors and techniques. Mobile vehicles and robots equipped with cameras, infrared sensors, laser scanners, radar, and ultrasonic devices can perform automated tunnel inspections at high speed. Vision-based systems are widely used for surface crack detection due to their efficiency and detail, while other NDT methods help identify more complex crack characteristics. The combination of these technologies, including image processing and data fusion, is key to achieving reliable and comprehensive tunnel lining assessments.

Chapter 3

Tunnel segmental lining defects

3.1. Introduction

Segmental tunnel linings can develop different types of defects during their lifecycle due to production processes, handling, installation, and operational conditions. The presence of these defects makes it necessary to understand their origin and characteristics in order to correctly evaluate tunnel condition and interpret inspection results.

This chapter describes the main defects affecting segmental tunnel linings based on research studies and technical guidelines. First, damages identified by the SIG Working Group are presented, including both technological damages related to manufacturing and installation, and structural damage caused by loading conditions. Then, defects included in the Italian Guidelines for Existing Tunnels are described, together with their classification based on extent and intensity. Additional defect types reported in the literature are also included. As a conclusion, defects not included in the Italian Guidelines for Existing Tunnels and that should be integrated in the case of segmental tunnel linings are identified.

3.1. Defects in tunnel segmental linings

The classification of defects in segmental tunnel linings presented in this section is mainly based on the report *Inspection and maintenance of precast tunnel segmental linings* developed by the ITA SIG Working Group 2 (2019). Damage to tunnel linings occurs throughout their lifecycle, from manufacturing defects to installation and operational failures. These damages can arise

during different phases of the segment life, from factory production including casting, demoulding (Figure 12a), handling, overturning, storage (Figure 12b), transportation and delivery on site, installation, until handover and service life operation. Special attention is given to two types of damage: technological damages, which are non-structural, and structural damages, which are related to the stress response of segments and precast linings during production Technological and structural damages may occur during the previously mentioned stages , or during the thrust phase (Figure 12d) .These damages result from various factors, including mechanical stresses, improper handling, and material deficiencies (Chiriotti, 2019).

(a) (b)

(c) (d)

Figure 12 a) Segments demoulding (ITA, 2019) b) Segments storage (ITA,2019) c) Segments transportation (Steel Fibre Reinforced Concrete for Tunnel Lining Segments, 2018) d) Segment installation during shield driving (Flath, T. ,2009, June 15)

Table 2 Types of segmental lining damage

Category	Phase	Damages
Technological damages	Post casting, demoulding, handling, overturning, storage	Concrete surface defects Insert presence defects Gasket damages Chipping of side and corners
	Handling and installation of the ring	Gasket damages Chipping of sides and corners Chipping of edges and corners
	Thrust phase	Gasket compression from jack's plate
	Grouting and operational phases	Gap and offset Water leakage from joints and bolt holes Unscrewing joint bolts chemical and thermal deterioration
Structural damages	Post casting, demoulding, handling, overturning, storage	Insert presence cracks Demoulding cracks Handling cracks Overturning cracks Storage cracks
	Handling and installation of the ring	Erector caused damages Handling and installation of the ring related damages
	Thrust phase	Transversal cracks Longitudinal cracks Chipping of sides and corners
	Grouting and service phases	Loss of connector and bolt performance spalling during fire

3.1.1 Technological damages

Technological damages are defects caused by problems in materials, production, installation, or construction quality, rather than by the tunnel carrying loads. In simple terms, they come from how the lining was made or built.

During the post-casting phase, which includes demoulding, handling, overturning, and storage, various surface defects can occur on the segment. These include concrete surface defects, insert presence defects, gasket damage, and chipping of sides and corners.

Concrete surface defects include hollows, exposed reinforcement, exposed aggregates (such as gravel nests or honeycombs), and the removal of the concrete skin. The severity of these defects depends on their location within the structure. Therefore, they should be classified based on the affected segment, which may include the extrados, intrados, perimetric surfaces, or specific areas like gasket grooves, niches, pockets, and holes.

Hollows consist of a small void on the surface or within the structure as shown in Figure 13. They are considered defects if they exceed 5 mm at extrados, intrados and perimetric surfaces and considered non-conformities if they exceed 1 mm on gasket groove. Hollows occur due to incomplete air expulsion during concrete pouring and segment casting. Air can be trapped between the mould and concrete or absorbed during transport between different containers (e.g., mixer to hopper). Hollows could be caused by poor vibration distribution and improper mix design.

Figure 13 Example of hollows (SIG WG2, 2019)

Exposed reinforcement is due to concrete failing to fully cover the steel bars, leaving them vulnerable to environmental conditions such as moisture, tunnel gases, and backfilling materials. This issue is primarily caused by:

- dense reinforcement spacing, when reinforcement bars are too closely packed, concrete may not flow properly around them.
- insufficient/inadequate vibration during casting preventing concrete from filling gaps between the reinforcement and the mould.
- misalignment of the reinforcement cage, as poor positioning can lead to areas where concrete coverage is insufficient.

Exposed aggregates (Figure 14) occur when large aggregate particles become visible on the segment surface due to a lack of fine materials like cement, sand, and additives. This typically happens because of:

- washout, i.e. excess water or overly fluid concrete can cause finer particles to be washed away, leaving behind only coarse aggregates.
- poor mixing, if concrete is not mixed properly, coarse particles can clump together, forming voids or nests. These conglomerates may not break apart during transport and casting, leading to uneven distribution in the segment.

Figure 14 Exposed Aggregates (SIG WG2, 2019)

Removal of Concrete Skin: it involves the removal of a concrete surface layer, typically 1–3 cm deep, without exposing reinforcement. It occurs more in corner areas and weak zones between the segment surface and concrete cover. Common locations include dowel sockets, erector gripper pockets, and insert areas. Causes include incorrect demoulding due to misaligned equipment or improper clamping, insufficient draft angles, and uneven demoulding agent distribution. Proper mould design and controlled demoulding processes are keys to preventing these defects.

Unscrewing/disconnection and insert absorption in the casting itself: It refers to insert disconnection (e.g. connection caps, threaded bearings, injection bearings) from its corresponding mould lodging and is embedded into the segment casting. This type of defect is mainly caused by two root causes, incorrect assembling of the insert not following manufacturer instructions including insufficient tightening torque during casting. This also leads to grout leaks as mentioned before. The second cause is due to incorrect coupling between insert and its corresponding lodging in the mould

Grout or grease leaks: Usually at grout sockets, grease or grout leakage can occur and spread on inserts retention link points on the mould. Connection issues and grease leakage can occur when lubrication is either insufficient where needed or applied incorrectly, affecting the integrity of the joints not on non-contact areas at sockets teeth or threads to ensure a secure and functional connection. Insert function is altered due to residual protective grease, which can cause assembly issues if not completely removed before production, especially after a prolonged stoppage.

Regarding grout, grout leaks mainly occur due to incorrect insert assembly or improper coupling with the mould lodging. It may loosen while casting not being tightened according to the manufacturer's specifications allowing gaps for leakage.

Double gaskets are mostly used for tunnel linings, to prevent leakage of water because of high groundwater pressure. Moreover, the use of two gaskets ensures a more robust seal. In case of one gasket failure or damaged, there is another gasket that still can maintain sealing properties of the gasket.

Anchored gaskets defects: One of the most common defects that could happen in anchored gaskets is the gasket sinking in the concrete longitudinal and circumferential joints and corners (Figure 15). The sinking is mainly due to incorrect gasket installation in its groove during casting,

as they could come over the groove not maintaining its correct position in the segment during moulding, also during installation or during casting as the gasket could deform forming a crease being forced inside the groove at one of its sides without being distributed all over the segment corner or longitudinal side. Another cause is the inadequate anchoring system, where there is no sufficient connection force applied at the mould during casting. Other causes that lead to corner sinking of the gasket in the concrete is the length of the gasket not sufficient in one or more of the sides of the segment, improper coupling of the gasket with the mould leading to gasket installation defects, as well as design mistakes of the gasket groove at the corner

Figure 15 Corner Gasket Damage (SIG WG2, 2019)

Concrete damages can include only concrete being damaged and it refers to cracking or breaking of concrete near gasket groove, concrete being damaged around the gasket areas and this is due to detachments around gasket along extended areas, and could be both gasket and concrete heavily damaged, which is mainly caused after demoulding , where damages affect both gasket and concrete along with cracks and concrete detachments

Glued gaskets defects: Corners deformation are common defects that happen to glued types of gaskets due to mispositioning of the gasket with segment corner. Similar causes adhere here to be due to incorrect gasket length and incorrect installation. Glued gaskets are prone to detachments due to several reasons including defects following the type of glue, environmental reasons like excess moisture and collisions or rubbing.

Chipping of sides and corners, representing breaks in the segment edges, is classified into three categories based on depth: less than or equal to 25 mm, between 25 and 50 mm, and greater than or equal to 50 mm.

Chipping (Figure 16) usually happens during casting due to incorrect distribution of demoulding agent either because of insufficient agent to cover all sides or the agent not being distributed uniformly along the sides and corners. Another cause is the collisions that happen during the casting. Segment chipping during demoulding is also caused by misalignment and excessive concrete cover thickness, making them more prone to damage.

Figure 16 Example of corner breaking (SIG WG2, 2019)

In the phase of handling and installation of the ring, some damage can occur due to how the segments are moved, handled, or placed. Among the most common are gasket damaging, chipping of sides and corners during handling, chipping of edges and corners during installation, and chipping of corners during installation. These types of defects result from impacts, misalignment, or mistakes during the installation process, and they should be checked based on where they happen and how serious they are.

The transportation and installation of lining rings involve precise handling, as they are first moved to the TBM's backup area and then positioned using a specialized crane system. A vacuum suction plate allows the erector to place the segments accurately, requiring skilled operation to ensure structural integrity (Marini, 2023). Several types of damage occur in these phases and are:

Gasket damaging, including expulsion or pull-out during installation, can occur during handling which describe transportation, shipping, and transfer to the job site, and installation exposes the gasket to potential damage from collisions or rubbing and are considered the main causes during

handling. For what concern ring installation phase, when installing a segment to an already installed segment, the gasket of the incoming segment may be expelled from its longitudinal side (Figure 17). During installation, gasket damage can be influenced by the longitudinal cut angle and the connection system. For instance, rectangular segments with a cut angle close to 0° increase the risk of gasket expulsion. Add to it gasket anchoring and adhesion issues including poor gasket lubrication where friction between the gaskets of adjacent segments can cause expulsion or displacement from the groove upon installation, and poor anchoring or poor gluing force.

Figure 17 Expulsion of gasket from one side SIG WG2, 2019)

Chipping of sides and corners during handling: Before installation and during post-casting phase, the segment is subjected to many handling operations which makes it prone to collisions specially at corners and /or edges. Having sharp edges or corners increases this risk of damaging, especially during the erector segment rotation phase.

Chipping of edges and corners during installation: Edges chipping (Figure 18) happen due to jack plate presses on the gasket during installation, it can cause concrete breakage or detachment between the gasket and the segment edge. Damage to gaskets can result from improper positioning due to smaller distance from the segment edge. Weakness in the segment edge due to poor concrete properties or lack of reinforcement which causes different mechanical properties that make areas at edges weaker than other surrounding concrete. Additionally, failure to comply with the design specifications, including joint gap limits and load distribution, can subject the gasket to excessive forces, causing the segment edges to break or the gasket to exceed the concrete's resistance.

Figure 18 Chipping of edge during installation (SIG WG2, 2019)

Additionally, corner chipping (Figure 19) during installation occurs when cracks form at the intrados or extrados corners, leading to concrete detachment. Main causes include collisions, weak concrete properties at the corner due to lack of reinforcement, gasket loads exceeding the concrete's strength, and improperly designed gasket corners with discontinuities causing excessive stress on the concrete during compression, leading to breakage.

Figure 19 Chipping of corners during installation (SIG WG2, 2019)

During the thrust phase, the TBM jacks' plates compress the segment gasket (Figure 20**)** with a certain degree of eccentricity (Figure 21) reducing its water-tightness capacity since this property cannot be fully recovered after compression. The causes of damage during the thrust phase are primarily related to the interaction and design of the TBM and segments. These issues occur when TBMs and moulds from different projects are used, leading to mismatches in design.

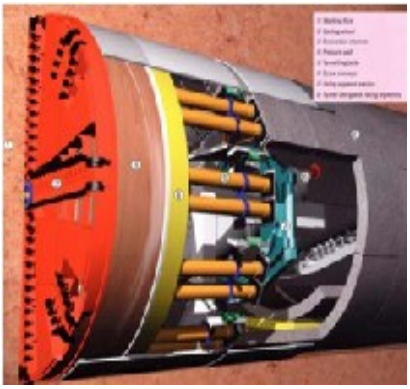

Figure 20 Thrust of TBM jacks on segment (SIG WG2, 2019)

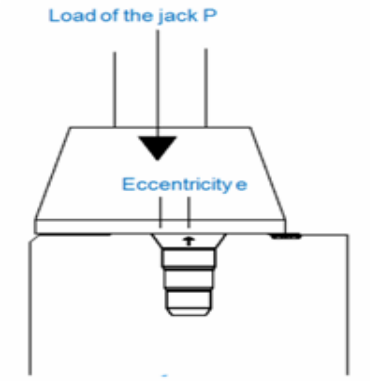

Figure 21 Layout of jacking cylinders and thrust with eccentricity (SIG WG2, 2019)

Issues related to the grouting and operational phases include the presence of gaps and offsets between segments, as well as water leakage through joints and bolt holes. These challenges often result from improper segment installation, where misalignment during assembly leads to joint dislocation and potential structural issues. Furthermore, deviations between the shield machine and the designed tunnel alignment can worsen these misalignments, increasing the risk of structural deficiencies and water ingress (Chakeri, 2021).

Excessive gaps and offsets in tunnel segments (Figure 22) can result from several factors related to installation and design. These limit values are related to the type of connection between the joints and the type of gasket. If segments are not assembled in their designated positions, the connection systems may fail to maintain the specified tolerances, leading to misalignment. This could be mainly due to the bituminous seams blocking the proper closing of the joint.

Incorrect sizing of bituminous pads for thrust force distribution can lead to improper joint closure as shown in Figure 22 , resulting in excessive gaps if the pads are too wide or not compressible enough. Excessive gaps and misalignment, due to reaction force generated by gaskets that can open the joint resulting from unbalanced thrust of the gasket when compressed exposing the tunnel's ring structure.

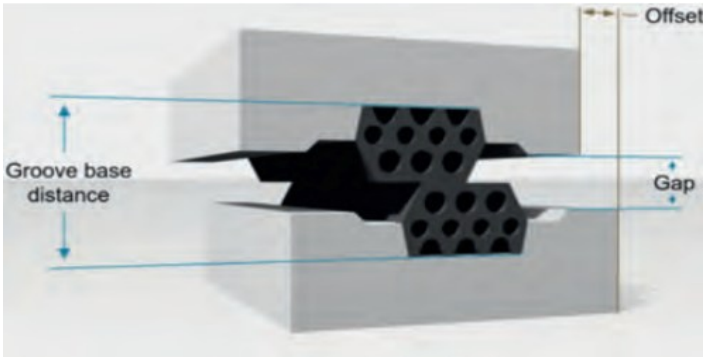

Figure 22 Gap and offsets (SIG WG2, 2019)

It is clearly visible that there is a slight bump in the segment towards the outer side, caused by an offset at the joint as shown in Figure 23. Additionally, there is a noticeable gap between the segments, which is likely due to improper alignment or inadequate gasket compression.

Figure 23 from left offset, from right a gap (SIG WG2, 2019)

Water leakage from joints and bolt holes: Water leakage (Figure 24) occurs when the waterproofing system fails to provide an adequate seal due to insufficient hydraulic sealing by the gaskets, which may not fully prevent water infiltration. In some cases, structural fissures extending through the entire segment thickness create pathways for water to bypass the gaskets and penetrate the tunnel lining. These issues can arise from improper gasket selection, installation errors, or concrete defects.

Figure 24 Water leakage from joints (SIG WG2, 2019)

3.1.2 Structural damages

Structural damages are defects that affect the lining because of stress, loads, ground pressure, or movements acting on the tunnel. In other words, they are linked to how the structure behaves under force. Structural damages as illustrated by SIG working group 2 research in the figure below:

Shield segment damage	Figure
Crack in axial direction	
Crack in circumferential direction	
Chipping at segment corner	
Scraping around segment joint	
Scraping around ring joint	
Crack/scraping around ring joint box	
Crack/scraping around segment joint box	
Scraping at outer surface	
hair crack at inner surface	
appearance of non-visible crack	
buckling of longitudinal rib (steel segment)	
deformation of rib (steel segment)	
break of joint bolt	

Figure 25 forms of segment damages during construction life cycle (SIG WG2, 2019)

During tunnel segments lifecycle, they undergo multiple operations, from manufacturing to installation with the TBM. These operations, post casting, demoulding, handling, overturning, storage, can result in structural defects due to overloading. Damages include cracks and fissures, which can arise from various stages: through-going cracks caused by inserts, cracks from incorrect demoulding, handling, overturning, or improper storage. Segments that have cracks or are not repaired are usually not allowed to be used in TBM. During this phase, cracks usually occur due to stress upon demoulding, handling, overturning, and storage. Some defects come from inserts, causing cracks between the erector gripper pockets and grout holes and grouped by their width: less than 0.2 mm, between 0.2 mm and 0.3 mm, and more than 0.3 mm.

During handling and installation of the ring, segments are placed together to form rings using an erector in which they experience various loads, such as those from the segment crane, gasket compression, and collisions. Due to the complexity of handling and installation, stress-induced cracks and fissures are the most common damages in this phase. The same specifications for cracks apply as in the previous stages. Cracks can result from improper handling or installation, and they are classified based on their width: less than 0.2 mm, between 0.2 mm and 0.3 mm, and more than 0.3 mm.

Figure 26 Segment cracks during erection (left) and ring erection (right) (SIG WG2, 2019)

A critical factor contributing to structural damage is the effect of jack thrust during construction due to excessive or uneven jack thrust. The huge load of concentrated stresses by thrust cylinders during TBM process backed with poor design in the segment can lead to splitting transversal cracks perpendicular to the thrust force (Figure 27). These cracks are smaller than 0.2 mm and are found around the area where the surface meets the concrete cover and make the waterproofing ineffective if damage is severed.

Figure 27 Splitting transversal cracks (SIG WG2, 2019)

It could lead also to longitudinal cracks along the tunnel as well as spalling cracks affecting the entire segment length and hindering leaks (Figure 28).

Figure 28 Longitudinal cracks along the tunnel and spalling cracks (SIG WG2, 2019)

Another serious effect is chipping of sides and corners, where rebars could be visible and when visible, corrosion is easy to occur disturbing.

Figure 29 chippings in the corners (SIG WG2, 2019)

During the thrust phase, segments can get damaged because of uneven force from the TBM to keep the machine aligned, with the lower ones carrying more load due to the TBM's weight. Often, the rams push on the segments with eccentricity, which adds extra stress causing spalling and cracking concrete cover and damage from ring grove displacement (Figure 30)

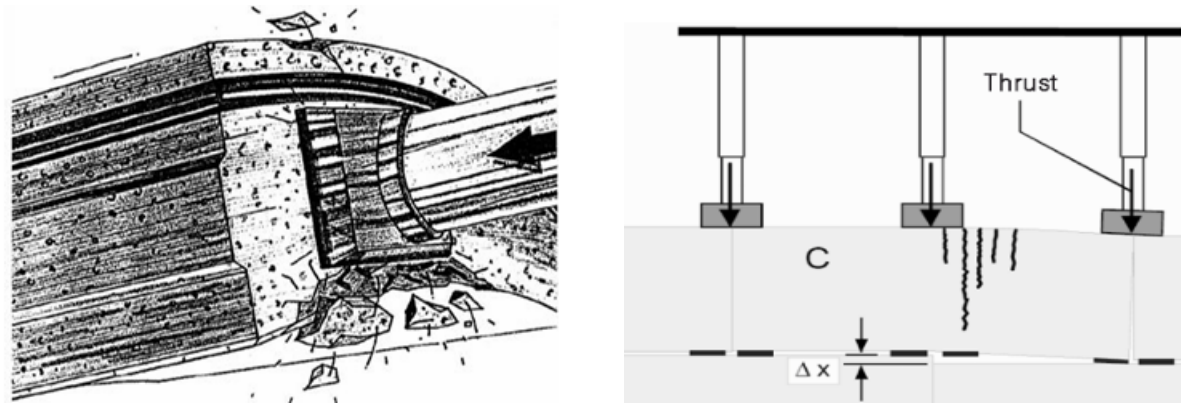

(a) (b)

Figure 30 a) Spalling and cracking concrete cover, b) Damage from displacement in the ring grove (SIG WG2, 2019)

The grouting and service phases can present specific defects. During these stages, various types of damage can occur, including the loss of connector and bolt performance, leading to misalignment, rotation, and sliding of segments. If fire resistance is inadequate, spalling may cause small concrete pieces to break off, weakening the structure. Cracks in segments can lead to leaks, compromising waterproofing and requiring repairs. Additional damage includes chipping of sides and corners and cracks forming in dry or wet conditions, sometimes leading to structural issues. These damages often result from connector and bolt failures, insufficient fire resistance, or concrete cracking.

Damage caused by oil or fire includes the deterioration or loss of the gasket's hydraulic sealing capacity due to contact with hydrocarbons present in the subsoil or exposure to flames, smoke, and high temperatures generated by fires inside the tunnel. If the presence of hydrocarbons in the subsoil is not properly assessed during design or construction, the gasket may suffer significant damage.

Concrete spalling may occur also, if the concrete lacks sufficient fire resistance. During the early stages of a fire, surface spalling can develop, where small pieces of concrete (up to 20 mm) are

gradually detached from the surface. This type of degradation is relatively slow and typically involves the dehydration of the cement matrix, followed by a loss of bond between the aggregate and matrix.

As the fire progresses and the concrete becomes increasingly compromised, small pieces may break off from the edges and corners of the structure, especially where cracks have already formed or the concrete is weak.

The most critical and dangerous form is explosive spalling, which usually occurs within the first 20–30 minutes of a fire when internal concrete temperatures reach between 150°C and 250°C. In this case, large fragments of concrete can be violently expelled over several meters. As each layer of concrete is removed, progressive explosive spalling can occur deeper into the cross-section, ultimately threatening the structural characteristics of the tunnel lining.

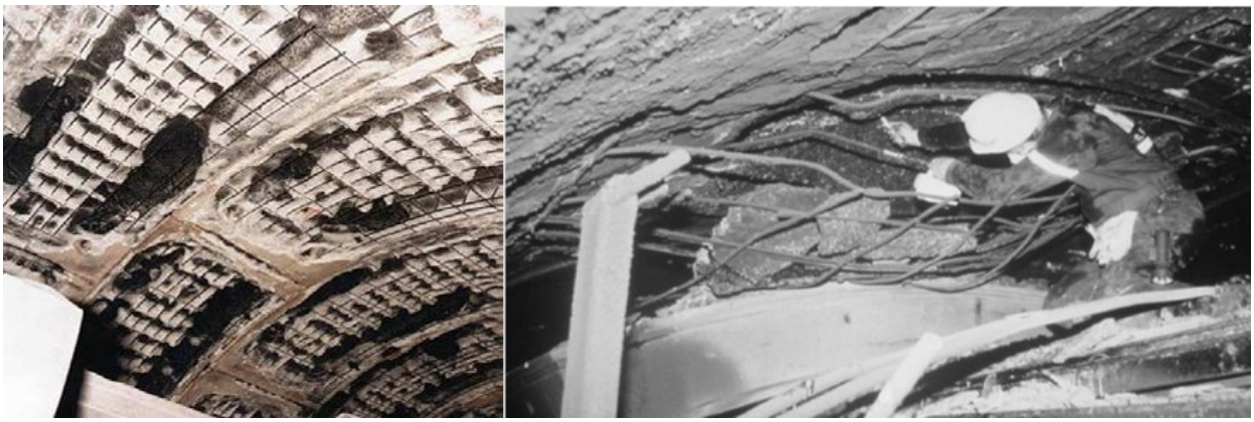

Figure 31 Fire damage in Channel tunnel (left) and in Cracks in the Store belt tunnel (right)l (SIG WG2, 2019)

Based on what is suggested by SIG W2 work, depending on the damage, some of the defects in the construction phase can be accepted and others lead to the discarding of the segment. As shown in Figure 31, damage to tunnel due to fire was heavily concentrated at the tunnel crown which will be deeply studied in this thesis in Chapter 4.

3.2 Italian Guidelines for Existing Tunnels Catalogue of Defects

The Italian guidelines provide a systematic approach to assessing defects in tunnel linings. Defects in tunnels are classified into structural defects, road surface defects, and non-structural elements and systems.

Additionally, defects are assessed by their extent (spatial distribution) and intensity (impact on structural elements), ensuring a consistent approach to monitoring and maintenance. During inspections, inspectors should focus on identifying defects rather than determining their causes, as assessments should be conducted later with specialists to avoid incorrect conclusions.

By defining defect levels, the guidelines help determine the necessary interventions, from regular maintenance to urgent structural repairs. High-severity defects (G=4) and medium-high severity defects (G=3) require immediate attention, especially when affecting critical structural elements. Meanwhile, medium-low (G=2) and low-severity defects (G=1) may only require monitoring and periodic maintenance. This structured assessment method allows engineers to prioritize actions effectively and manage tunnel defects efficiently.

During tunnel inspections, the tunnel manager assigns a gravity value (G) to each defect based on its extent (k_1) and intensity (k_2). Extent (k_1) represents the defect's spread, calculated as the ratio of its length or area to a reference section:

For linear defects, the parameter k_1 is defined as:

$$k_1 = \frac{\text{length of defect}}{\text{length of reference concrete}} \quad (3.1)$$

For surface defects, the parameter k_1 is defined as:

$$k_1 = \frac{\text{area of defect}}{\text{area of reference area}} \quad (3.2)$$

It is classified as low (0.2), medium (0.5), or high (1). Intensity (k_2) reflects defect severity, also ranging from low (0.2) to high (1), depending on characteristics like water inflows, cracks, or voids. Assigning k_1 and k_2 values ensures a structured assessment of tunnel conditions (Ministero delle Infrastrutture e della Mobilità Sostenibili, 2022).

Based on the Italian Guidelines for Existing Tunnels, several types of defects can be identified during visual inspections of tunnel linings. The following section describes some of the most common defects affecting segmental linings, together with their characteristics and possible causes.

Water infiltration (Stillicides) is a common defect in tunnel linings. It is the presence of stillicides (Figure 32), which result from the repeated passage of small amounts of water over the tunnel surface. This defect appears as discoloration in areas where water infiltrates through cracks, joints, or construction discontinuities. This phenomenon may be due to other defects that may be present, such as geological discontinuities, leaks in waterproofing systems, obstruction and/or deterioration of drainage discharges.

Figure 32 Stillicides (Ministero delle Infrastrutture e della Mobilità Sostenibili, 2022

Table 3 Classification of stillicides based on their extension and intensity in segmental lining tunnels.

Extent k1	0.2 (barely present)	0.5 (~50% surface)	1 (~entire surface)
Intensity k2	0.2 (low)	0.5 (medium)	1 (high)

Effects of frost (traces of salts) is another defect where frost appears at the surface of segments in ice sheets form or stalactites and is mainly due to freeze-thaw cycles (Figure 33). Freeze-thaw cycles over further period could lead to flaking and detachments of small portions of surface.

Figure 33 Frost (salt traces on surface) (Ministero delle Infrastrutture e della Mobilità Sostenibili, 2022)

Table 4 Classification of stillicides based on their extension and intensity in segmental lining tunnels

Extent k1	0.2 (barely present)	0.5 (~50% surface)	1 (~entire surface)
Intensity k2	0.2 (low)	0.5 (medium)	1 (high)

Efflorescence on concrete shows up on concrete as white, powdery spots or thin, fragile filaments caused by salt coming to the surface (Figure 34). It usually happens with older or sprayed concrete and mortar coatings. In which, it can point to deeper problems like coating damage, cracks, or material peeling off.

Figure 34 White coatings on surface of concrete (MIMS, 2022)

Table 5 Classification of deterioration severity based on extension (k1) and intensity (k2)

Extent k1	0.2 (barely present)	0.5 (~50% surface)	1 (~entire surface)
Intensity k2	0.2 (low)	0.5 (medium)	1 (high)

Deterioration of the tunnel entrance portals show signs of deterioration such as cracking, surface degradation, waterproofing issues, or movement of cladding panels, all caused by pressure from surrounding soil or shifting ground (Figure 35). These problems can be linked to the rotation of the arch's tympanum or instability in the terrain above. These issues may also indicate larger underlying problems like slope instability or water infiltration.

Figure 35 Deterioration of the entrance portals (MIMS, 2022)

Table 6 Classification of deterioration severity for entrance portals based on extension (k1) and intensity (k2)

Extent k1	0.2 (barely present)	0.5 (~50% surface)	1 (~entire surface)
Intensity k2	0.2 (low)	0.5 (medium)	1 (high)

Instability of Slopes happens when soil or rocks from natural slopes shift or collapse, often pushing debris toward or near tunnel entrances (Figure 36). This can be caused by things like fractures in the ground, water runoff, or even vegetation being disturbed.

.

Figure 36 slope instability causing debris flow & structural damage on tunnel entrance (MIMS, 2022)

Table 7 Classification of slope instability severity based on extension (k1) and intensity (k2)

Extent k1	0.2 (barely present)	0.5 (~50% surface)	1 (~entire surface)
Intensity k2	0.2 (low)	0.5 (medium)	1 (high)

Lesions and Detachments due to Compressive Load is a type of defects that can be seen as cracks along the tunnel lining, with pieces of concrete detaching especially in cast-in-place concrete happening in different sections of the tunnel (Figure 37). During inspection, you can use lighting and sound tapping to locate and evaluate the damage, checking how widespread it is and whether the cracks are recent or have signs of aging.

Figure 37 Visible cracking and material detachment on a tunnel ceiling caused by compressive stress (MIMS, 2022)

Table 8 Severity classification of detachment defects due to compressive loads based on extent (k1) & intensity (k2)

Extent k1	0.2 (barely present)	0.5 (~50% surface)	1 (~entire surface)
Intensity k2	0.2 (low)	0.5 (medium)	1 (high)

Damage and detachment due to corrosion of the reinforcements happens when the concrete cover layer breaks off, exposing the steel reinforcements inside to air and moisture, which causes corrosion (Figure 38). It usually affects the reinforced areas, especially near tunnel entrances. During inspections, lights and tapping can help identify how much concrete is missing and how badly the steel is rusted.

Figure 38 Concrete damage and steel exposure caused by corrosion of reinforcements. (MIMS, 2022)

Table 9 Classification of the extent and intensity of damage due to reinforcement corrosion.

Extent k1	0.2 (barely present)	0.5 (~50% surface)	1 (~entire surface)
Intensity k2	0.2 (low)	0.5 (medium)	1 (high)

Insufficiency of the drainage system for wastewater is due to an insufficient drainage system that can't properly handle surface or infiltrated water, including leaks or external sources like firefighting water (Figure 39). It shows up as puddles or damp areas on the road. During inspections, it's important to check for visible infiltration points, damaged drains, or missing waterproofing. Over time, this can lead to road damage like cracks, bulges, or surface deformations.

Figure 39 Poor drainage causing water accumulation (MIMS, 2022)

Table 10 Classification of drainage system defects severity based on extent (k1)&intensity (k2)

Extent K1	-	-	1(~entire surface)
Intensity K2	-	-	1(high)

Insufficiency of the drainage system for wastewater is due to an insufficient drainage system that can't properly handle surface or infiltrated water, including leaks or external sources like firefighting water (Figure 40). It shows up as puddles or damp areas on the road. During inspections, it's important to check for visible infiltration points, damaged drains, or missing waterproofing. Over time, this can lead to road damage like cracks, bulges, or surface deformations.

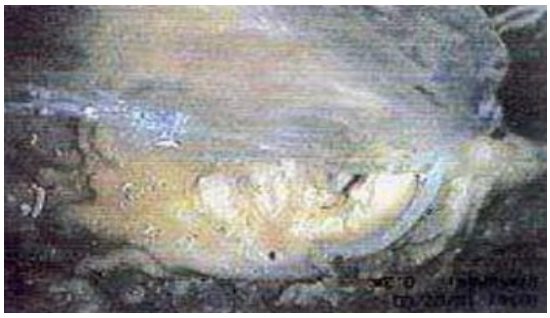

Figure 40 water collection system deterioration (MIMS, 2022)

Table 11 Classification of the deterioration levels of the water collection system based on extension defect k1 and intensity k2

Extent k1	0.2 (barely present)	0.5 (~50% surface)	1 (entire surface)
Intensity k2	0.2 (low)	0.5 (medium)	1 (high)

Insufficiency of the drainage system for wastewater is due to an insufficient drainage system that can't properly handle surface or infiltrated water, including leaks or external sources like firefighting water (Figure 41). It shows up as puddles or damp areas on the road. During inspections, it's important to check for visible infiltration points, damaged drains, or missing waterproofing. Over time, this can lead to road damage like cracks, or surface deformations.

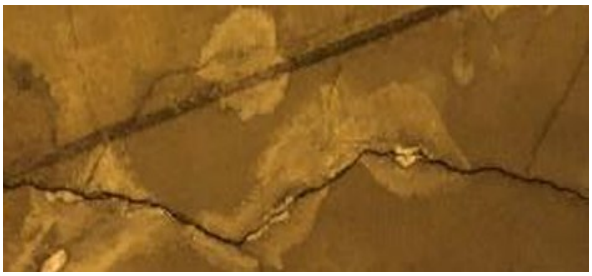

Figure 41 longitudinal cracks along the tunnel coating, aligned with the tunnel axis (MIMS, 2022)

Table 12 Classification of longitudinal crack defects based on extension (k1) and intensity (k2) of the affected tunnel lining surface.

Extent k1	0.2 (barely present)	0.5 (~50% surface)	1 (entire surface)
Intensity k2	0.2 (low)	0.5 (medium)	1 (high)

Diagonal cracks, also called oblique cracks, form at an angle to the tunnel axis and usually appear in sequences (Figure 42).They're common in cast concrete where they tend to be wider than typical shrinkage cracks.

Figure 42 Diagonal Cracking (MIMS, 2022)

Table 13 Classification of diagonal crack defects based on extension (k1) and intensity (k2) of the tunnel lining.

Extent k1	0.2 (barely present)	0.5 (~50% surface)	1 (entire surface)
Intensity k2	0.2 (low)	0.5 (medium)	1 (high)

Vertical Cracks run perpendicular to the tunnel's axis and can appear in any section (. In cast concrete they're often wider than shrinkage cracks. Inspections focus on the number, width, and depth of these cracks to evaluate potential damage. These cracks may lead to cladding deformation, resonant empty areas, block damage, or surface cracks on the roadway.

Table 14 Classification of vertical cracks by extension (k1) and intensity (k2) in tunnel linings.

Extent k1	0.2 (barely present)	0.5 (~50% surface)	1 (entire surface)
Intensity k2	0.2 (low)	0.5 (medium)	1 (high)

Curvilinear cracks are characterized by their uniformly curved, crescent-like shape, appearing between construction joints (Figure 43). These cracks can indicate localized stress concentrations or detachment of thin lining panels, particularly in tunnel claddings. During inspections, they are assessed by their surface extent and intensity using a standard rating table. Their detection may

also involve tapping methods to locate voids, suggesting hollow-sounding areas due to detachment. Associated degradation phenomena include separation of thin panels from the tunnel lining.

Figure 43 Curvilinear cracks observed in the tunnel lining (MIMS, 2022)

Table 15 Classification criteria for curvilinear cracks based on surface extension (k1) and intensity (k2).

Extent k1	0.2 (barely present)	0.5 (~50% surface)	1 (~entire surface)
Intensity k2	0.2 (low)	0.5 (medium)	1 (high)

Reduction in symmetric deformation - asymmetric deformation (Figure 44) is a defect that can be either symmetrical or asymmetrical between segments at the top arch and can be seen as deformation in the tunnel lining section framework, with a curvature radius increase in the arch upper part of the tunnel, a side walls separation and a lowering of the vault at the key. Displacement of the segments could be due to unforeseen thrusts of the mass or landslides.

If it is symmetrical deformation, this deformation affects only one side of the arch between base and side wall and can be clearly visualized in tunnels with slender profiles. This defect can be allocated through visual inspection and classified according to extent of surface and degree of deformation. Effects of this phenomenon could be possible cracks at the key vault of the tunnel. In the case of asymmetric deformation, possible wide horizontal cracks on the thrust side, shear cracks, chipping at key vaults, hollow sound areas and water seepage

Figure 44 asymmetric deformation (MIMS,2022)

Table 16 Classification criteria for reduction deformation based on surface extent (k1) and intensity (k2).

Extent k1	0.2(Barely present)	0.5(~50% surface)	1(Entire surface)
Intensity K2	0.2(low)	0.5(medium)	1(high)

Deterioration of the reverse arch shows up through small movements as shown in Figure 45 either the arch pushing upward or settling. This leads to cracking, visible gaps, or uneven surfaces that can impact structural stability. Close inspection of these deformities and an assessment of the degree of cracking help in determining how severe the damage is and what repair steps might be needed. Deterioration of the reverse arch Related degradations could be water infiltrations, abnormal deterioration of the vault (detachments at the key to the arch, various extents and shapes of cracks) and in the lateral walls.

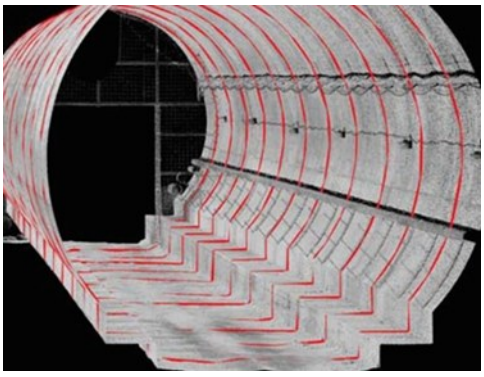

Figure 45 Illustration demonstrating the typical deterioration pattern of the reverse arch (MIMS,2022)

Table 17 Classification criteria for reverse arch deterioration based on surface extent (k1) and intensity (k2).

Extent k1	0.2(barely present)	0.5(~50% surface)	1(~entire surface)
Intensity k2	0.2 (low)	0.5(medium)	1(high)

Breakage of the arch (referred to as the "kidneys" or "dome" of the vault) involves deformative shifts in the tunnel lining, where successive layers or blocks no longer align with the original shape (Figure 46)Sometimes this manifests as protrusions, collapses, or cracking that may begin subtly but can lead to more serious failures. While sudden collapse is possible, various warning signs (e.g., wide cracks, flaking surfaces, tilted sections) usually become evident beforehand.

Figure 46 Huge signs of arch breakage in the tunnel lining. (MIMS,2022)

Table 18 classification based on extent and intensity

Extent k1	0.2 (barely present)	0.5 (~50% surface)	1 (~entire surface)
Intensity k2	0.2 (low)	0.5(medium)	1(high)

Presence of voids near the intrados of the lining refer to gaps or empty spaces that form behind the interior surface of the tunnel structure (Figure 47). These gaps can develop due to factors like poor construction practices, material shrinkage, or ongoing deterioration. If left unaddressed, they may compromise structural integrity by reducing the effective thickness of the lining and allowing water or other corrosive agents to penetrate.

Figure 47 void formation behind the intrados of the tunnel lining. (MIMS,2022)

Table 19 Classification based on extent and intensity

Extent k1	0.2 (barely present)	0.5 (~50% surface)	1 (~entire surface)
Intensity k2	0.2 (low)	0.5(medium)	1(high)

Deterioration of concrete joints is a defect commonly observed at the interface between adjacent segment rings, often manifesting as cracks, surface flaking, or loss of joint filling (Figure 48). These forms of degradation affect continuity and integrity of the concrete ring and are usually accompanied by detached aggregates or filler separation. In precast segmental linings, such issues are typically due to poor joint filling or improper assembly. Degradation is often associated with the presence of moisture, which boosts the deterioration process through microcracking and surface disintegration. Inspection should verify whether the joint is adequately filled and if disintegration is isolated or widespread.

Figure 48 Deterioration of concrete joints. (MIMS,2022)

Table 20 classification based on extent and intensity

Extent k1	0.2 (barely present)	0.5 (~50% surface)	1 (~entire surface)
Intensity k2	0.2 (low)	0.5(medium)	1(high)

Surface defects in concrete are characterized by irregularities in color, texture, or pattern, primarily affecting the underside of the tunnel lining (Figure 49). Common signs include water surfacing, localized rust stains, traces of reinforcement outlines, and formwork deformations. These defects may indicate underlying issues such as poor material compaction, segregation, or exposure to moisture. They are commonly assessed visually and confirmed through tactile inspection and surface hardness measurements (e.g., sclerometer tests). When accompanied by dull acoustic responses or cracking, these defects may signal more serious degradation like voids or localized delamination.

Figure 49 Surface Defects (MIMS,2022)

Table 21 classification of surface defect based on Extent and Intensity

Extent k1	0.2 (barely present)	0.5 (~50% surface)	1 (~entire surface)
Intensity k2	0.2 (low)	0.5(medium)	1(high)

Exposure to fire (Figure 50) specifically heat and smoke leads to degradation which primarily affect the crown (upper surface) of the tunnel lining. The effects of fire on tunnel linings can vary widely depending on the type of lining, as well as the intensity and duration of exposure. Typical signs of fire-related deterioration include colour changes in the concrete, deep detachments such

as craters, superficial detachment, surface melting, and the development of deep cracks. These forms of damage are usually most pronounced in the vault, where the highest temperatures during a fire are reached.

Several elements can be observed during inspections to help identify and classify fire-induced defects. Inspectors can note the location and extent of the affected tunnel section, including the beginning and end of the damaged area and any visible changes in colour. The consistency and condition of the material can be evaluated using auditory inspection techniques, such as tapping with a hammer. In addition, local measurements can be taken to determine the dimensions and depth of detachment areas or spalling and to identify any cracking. The surface hardness of the concrete may also be measured using a sclerometer.

Fire exposure can also lead to broader degradation related phenomena. These include the reduction of mechanical properties in the surrounding concrete even in areas that appear visually intact the loss of the lining's waterproofing capacity, and potential damage to the tunnel's drainage system.

Figure 50 damage due to fire (MIMS,2022)

Table 22 classification of fire defect based on extent and intensity

Extent k1	0.2 (barely present)	0.5 (~50% surface)	1 (~entire surface)
Intensity k2	0.2 (low)	0.5(medium)	1(high)

3.3 Other types of defects

This section presents a systematic classification of tunnel defects taken from the defects catalogue of a specific concessionaire with attention to their causes, main characteristics, and inspection criteria.

The primary defects observed in segmental lining tunnels include cracking, water infiltration, misalignment of segments, joint failures, and surface deterioration. These issues can result from material aging, poor construction practices, environmental exposure, or mechanical stresses. Water-related defects, such as active moisture stains and runoff traces, are particularly critical, as they can lead to reinforcement corrosion and loss of concrete integrity.

Segmental misalignment or improper joint sealing can create structural discontinuities that affect the tunnel's load distribution. By categorizing these defects and their severity, the catalogue serves as a valuable reference for inspection and maintenance strategies. Understanding these common deterioration patterns allows for early intervention, reducing the risk of extensive structural damage and ensuring the long-term safety of tunnel infrastructure.

The following is a comprehensive overview of the most common defects affecting new segmental lining tunnels, as outlined in the “Catalogo Difetti”. Each defect is described based on its characteristics, possible causes, and classification criteria:

Concretions – Deposits – Encrustations: Mineral encrustations and deposits commonly form on concrete structures due to prolonged exposure to water infiltration. These deposits, known as concretions, result from the crystallization of minerals carried by water, which accumulates on surfaces over time. They are categorized into limestone concretions, which appear as yellowish stains caused by calcite crystallization in cracks and porous areas, and sulphate concretions, which are whitish deposits of gypsum typically found in surface joints. The presence of these encrustations not only affects the aesthetic appearance of structures but may also indicate underlying moisture issues that could compromise durability.

Table 23 Classification of Concretions Based on Extent and Thickness for Defect Assessment

Extent (k1)	0.2 (barely present)	0.5 (~50% surface)	1 (entire surface)
Intensity (k2)	0.2 (thickness < 1 cm)	0.5 (1 cm < thickness < 3 cm)	1 (thickness > 3 cm)

This table categorizes defects based on their extent and intensity, specifically assessing the position, spread, and thickness of concretions.

Crumbling and voids in concrete structures, known as "Sgretolamenti – Vespai", is a common defect in aging concrete structures, where certain areas lose fine aggregate particles, either visibly exposed on surface or hidden beneath a thin surface layer. The loss of fine materials compromises the concrete's structural integrity, leading to increased porosity and potential water infiltration, which affects the volume of the material which, making it a significant concern for long-term durability.

The following table below classifies defects in concrete structures based on their extent (k1) and intensity (k2), considering both surface coverage and material deterioration. Higher values indicate more severe and widespread defects, with the most critical cases involving open joints and material detachment, which may compromise structural integrity.

Table 24 classification of Defects Based on Extension and Intensity

Extent k1	0.2(barely present)	0.5(~50% of the surface)	1(~entire surface)
Intensity k2	0.2(closed joint but with deterioration/superficial defects)	0.5(open joint with surface defects but no detachments (resistant to hammering)	open joint with surface defects with detachment of material, including non-structural

Dripping Water Stains (Stillicidi) appears as areas of discoloration different from the intact material, caused by the repeated passage of small amounts of water over the surface of structural

elements. In segmental lining tunnels, these stains typically occur where there is an anomaly in the coating, such as cracks, holes, or discontinuities between different construction elements.

This table categorizes defects based on their extent and intensity highlighting different severity levels, from minor surface films to significant water infiltration under pressure.

Table 25 Classification of Defects Based on Extension and Intensity

Extension k1	0.2 (barely present)	0.5 (≈50% of the surface)	1 (≈entire surface)
Intensity k2	0.2 (film on surface < 1mm)	0.5 (film on surface > 1mm)	1 (pressurized water)

Water Flows is represented as areas of a different color than the concrete one and mainly caused by water repeated passage on the surface. Moreover, in the case of segmental lining tunnels, water infiltration is due to abnormalities, which could be caused by either coating, cracks, holes or discontinuities between segments.

The table below outlines the key elements detectable during an inspection to assess this defect, focusing on infiltration location, drainage deterioration, and jet recovery. It categorizes defect extent (k1) and intensity (k2), indicating progression from minimal presence to severe issues like pressurized water infiltration.

Table 26 Classification of water infiltration defect

Extent k1	0.2 (barely present)	0.5 (≈50% of the surface)	1 (≈entire surface)
Intensity k2	0.2 (film on surface < 1mm)	0.5 (film on surface > 1mm)	1 (pressurized water)

Efflorescence on concrete consists of salt crystallizations that form on the external surface or near the surface of the lining and appear as a white powdery coating. This deterioration is mainly caused by sulphates that could over time lead to surface scaling, disintegration, exfoliation, swelling and flaking, compromising durability. (Neville, 2011Efflorescence in concrete is evaluated based on its location, surface coverage, and intensity, which can range from minor deposits to significant swelling that may indicate deeper material deterioration.

Table 27 Classification of efflorescence in concrete based on its extent and intensity

Extent k1	0.2 (barely present)	0.5 (≈50% of the surface)	1 (≈entire surface)
Intensity k2	0.2 (thickness < 5 mm)	0.5 (thickness > 5 mm)	1 (Efflorescence with swelling)

Shrinkage cracks are thin cracks (visible from 0.1 mm) that occur in unreinforced concrete castings, with widths typically not exceeding 1-2 mm (Figure 51). These cracks are caused by the loss of moisture during the curing process, leading to volume reduction and cracking. Shrinkage cracks develop in prefabricated or cast-in-place elements. However, if the tunnel profile deforms, some cracks may form due to structural reasons rather than shrinkage. In such cases, these cracks should be classified as horizontal, diagonal, or vertical structural cracks rather than shrinkage cracks.

Figure 51 shrinkage cracks on a segment surface

The table below presents inspection criteria for cracks, including their position, quantity, width, and potential abnormal widening over time, along with classifying cracks by extension and intensity.

Table 28 Classification criteria based on extension and intensity

Extension k1	0.2 (barely present)	0.5 (≈50% of the surface)	1 (≈whole surface)
Intensity k2	0.2 (opening < 0.5 mm)	0.5 (0.5 mm < opening < 1 mm)	1 (opening > 1 mm but < 2 mm)

Vertical Cracks in Tunnel Linings form perpendicular to the tunnel's length and can appear anywhere in the structure. In prefabricated sidewalls, they usually develop at segment joints, while

in cast-in-place concrete, they are more irregular and wider due to material shrinkage and construction conditions. Monitoring these cracks helps assess structural stability.

Figure 52 vertical cracks

Crack inspections assess position, width, edge deterioration, and propagation through materials, to determine structural impact and potential repairs. Classifications are shown in the following table.

Table 29 Classification criteria

Extension k1	0.2 (barely present)	0.5 (≈50% of the surface)	1 (entire surface)
Intensity k2	0.2 (opening < 3 mm)	0.5 (3 mm < opening < 5 mm)	1 (opening > 5 mm)

Horizontal Cracks run parallel to the tunnel's longitudinal axis (Figure 53). Their characteristics vary depending on the type of lining. In cast-in-place concrete, they are usually wider than shrinkage cracks and usually caused by construction issues, temperature changes, or poor curing, which create stress along the tunnel wall.

Figure 53 Horizontal Crack

Crack inspections check the location, width, edge damage, and spread of cracks. Tools like crack gauges and sound tests help measure them.

Table 30 Classification criteria of horizontal cracking

Size k1	0.2 (barely visible)	0.5 (about 50% of the surface)	1 (covers almost the whole surface)
Width k2	0.2 (opening < 3 mm)	0.5 (opening between 3 mm and 5 mm)	1 (opening > 5 mm)

Diagonal Cracks, also called oblique cracks, form at an angle to the tunnel's axis (Figure 54). They often appear in a series rather than as single cracks. Their characteristics depend on the type of lining. In cast-in-place concrete, these cracks are usually wider than shrinkage cracks.

Figure 54 Diagonal crack

Criteria for inspecting and qualifying cracks in a structure, including their position, width, edge deterioration, and whether they follow construction joints or affect multiple segments.

Table 31 Classification criteria of diagonal cracks

Extent k1	0.2 (barely present)	0.5 (≈50% of the surface)	1 (entire surface)
Intensity k2	0.2 (opening < 3 mm)	0.5 (3 mm < opening < 5 mm)	1 (opening > 5 mm)

Curvilinear cracks have a smooth, crescent-shaped path and usually start and end at a construction joint (Figure 55). They are often found in segmental lining tunnels and can indicate structural movement or weaknesses in the material.

Figure 55 curvilinear cracks

Table 32 Curvilinear cracks classification criteria

Extent k1	0.2 (barely present)	0.5 (≈50% of the surface)	1 (entire surface)
Intensity k2	0.2 (opening < 3 mm)	0.5 (3 mm < opening < 5 mm)	1 (opening > 5 mm)

Deterioration of the highway drainage system leads to water accumulation on the road, indicating defects in the underlying drainage structures (Figure 56). It usually results from partial or complete blockages due to lack of cleaning or deposits, crushing deformations, or structural breakages.

Figure 56 deposits along the roadside could lead later to water accumulation

Table below shows the inspection criteria for identifying defects in drainage systems, focusing on blockage causes, narrowing of the drain, and affected pavement areas.

Table 33 Classification of drainage system defects

Extent k1	0.2 (barely present)	0.5 (≈50% of the surface)	1 (entire surface)
Intensity k2	0.2 (low)	0.5 (medium)	1 (high)

Visible Reinforcement due to insufficient concrete cover in tunnels constructed with prefabricated segments, an inadequate concrete cover over the reinforcement can lead to visible rebar on the surface, exposing the reinforcement to potential corrosion and reducing the overall lifespan of the tunnel (Figure 57).

Figure 57 Exposed Reinforcement

Inspections assess the location, size, connection to reinforcement, and shrinkage cracks presence .

Table 34 Classification of exposed reinforcement defect

Size k1	0.2 (barely visible)	0.5 (about 50% of the surface)	1 (whole surface coverage)
Intensity k2	0.2 (barely visible defect with no shrinkage cracks)	0.5 (visible defect with some shrinkage cracks)	1 (clearly visible defect with widespread shrinkage cracks)

Chipping and Detachments can be visualized as fragments being detached from the edges of the segment, causing discontinuities of the material composing it (Figure 58). Detachments and chipping are mainly caused by impact damage, incorrect formwork removal, or incorrect positioning of prefabricated segments.

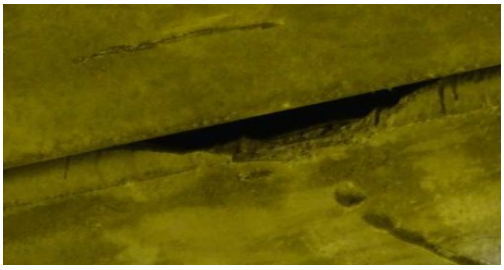

Figure 58 Detachment of concrete segment side

Table 35 Detachment and chipping defect criteria of classification

Extent k1	0.2 (barely present)	0.5 (≈50% of the surface)	1 (entire surface)
Intensity k2	0.2 (depth loss < 5 cm)	0.5 (5 cm < depth loss < 20 cm)	1 (depth loss > 20 cm)

Concrete surface defects include all defects that affect the appearance, color, or uniformity of the tunnel's intrados surface (Figure 59). Common issues include bubbles, water seepage, color variations, visible reinforcement outlines, rust stains, and localized formwork deformations. These defects may not always impact structural integrity but can indicate deeper problems or poor construction quality.

Figure 59 surface defects

The defect's location and size, the detection of hollow sounds through surface hammering, the concrete surface hardness measured with a sclerometer, and the deterioration extent quantified through measurements help assess the material's quality.

Table 36 Surface defects classification criteria

Extent k1	0.2 (barely present)	0.5 (≈50% of the surface)	1 (entire surface)
Intensity k2	0.2 (presence of spots and color changes)	0.5 (cracking of the intrados)	1 (superficial detachments < 1 cm)

Deterioration of Protective Screens such as corrugated panels of galvanized metal, fiber cement, or plastic, occurs through deformations, impact damage, oxidation perforations, and corrosion of

anchors (Figure 60). These issues weaken their structural integrity and protective function, highlighting the need for regular inspection and maintenance.

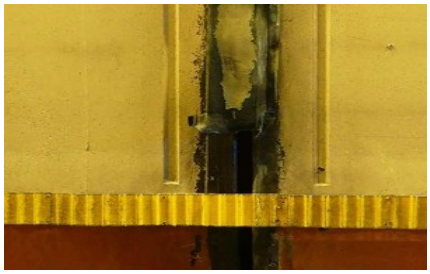

Figure 60 Deterioration of Protective Screens

The assessment of protective screen deterioration considers defect position, oxidation level of anchors and panels, and misalignment or overlapping of corrugated sheets, as summarized in the table below.

Table 37 Classification of Defect Extent and Intensity in Protective Screens

Extent k1	0.2 (barely present)	0.5 (≈50% of the surface)	1 (entire surface affected)
Intensity k2	0.2 (moisture on the outer surface of the panel)	0.5 (damaged/deformed panel with dripping water)	1 (damaged/deformed panel with water streaks)

Deterioration of tunnel entrance portals is often characterized by crack patterns and typical surface degradation phenomena affecting concrete (Figure 61).

.

Figure 61 Tunnel Entrance Defect

Table 38 Classification Criteria of Entrance Defects

Extent k1	0.2 (barely present)	0.5 (≈50% of the surface)	1 (entire surface affected)
Intensity k2	0.2 (narrow cracks, opening < 1 mm)	0.5 (open cracks up to 5 mm)	1 (open cracks > 5 mm with visible structural deformation)

Active Moisture refers to lack of concrete covering layers of longitudinal and transverse reinforcements which will lead to consequent exposure to moisture and CO2 contributing to oxidizing rebars and making them prone to corrosion (Figure 62). Moreover, the most exposed elements, such as the edges of structural elements, which have a high surface-to-volume ratio., are particularly prone to cover concrete detachment due to exposure to external agents.

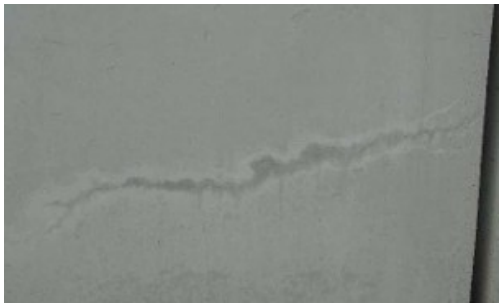

Figure 62 Active Moisture on walls

Table 39 Active moisture defect classification criteria

Extent k1	0.2 (barely present)	0.5 (≈50% of the surface)	1 (entire surface)
Intensity k2	Always = 1		

Spiderweb Cracks refers to small, irregular cracks spread across the surface of elements, especially in areas highly affected by moisture (Figure 63).

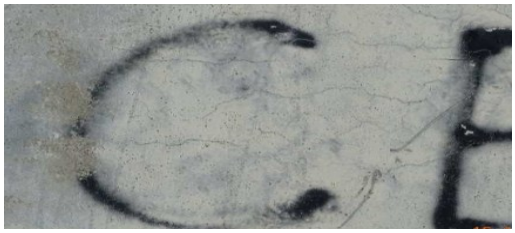

Figure 63 Spiderweb Cracks

Table 40 Spiderweb cracks defect classification criteria

Extension k_1	0.2 (barely present)	0.5 (≈50% of the surface)	1 (entire surface)
Intensity k_2	Always = 1		

3.4 Defect comparison

The three sources analyzed, specifically SIG Working Group Research, the Italian Guidelines for Existing Tunnels and the other defects listed in the defects catalogue of a motorway concessionaire, show both similarities and differences in how they approach segmental lining defects. All three mention the most common and widely known defects, such as cracks, water infiltration, and surface deterioration, which are the main defects considered to be structural and visually easy to detect. However, some defects are only included in specific documents. For example, SIG document has a more detailed and technical study approach, conceptualizing defects in all construction phases of the segmental lining tunnel specifically. On the other hand, the Italian Guidelines for existing tunnels address defects in all tunnel types, including segmental lining tunnels, within the broader category of "existing tunnels." They also include general categories such as geometric irregularities and joint misalignments, which are not developed in depth in the other two sources.

Unlike the SIG document and other types of defects, the Italian Guidelines do not mention the possible causes of the defects but rather focus on their severity based on two main parameters: intensity and extent. The SIG document, instead, tends to group defects by structural and technological relevance. The following tables provide a comparative analysis of defects identified in tunnel segmental linings as documented in three different sources. The aim is to identify

commonalities and discrepancies in defect classifications and presence across these guidelines, with each defect categorized based on its relevance to the source.

The tables use P for "Present" and N for "Not Present" to indicate whether a specific defect is mentioned in each guideline.

Table 41 Surface defects

Defect Type	SIG Research	Other Catalogue	Italian Guidelines
Hollows	P	N	N
Exposed aggregates	P	N	N
Exposed reinforcement	P	P	P
Surface deterioration	P	P	P
Concrete surface defects (general)	P	P	P
Chipping / detachment	P	P	P
Crumbling / voids	N	P	P (near intrados)
Dripping water stains	N	P	N
Deterioration of protective screens	N	P	N
Wall defects	N	P	N

Table 42 Cracks and Fissures

Defect Type	SIG Research	Other Catalogue	Italian Guidelines
Shrinkage cracks	N	P	N
Vertical cracks	P	P	P
Horizontal cracks	P	P	P
Diagonal cracks	P	P	P

Defect Type	SIG Research	Other Catalogue	Italian Guidelines
Curvilinear cracks	N	P	P
Longitudinal cracks	P	P	P
Insert cracks	P	N	N
Spalling cracks	P	N	N
Non-visible cracks	P	N	N
Cracking (generic)	P	P	P (“lesions”)

Table 43 Water and Moisture Related Defects

Defect Type	SIG Research	Other Catalogue	Italian Guidelines
Water infiltration	P	P	P
Efflorescence on concrete	N	P	P
Moisture activity / active moisture	N	P	N
Dripping water stains	N	P	N
Water leaks from joints	P	N	P
Water flows	N	P	N
Concretions / deposits	N	P	N
Frost, traces of salts	N	N	P
Insufficiency of drainage system	N	P	P
Deterioration of water collection system	N	P	P

Table 44 Joints, Gaskets, and Connection Defects

Defect Type	SIG Research	Other Catalogue	Italian Guidelines
Gasket defects (anchored, glued, etc.)	P	N	N
Segment misalignment	P	P	P
Joint failures / deterioration	P	P	P
Intrados voids near joints	N	N	P
Gap and offset in joints	P	N	P
defects of joint bolts	P	N	N
Deterioration around gasket	P	N	N

Table 45 Structural, Installation, and Other Defects

Defect Type	SIG Research	Other Catalogue	Italian Guidelines
Installation defects	P	N	N
Thrust phase defects	P	N	N
Loss of connector/bolt	P	N	N
Misalignment, rotation,	P	P	P
Deterioration of protective	N	P	P
Reverse arch damage	N	N	P
Breaking of arch	N	N	P
Corrosion-related	P	P	P
Slope instability	N	N	P
Spider web cracks	N	P	N
Symmetric/asymmetric	N	N	P
Fire damage	P	N	P

The document of “Damages of Segmental Lining" proposed by Working Group 2 of the Italian Society of Tunnels (2018) addresses various types of damages, defects, and loss of functionality in tunnel segmental linings caused by mechanical actions during both installation and operational phases.

During installation and pushing, defects include damages from impacts during transport to the erector, stresses induced by the erector itself, gasket damage and loss of gasket effectiveness due to faulty ring assembly, segment defects and detachments caused by jack thrusts, damages occurring during back injection or secondary injections, and damages from contact between the ring and the shield tail, especially in curved sections.

During operation, the document highlights defects such as defects caused by thrusts from the surrounding rock mass and water that is usually linked to design flaws reciprocal segment displacements, damages from uneven thrusts due to poor back-injection leading to inadequate contact between the ring and the ground, damages caused by landslide induced movements primarily along sliding surfaces, and loss of waterproofing functionality due to insufficient clogging behind the lining.

The defects catalogue and the Italian Guidelines for Existing Tunnels explain how to identify the location of defects along the tunnel arch. This is especially important when universal segments are used, because these segments can be placed in different positions within the ring and therefore do not have a fixed location. Since these segments can be installed in any orientation, it is not possible to assign defects to a specific segment number. Instead, both sources adopt a geometrical reference system based on the arch's angular position.

As viewed from other catalogue, defects are located using a polar coordinate approach, where the crown is generally considered as reference (0° or 12 o’clock), and positions are defined clockwise or counterclockwise along the intrados of the lining. Similarly, the Italian Guidelines utilize a standard classification that divides the tunnel cross-section into sectors or angular intervals (e.g., 0°–30°, 30°–60°, etc.), allowing for consistent defect mapping regardless of segment orientation. This method ensures that the location of anomalies, cracks, and other damage can be systematically recorded, analyzed, and compared between inspections or across different tunnels.

Finally, as shown in the comparison tables 41 to 45, it would be useful to include the defects that are not covered by the Italian guidelines and are covered by other references and italian research.

Chapter 4

Numerical model of fire-induced damage

4.1 Introduction

Fire incidents in tunnels pose significant threats to the structure of segmental linings, which results in spalling, cracking, or detachment of lining components (Khoury, 2000). These effects are caused by steep thermal gradients that develop in concrete due to its low thermal conductivity during fire exposure (Mindeguia, 2009). The internal stress generated by these gradients, along with pore pressure buildup, leads to explosive spalling in high strength concrete (Kalifa et al., 2000). Due to these severe structural risks, the assessment of tunnel lining behaviour under fire conditions is required by the Italian Legislative Decree D.Lgs. 264/2006 and the Italian Guidelines for Existing Tunnels, which define catastrophic fire scenarios (Level 4) and require the evaluation of tunnel structural stability under extreme thermal loading.

Historical tunnel fires have highlighted the severity of thermal degradation. For example, the 1996 Channel Tunnel fire resulted in major spalling, reducing the thickness of the concrete lining from 450 mm to less than 50 mm in some sections (Carvel & Both, 2002). Similarly, the Mont Blanc Tunnel fire in 1999 exposed linings to temperatures above 1000°C, causing extensive structural damage and prolonged service disruptions (Beard & Carvel, 2005).

Numerical modeling is widely used to simulate the mechanical behavior of tunnel structures under fire induced conditions. This chapter presents a two dimensional finite element analysis using Rocscience RS2 software, which is well suited for analyzing stress redistribution, deformation,

and stability in geotechnical systems (Rocscience, 2024).This phenomenon alternatively caused thermal expansion and strength degradation for concrete (Fire Safety Journal, 2025)

The simulation focuses on the removal of the tunnel lining at the crown (between –45° and +45°), which replicates the loss of support typically seen under high temperature conditions (Zhou & Wu, 2023). The modelling approach adopted in this study represents a simplified method to simulate fire-induced damage by removing the tunnel crown, which reflects the loss of structural support that may occur under severe fire conditions. However, this approach does not explicitly simulate the thermo-mechanical behaviour of concrete, such as temperature distribution, thermal stresses, or the progressive degradation of material properties due to elevated temperatures. Instead, the analysis focuses on evaluating the structural response of the tunnel system to a localized loss of support. This simplification allows for the investigation of deformation patterns, plastic zone development, and failure mechanisms under different rock mass conditions.

In addition to internal deformation, crown degradation can lead to surface-level ground settlements, especially in shallow tunnels or weak rock masses (Liu et al., 2015). The lack of confinement allows stress migration toward the surface, resulting in measurable ground deformations or surface instability (Brady & Brown, 2006).

Simulation results are analyzed in terms of yielded elements, plastic zone development, and ground surface deformation. The findings aim to improve understanding of tunnel performance under fire damaged conditions and support the development of resilient design and risk mitigation strategies.

4.2 Modelling geometry and input parameters

In this study, finite element analysis was used to develop scenarios by removing the tunnel crown to represent the loss of structural support that can occur under severe fire conditions. For simplicity and to save computational time, the analyses are limited to a 2D model representation which is considered conservative as we are assuming that the whole tunnel crown length is going to be damaged by fire. The numerical models were developed to cover the complete evolution of the tunnel, starting from the initial geostatic condition and progressing through the excavation process, the installation of both the preliminary and final linings, and their subsequent degradation phases.

Three different types of rock masses were considered in the analysis to represent a wide range of geological conditions and to simulate how this type of damage develops under different ground and structural conditions.

The first corresponds to a poor-quality rock mass composed of flysch-type sediments, typical of formations found in Greece represented as scenario R1, typically characterized by low strength and significant anisotropy due to interbedded layers of sandstone and shale (Hoek & Brown, 1997; Marinos & Hoek, 2000).

The second represents an average-quality rock mass consisting of quartz–mica schist, with moderate stiffness and a foliated texture represented as scenario R2, characteristic of geological conditions in India.

The third type is a massive and strong rock mass composed of gneiss, characterized by high stiffness and low deformability (Palmström, 2001) similar to those encountered in Argentina as scenario R3, where rock bolts were applied to provide additional support following the general support concepts described by Barton et al. (1974) and Hoek et al. (2002). This resulted in nine main numerical models, with additional models used to investigate limit conditions.

To investigate the influence of tunnel depth on structural response, three tunnel configurations were considered at different overburden depths. These configurations represent shallow, intermediate, and deep tunnel conditions, allowing a comparison of their behaviour under the same modelling assumptions. The layout and relative positions of the tunnels within the rock mass domain are shown in Figure 64.

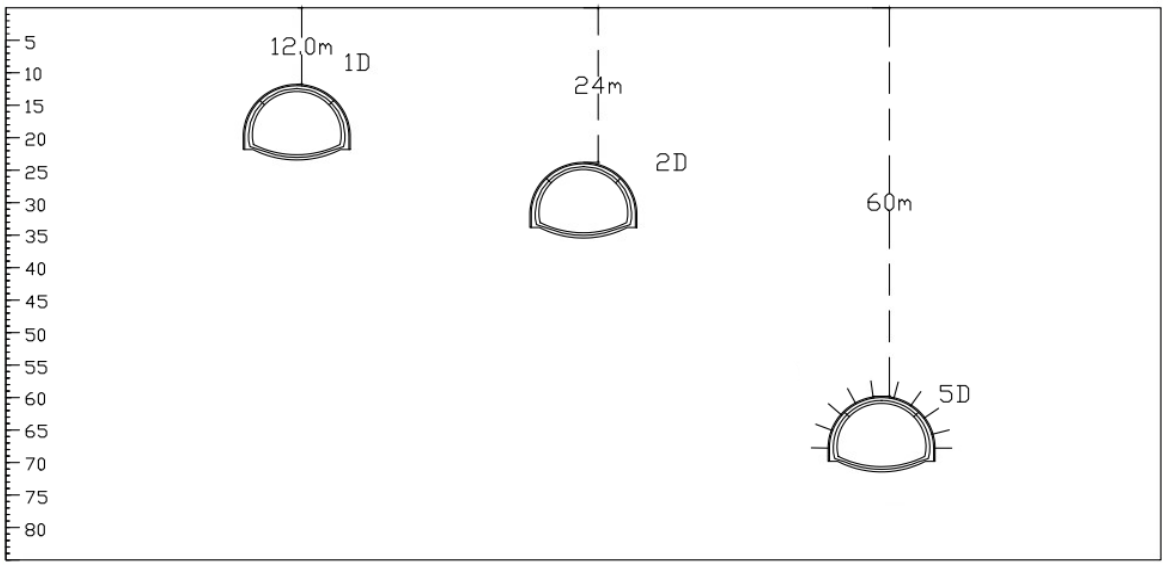

Figure 64 Layout of tunnels R1, R2 and R3 characterized by a cover of 12 m, 24 m, and 60 m.

The tunnel used in numerical modelling is horseshoe-shaped cross-section with a total width of 16 m and a height of 12 m (Figure 65). It consists of two structural linings: a 200 mm preliminary lining made of (C20/25) shotcrete reinforced with steel and an 800 mm final C30/37 concrete.

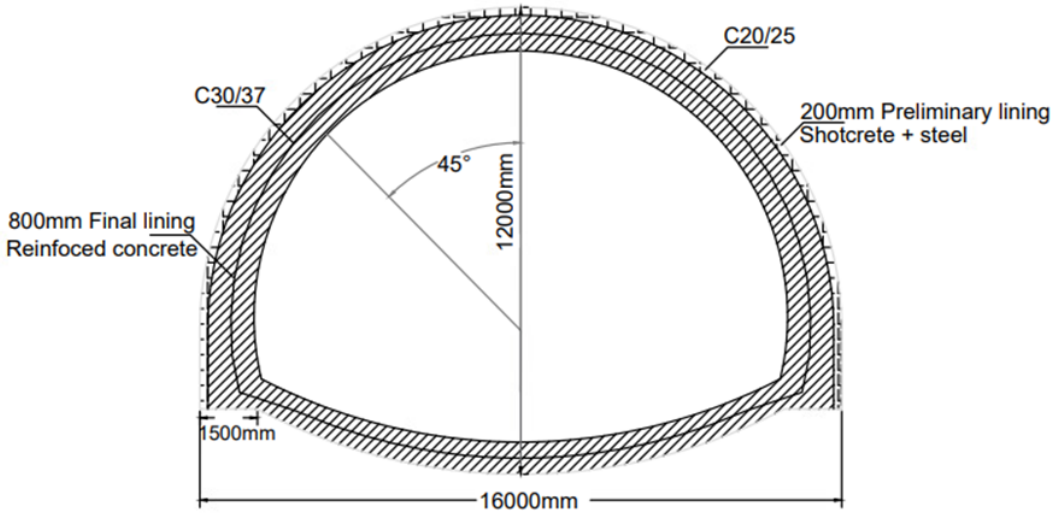

Figure 65 R1&R2 Tunnel lining cross section

The same tunnel geometry and lining dimensions were adopted for all simulated rock mass conditions to maintain consistency in the comparison. For the R1 and R2 rock masses (Figure 65), only the linings were applied. In contrast, for R3 4.2 m-long rock bolts were added (Figure 66).

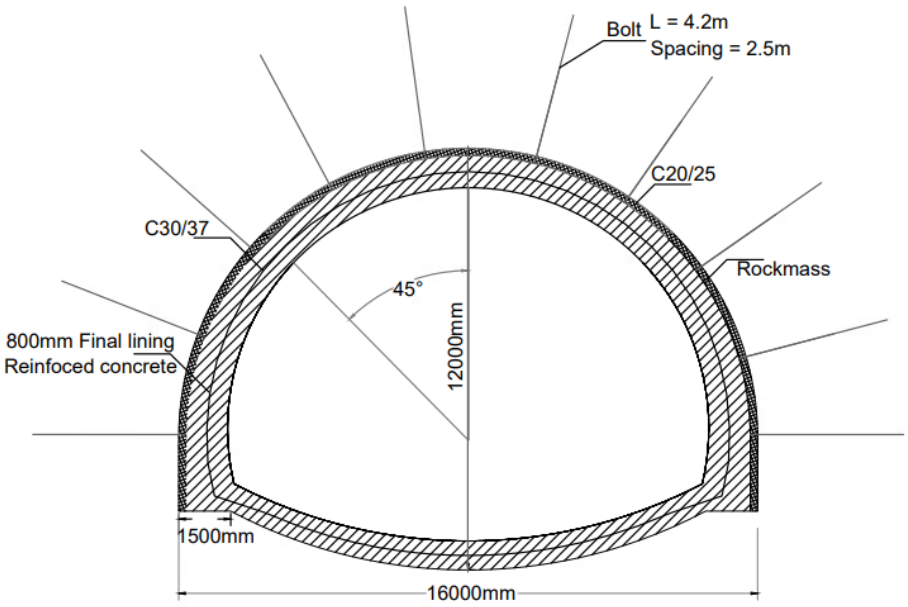

Figure 66 R3 tunnel lining cross section with bolts

The removal of the preliminary lining and, subsequently, the removal of the bolts were carried out in the model to simulate the long-term degradation of the tunnel The simulation continues up to the stage representing the deterioration of the tunnel crown, where the damaged portion is fully removed to reproduce the effects of fire-induced degradation (Figure 67).

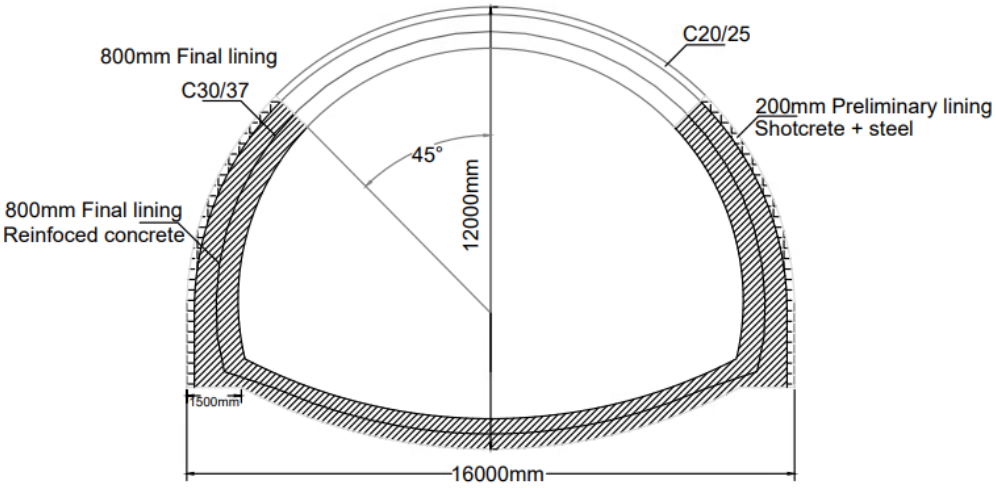

Figure 67 R1 & R2 crown degradation

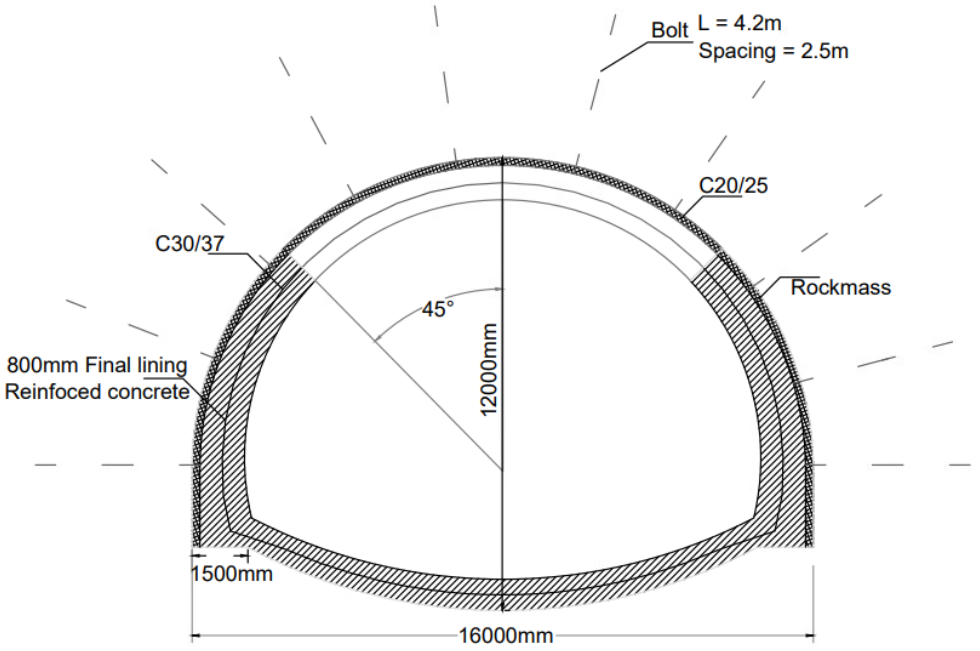

Figure 68 R3 crown & bolts removal

Table 46 summarizes the mechanical parameters adopted for tunnel concrete and shotcrete structure. The adopted unit weights are 22 kN/m³ for the flysch-type rock (Fine Software, 2024),

25 kN/m³ for the quartz–mica schist (Kumar et al., 2013), and 27 kN/m³ for the gneiss (Universidad de Alicante, 2024).

Table 46 Concrete & shotcrete characteristics

Strength parameters	**C30/37**	**C20/25**
R_{ck} [MPa]	37.0	25.0
f_{ck} [MPa]	30.7	20.8
f_{cd} [MPa]	17.4	11.8
f_{ctm} [MPa]	2.94	2.27
f_{ctd} [MPa]	1.96	1.51
Φ[°]	34.34	34.66
c [MPa]	4.99	5.38

The tunnel characteristic curve Figure 69 represents the relationship between the fictitious pressure acting on the tunnel walls and the corresponding radial displacement for determining the optimal location and timing for installing the support system, as tunnel walls deform progressively along the excavation face.

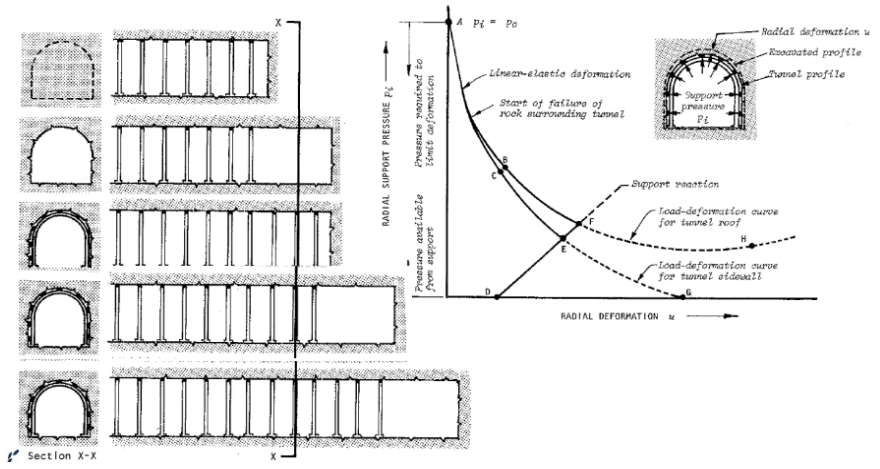

Figure 69 Advance of the tunnel face and installation of supports (left) and Tunnel characteristic curve (after Panet, 1995)

Anchor bolts and shotcrete are the most common support systems used in tunneling. These can be installed either as a temporary measure prior to final lining or as permanent reinforcement. The efficiency of these systems is analyzed by determining the characteristic line of the support and evaluating its interaction with the characteristic curve of the tunnel, which defines the convergence confinement relationship.

The Q-system (Barton & Grimstad, 2004) classifies rock mass based on six parameters: RQD (Rock Quality Designation), Jn (number of joint sets), Jr (joint roughness), Ja (joint alteration), Jw (joint water reduction factor), and SRF (stress reduction factor).

The Q-support chart (Figure 70) defines the support categories according to the tunnel span, height, bolt length, and rock mass quality.

In situations where the Q-value cannot be easily determined, it may be correlated with the Rock Mass Rating (RMR) system (Bieniawski, 1993). The following empirical correlation is commonly used:

$$RMR = 9\ln(Q) + 44 \qquad (4.1)$$

$$MR = 13.5\,log(Q) + 43 \qquad (4.2)$$

$$RRMR = 50 + 15\,log(Q) \qquad (4.3)$$

Starting from the R3 scenario, verification was carried out for the use of a bolt support system. The design follows the criteria of the Q-system and RMR method described above.

The geomechanical parameters of the rock mass are presented in Table 47. An essential parameter for the support design is the Excavation Support Ratio (ESR), which depends on tunnel purpose and is selected following Grimstad and Barton (2014), as shown in Figure 70.

Table 47 Excavation support ratio

Type of Excavation		ESR (1994)	ESR (2014)
A	*Temporary mine openings, etc.*	ca. 2-5	*ca. 2 to 5*
B	*Permanent mine openings, water tunnels for hydropower (exclude high pressure penstocks), pilot tunnels, drifts and headings for large openings, surge chambers*	1.6-2.0	*1.6 to 2.0*
C	*Storage caverns*, water treatment plants, minor road and railway tunnels, *access tunnels*	1.2-1.3	0.9 to 1.1 *Storage caverns 1.2-1.3*
D	*Power stations*, major road and railway tunnels, *civil defence chambers, portals, intersections*	0.9-1.1	Major road and rail tunnels 0.5 to 0.8
E	*Underground nuclear power stations, railway stations, sports and public facilities, factories, major gas pipeline tunnels*	0.5-0.8	*0.5 to 0.8*

Based on the geological and hydrological conditions, the RMR value was determined as 67 using formula (4.1). The Q-system analysis produced the following results:

In Table 48, case 1 follows Equation (4.1), case 2 follows Equation (4.2), and case 3 follows Equation (4.3). Each equation represents a different empirical relationship between RMR and Q rock mass classification systems, applied according to specific conditions considered in each case.

Table 48 Q-system

Case		Q-value
Case 1	*4.1*	12.878
Case 2	*4.2*	59.948
Case 3	*4.3*	13.594
Average Q		28.807

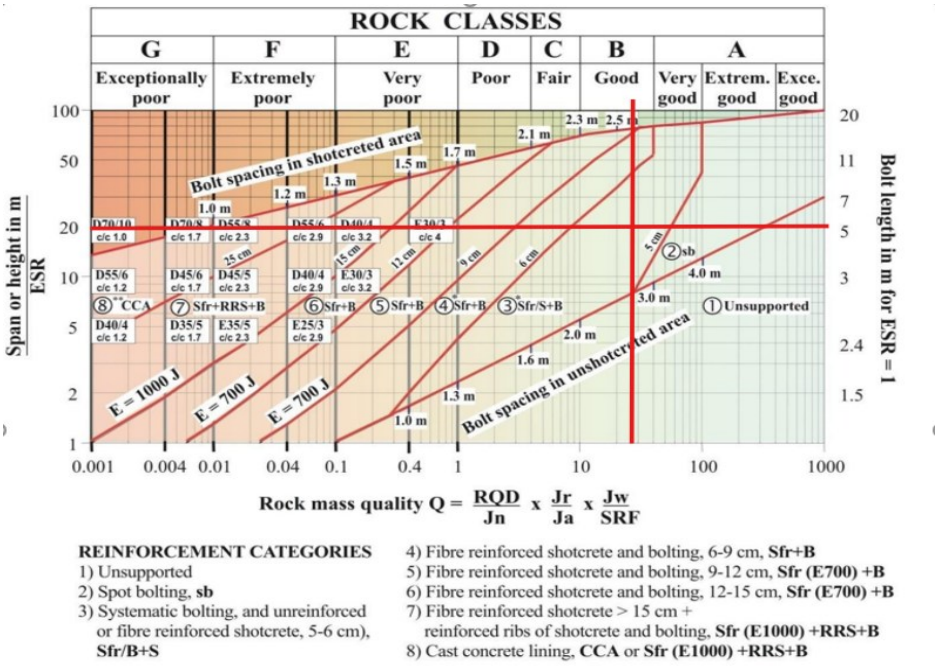

Figure 70 Q-Support chart

Figure 70 shows the resulting design class derived from the Q-support chart. The analysis corresponds to Category 3 reinforcement, recommending systematic bolting and unreinforced or fibre-reinforced shotcrete (5–6 cm), defined as Support Type=Sfr/B+S, with bolt spacing up to 2.5 m.

The plastic radius (R_p) of the tunnel was estimated using the following expression:

$$R_p = a\left(\frac{(p_0 + c_r \cot \phi_r) - (p_0 + c_p \cot \phi_p)\sin \phi_p}{p_i + c_r \cot \phi_r}\right)^{\frac{1}{N_r - 1}} \qquad (4.4)$$

Table 49 Input parameters for tunnel with bolts in good quality rock mass

	Symbol	Value	Unit
Equivalent tunnel radius	Req	9.75	m
In-situ stress ratio	K0	1	–
Vertical stress	p0	0.8856	MPa
Horizontal stress	σ_h	0.8856	MPa
Internal pressure	p_i	0	MPa
Cohesion	c	2.0416	MPa
Friction angle	φ	42.97	°
Stress exponent	Nr	5.28	–
Critical pressure	pcr	−1.2118	MPa
Plastic radius	Rpl	8.08	m

The estimation of the plastic radius of the tunnel is equal to 8 m. Therefore, it is recommended to use bolts with a length equal to 8-4.8=3.125+1=4.2 m, having spacing between bolts taken from the graph to be equal to 2.5 m.

4.3 Modeling computational stages

Three rock mass qualities were analysed, i.e. poor, average, and good quality rock mass. For each rock mass type, three tunnel depths were considered (1D, 2D, and 5D, where D is the tunnel diameter). Rock masses strength and deformability properties are listed in Table 50

Table 50 Rock mass strength and deformability properties (Hoek,2002)

Parameter	Unit	Poor Rock	Average Rock.	Strong Rock
Young's Modulus (E)	MPa	480	13,000	43,000
Poisson's Ratio (v)	–	0.3	0.3	0.3
Cohesion (c)	MPa	0.135	2	9.4
Friction Angle (ϕ)	°	22.4	40	43
Unit Weight (γ)	kN/m^3	22	25	27
Intact rock strength (σ_{ci})	MPa	7.5	30	110
GSI	–	20	65	75
Hoek-brown constant (m_b)	–	0.55	4.5	7.25
Hoek-brown constant (s)	–	0	0.02	0.062
constant (a)	–	0.5	0.5	0.5

For all quality rock masses, tunnel simulations were carried out using 15 calculation stages. Stage 1 represents the geostatic stress condition, in which the in-situ stresses are applied to the intact rock mass prior to excavation.

From Stages 2 to 12, tunnel excavation is simulated through a gradual internal pressure release. The unloading is applied in 10% increments, representing the progressive stress release associated with excavation.

The primary lining in poor and average quality rock masses, consisting of steel sets and shotcrete, is installed at Stage 8, after 50% stress release of the original stress, to contribute to tunnel stability during the remaining excavation and stress redistribution phases. For models with good quality rock mass, rock bolts are installed at Stage 8 as well after 50 % stress release.

At Stage 13, the final lining (concrete lining) is installed after 100% stress release. This stage represents the completed tunnel configuration under normal operating conditions, with both primary and final linings active.

The subsequent stages are used to simulate support degradation.

At Stage 14, the primary lining is degraded by setting its strength properties to zero. This approach represents a complete loss of structural capacity of the primary lining while maintaining its geometry in the model. In this stage, rock bolts were removed to simulate bolts reinforcement long term deterioration only.

At Stage 15 in all models, a localized damage at the tunnel crown is simulated. The crown is defined as the portion of the lining between –45° and +45° from the tunnel axis. This stage represents severe local degradation, which may occur due to extreme events such as fire exposure. In this stage, rock bolts are also removed combined with crown damage to simulate long term deterioration of reinforcement elements combined with crown damage in case of good quality.

Stages from stage 1 to 15 for tunnel without and with bolts are illustrated in Figure 71 and Figure 72 respectively.

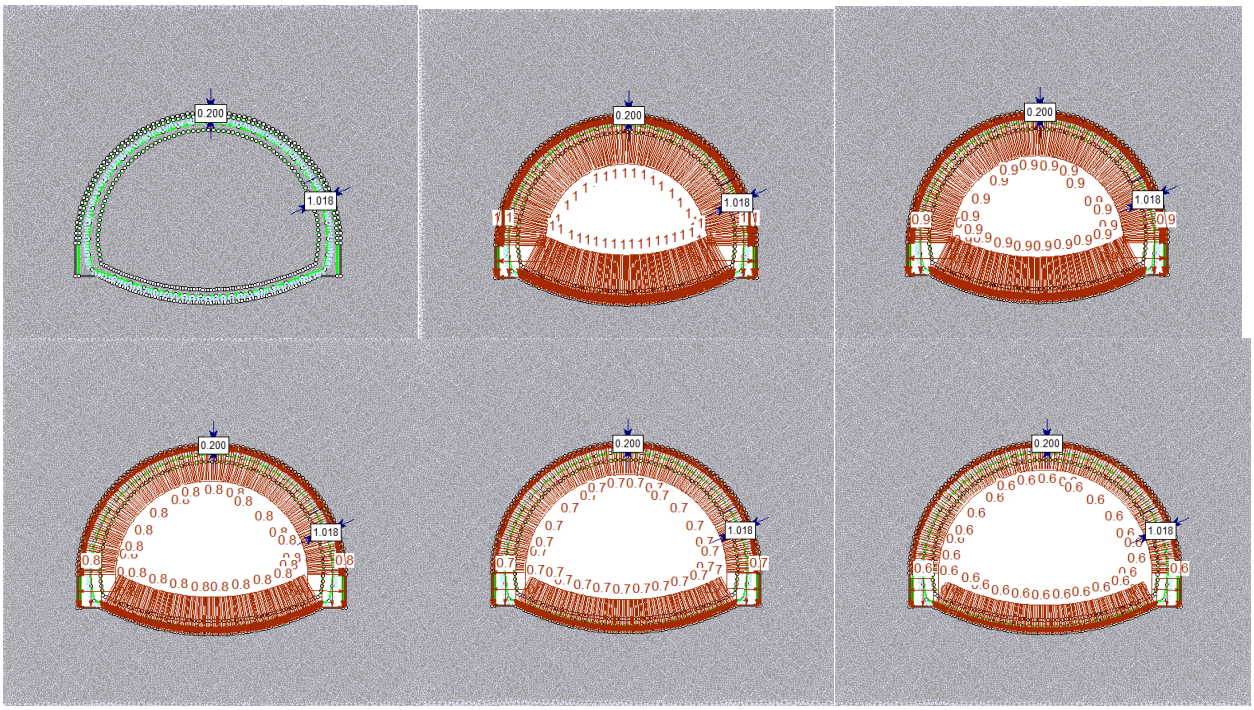

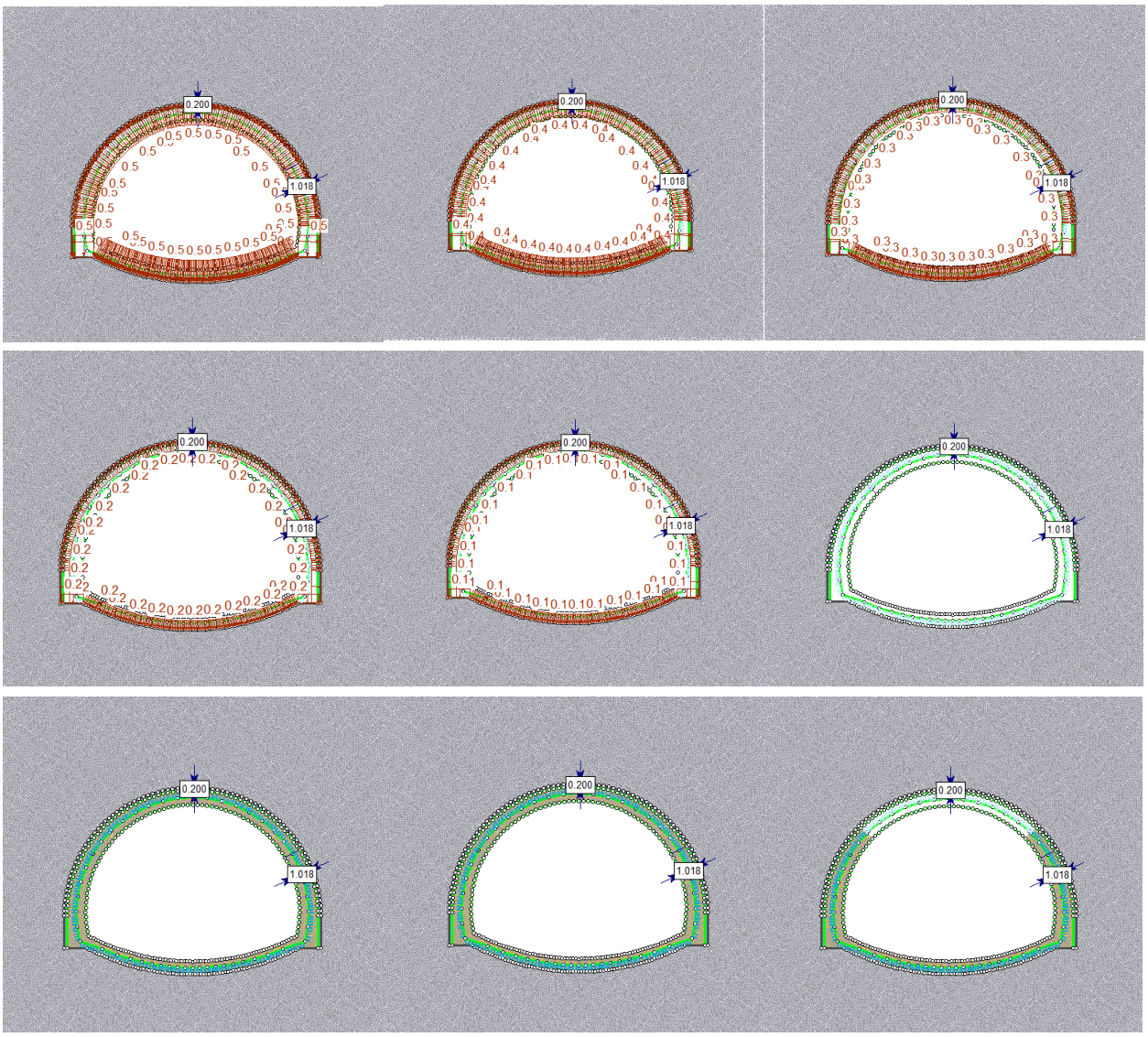

Figure 71 Model excavation and degradation stages for tunnel without bolts

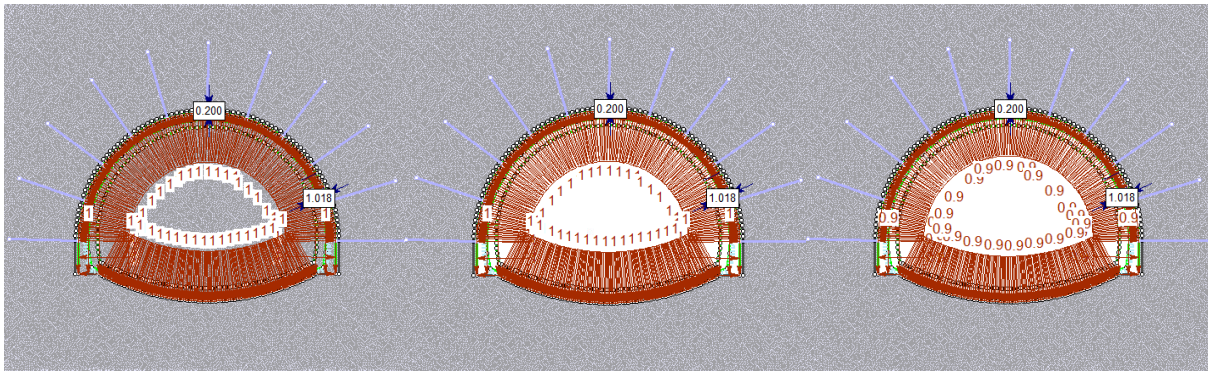

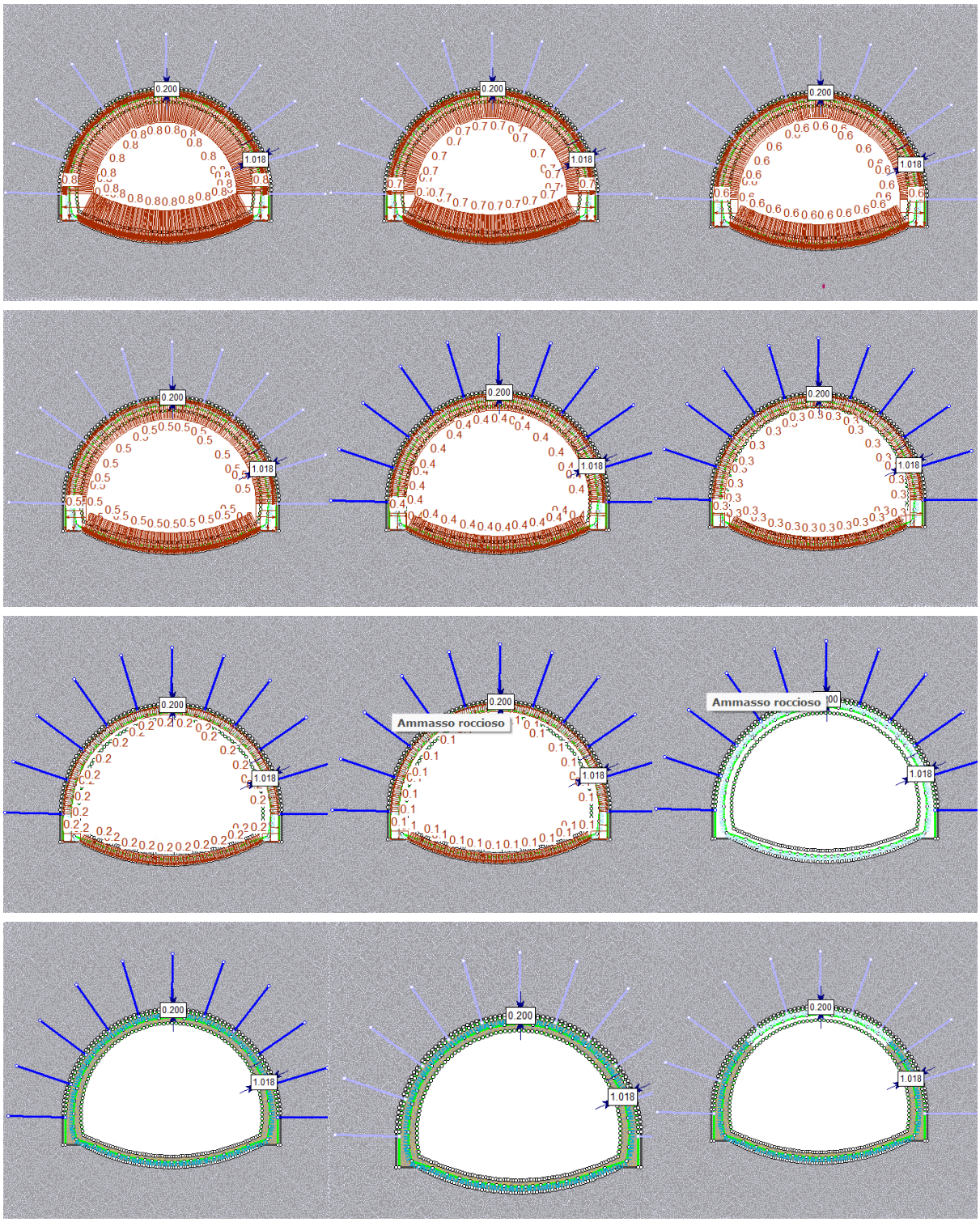

Figure 72 Model excavation and degradation stages of tunnel with bolts

4.4 Results and analysis

Looking at the numerical results obtained from the RS2 analyses, with specific reference to the screenshots of the models presented in Figures 71 to 90, the results are discussed in terms of total displacement, plastic zone development, and maximum plastic strain, for different rock mass qualities and tunnel depths.

4.4.1 Deformations

Figures 71 to 73 show the total displacement contours for the poor-quality rock mass (PQ – flysch) at shallow (1D), intermediate (2D), and deep (5D) tunnel depths. At Stage 15, corresponding to the complete removal of the crown lining, the numerical solution did not converge for any of the tunnel depths considered. This behavior indicates that the tunnel ground system was unable to reach mechanical equilibrium.

In the 1D condition, the displacement field is strongly influenced by the proximity of the ground surface. After crown degradation, large vertical displacements develop above the tunnel, indicating loss of confinement and redistribution of stresses toward the surface. The maximum displacements are concentrated at the crown and extend upward, suggesting a higher risk of surface settlement for shallow tunnels in weak rock masses.

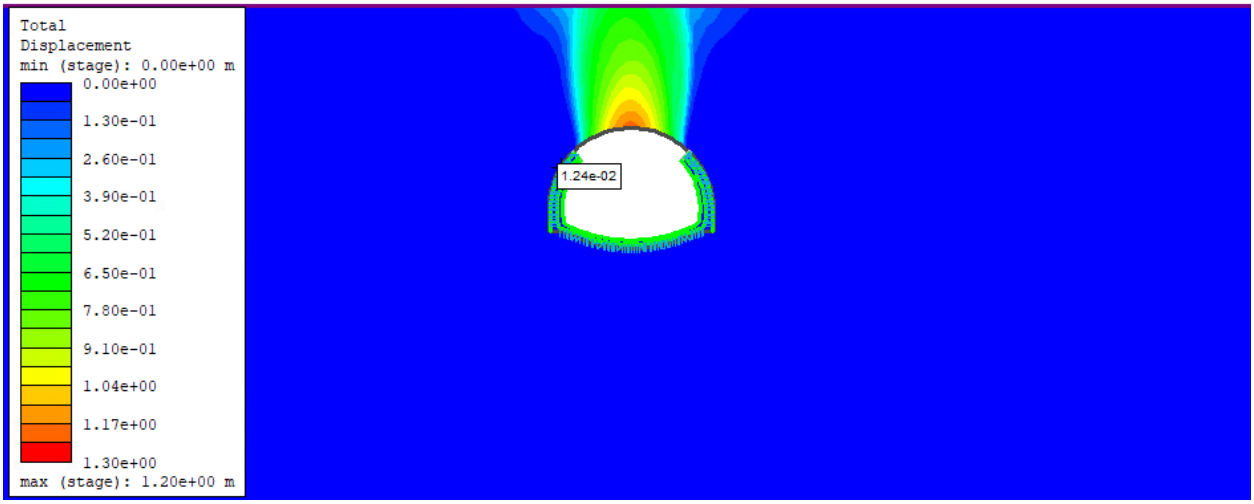

Figure 73 Total displacement contours for PQ-1D

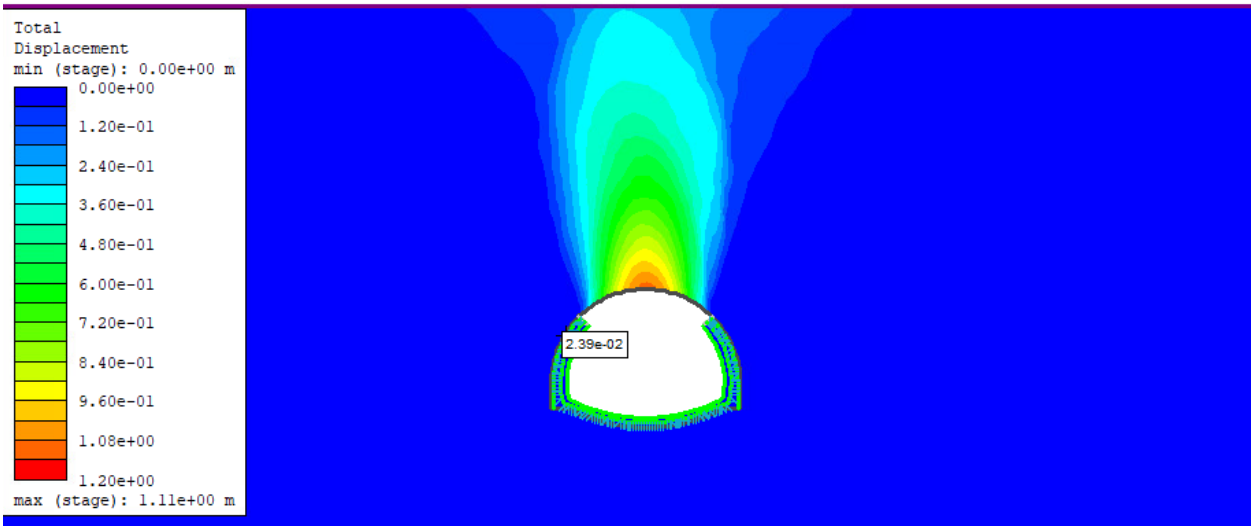

Figure 74 Total displacement contours for PQ-2D

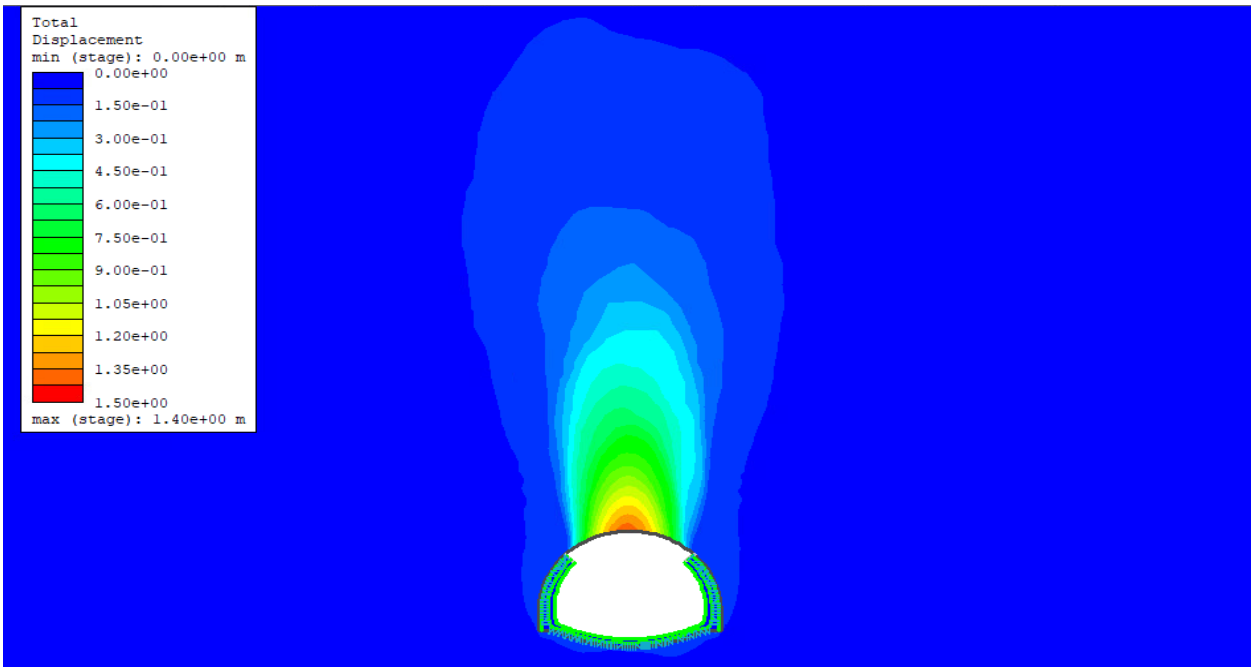

Figure 75 Total displacement contours for PQ-5D

Figures 74 to 76 present the displacement contours after tunnel crown removal for the average quality rock mass (AQ – quartz–mica schist). Compared to the poor rock mass, the displacements are clearly lower for all depths. In the shallow case, deformation is still visible near the crown, but its magnitude and spatial extension are limited. At 2D and 5D depths, the tunnel shows a more stable response, with displacements mainly concentrated close to the lining and no significant upward propagation.

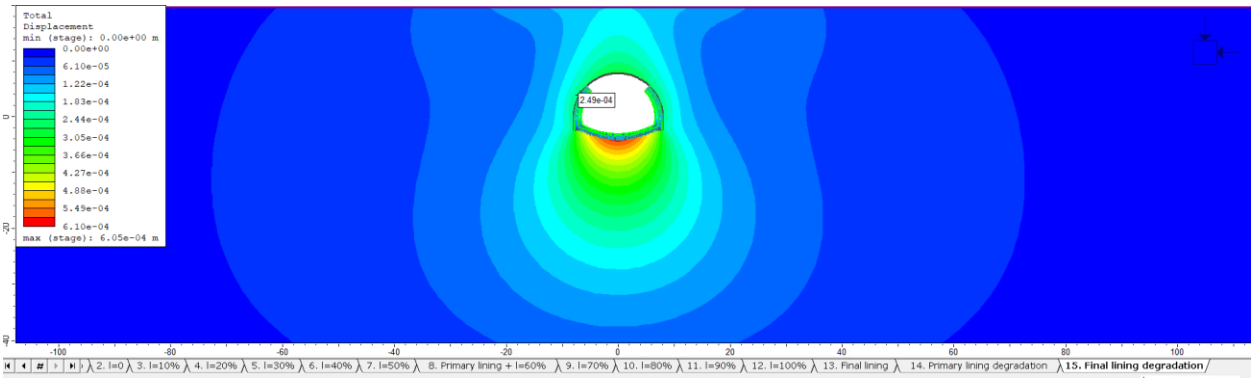

Figure 76 Total displacement contours for AQ-1D

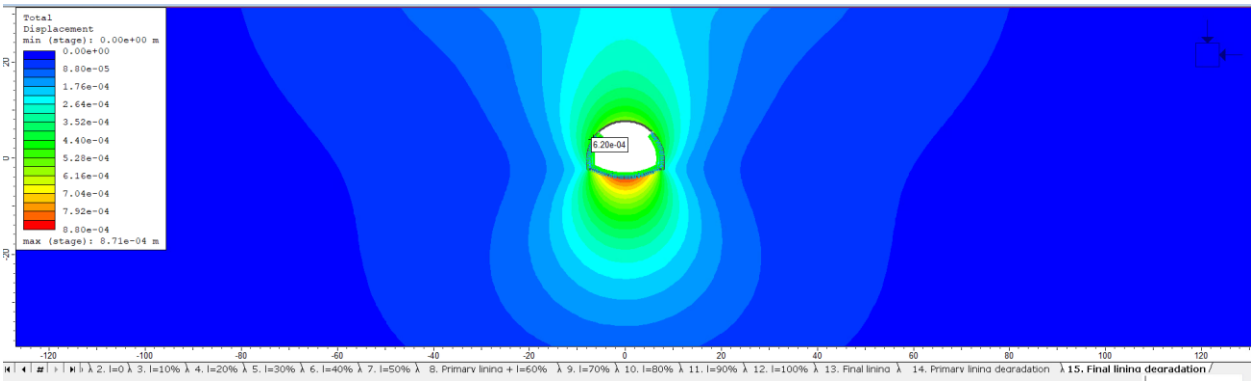

Figure 77 Total displacement contours for AQ-2D

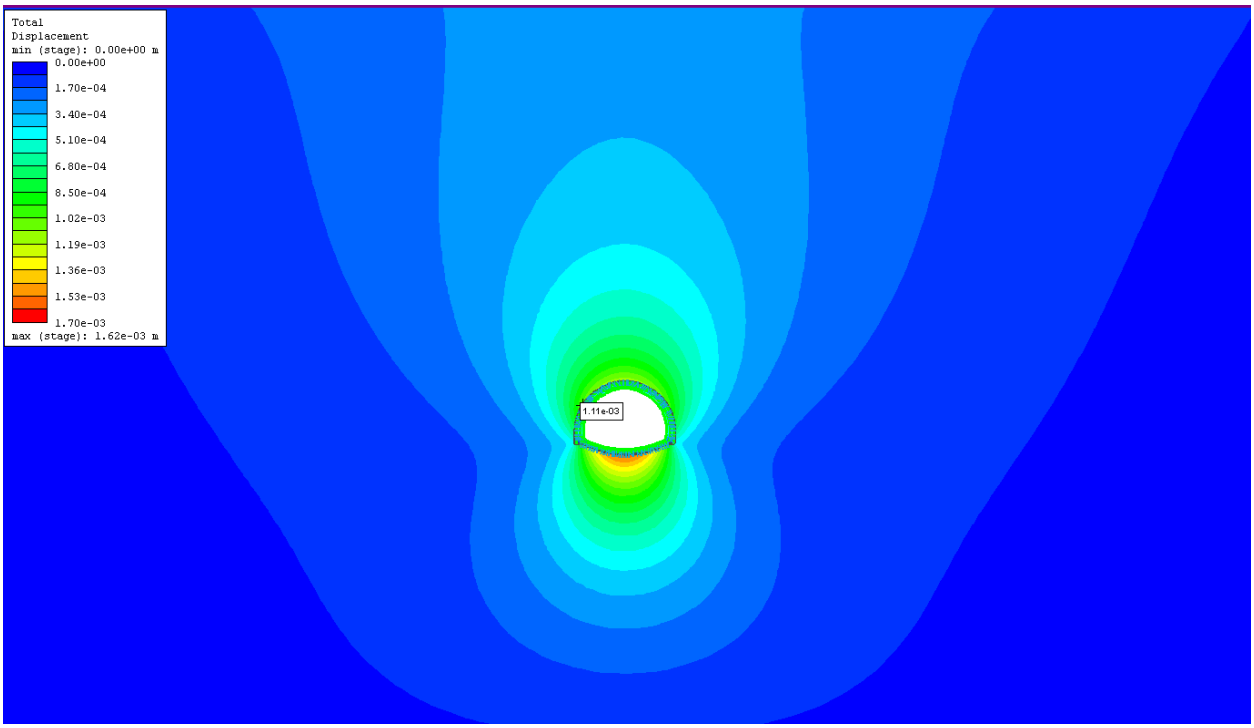

Figure 78 Total displacement contours for AQ-5D

Figures 77 to 79 show the results for the strong rock mass (GQ – gneiss) with bolt support. Even after the removal of the crown lining and bolts, the total displacements remain very small. Although the displacement contours appear significant in the plot, the actual magnitude of

deformation is very small. These results highlight the effectiveness of good rock quality and reinforcement systems in limiting tunnel deformation under severe damage scenarios.

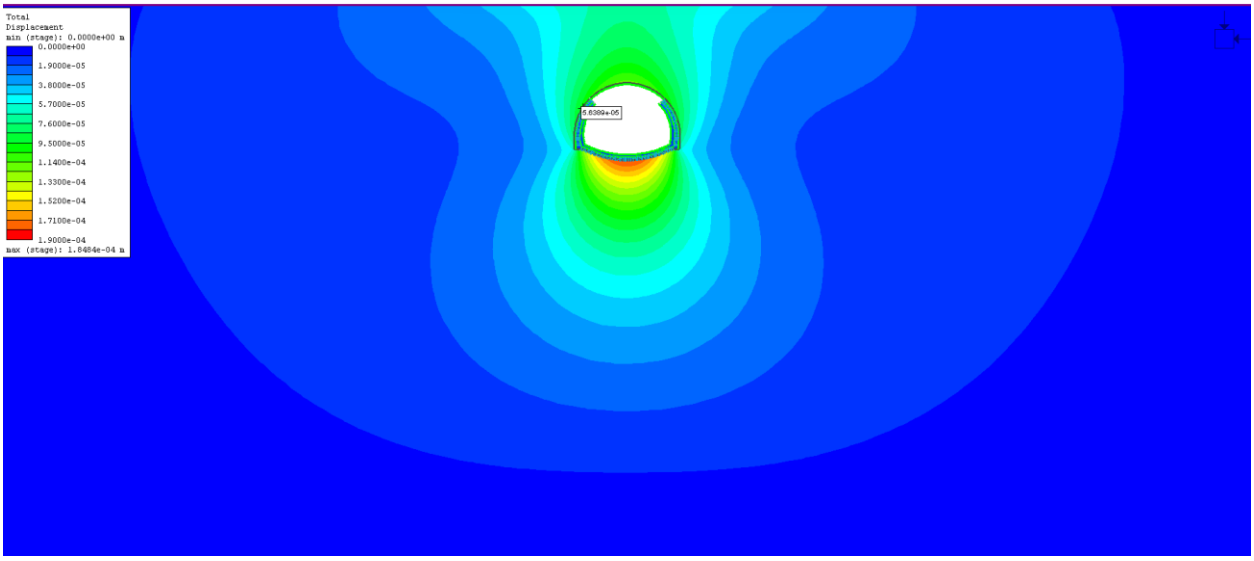

Figure 79 Total displacement contours for GQ-1D

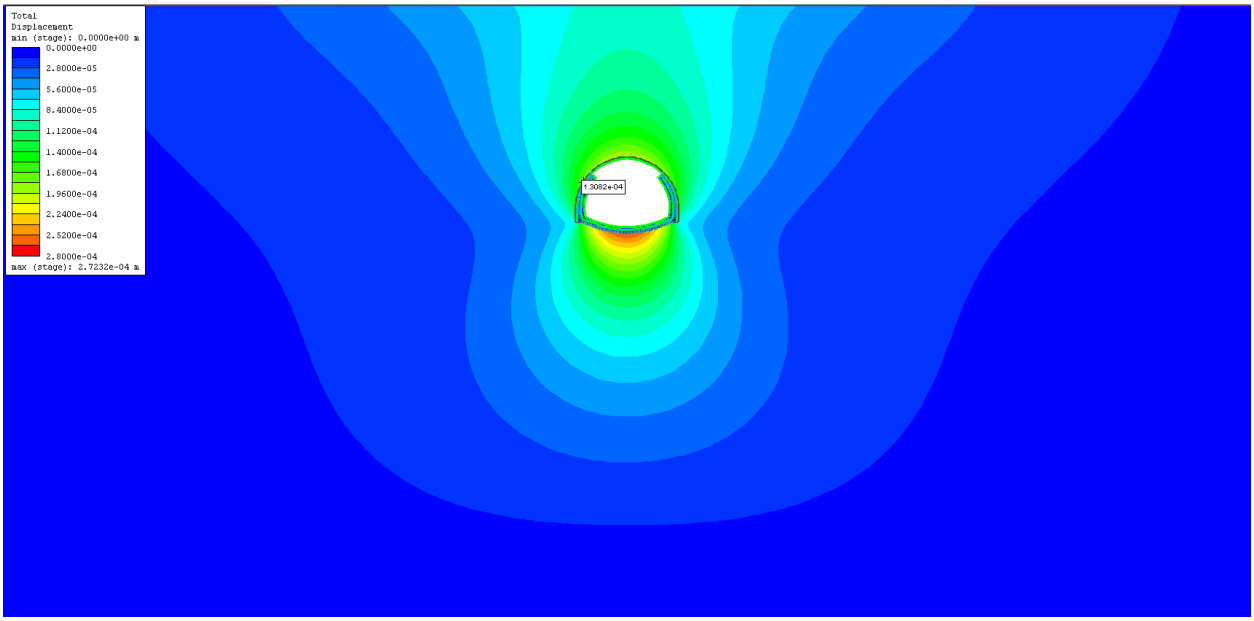

Figure 80 Total displacement contours for GQ-2D

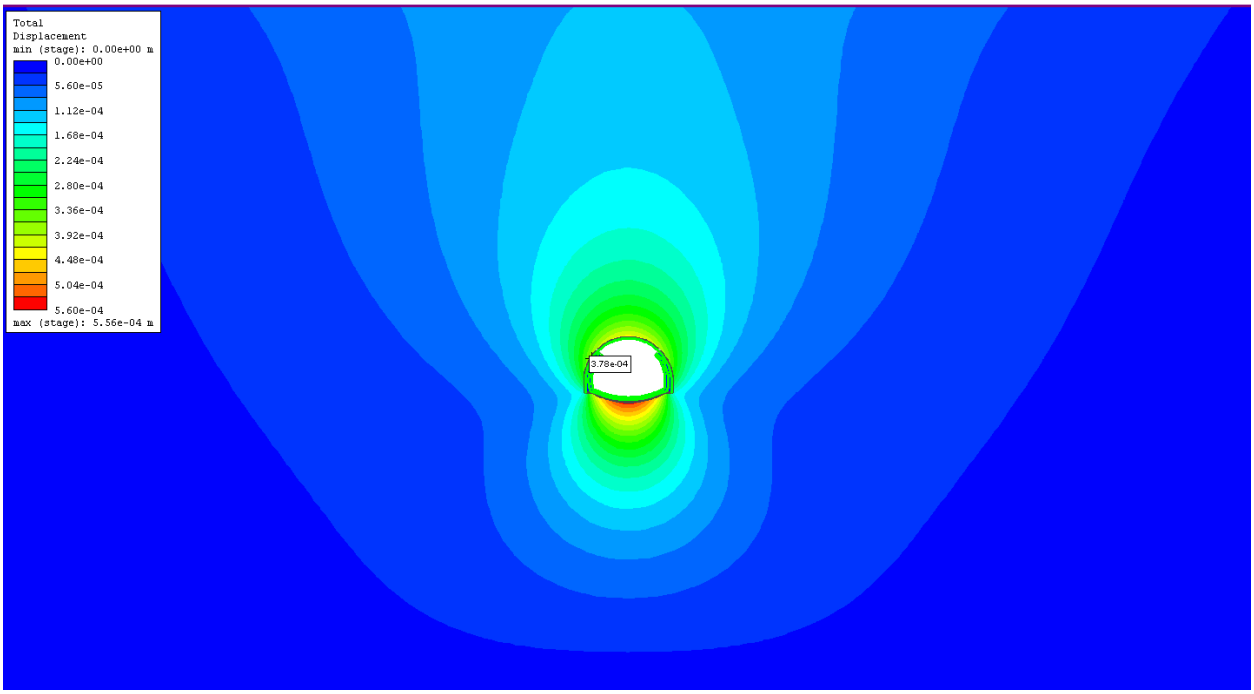

Figure 81 Total displacement contours for GQ-5D

The poor rock mass exhibits the highest displacement values overall, with displacement magnitude increasing with depth due to higher in-situ stresses, while the average and strong rock masses show progressively lower values for the same depth conditions. The strong rock mass presents almost negligible surface displacement.

4.4.2 Plastic zone

The extent of yielded elements around the tunnel is shown in Figures 80 to 82 for the poor-quality rock mass. In the shallow tunnel case (PQ-1D), yielding initiates along the tunnel sidewalls and the immediate excavation boundary. The first yielded elements develop around the tunnel periphery and then propagate outward, extending toward the ground surface on both the left and right sides.

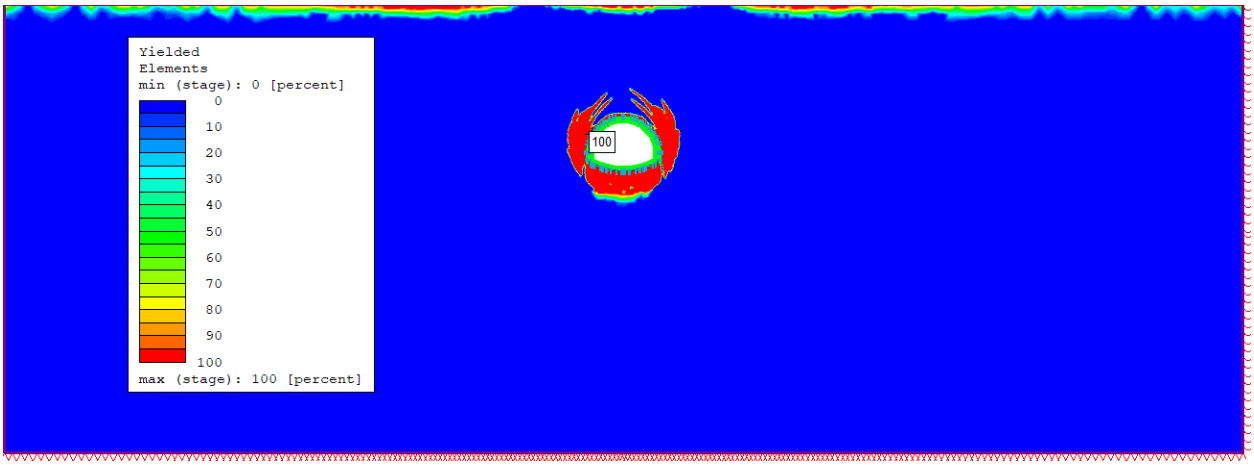

Figure 82 Yielded elements (%) around the tunnel for stage 14 (same for all depths)

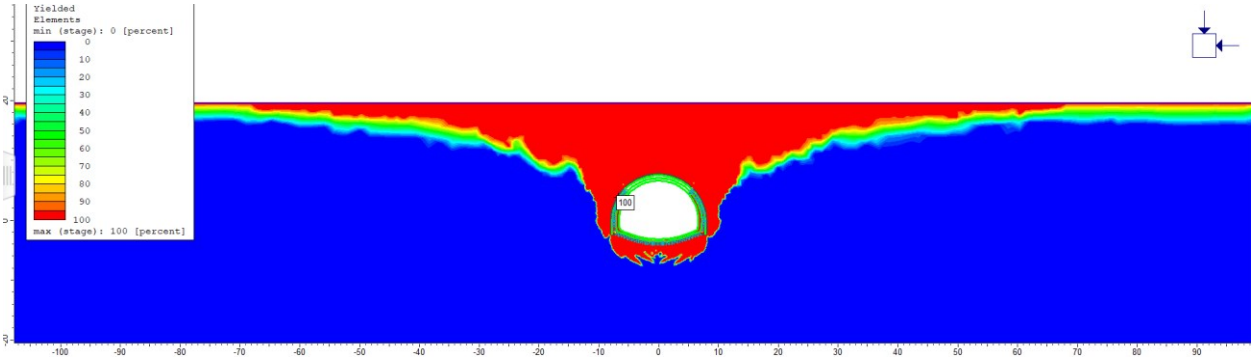

Figure 83 Yielded elements (%) around the tunnel for PQ-1D

At depth (PQ-2D), the number of yielded elements increases, and the plastic zone expands both radially and vertically around the tunnel profile. The higher overburden stress leads to greater stress concentration after crown removal at stage 15(Figure 84) compared to stage 14(Figure 82), promoting progressive yielding of surrounding rock mass.

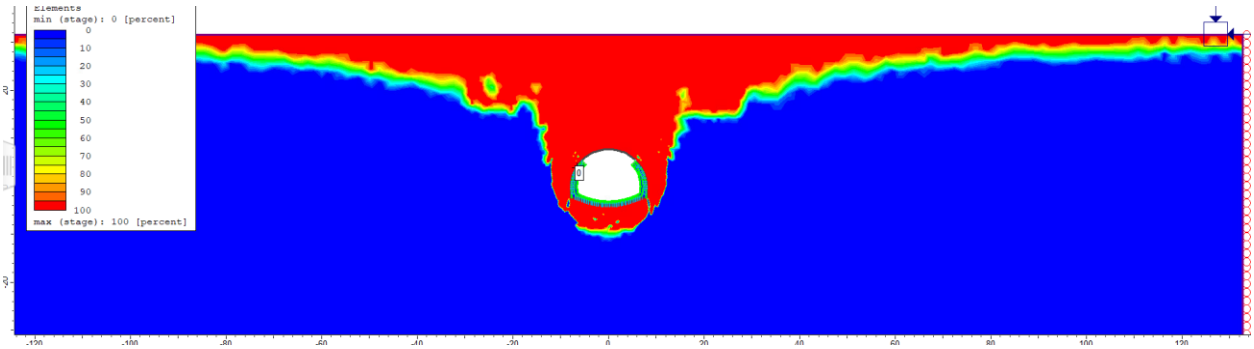

Figure 84 Yielded elements (%) around the tunnel for PQ-2D at stage 15

In the deep tunnel case (PQ-5D), the yielded elements significantly increase, and the plastic zone becomes much more extensive, surrounding a large portion of the excavation boundary. This behaviour clearly indicates that increasing depth, and therefore higher in-situ stress, strongly amplifies plastic deformation once structural support is lost. The expansion of the plastic zone with depth reflects a transition from localized damage to a more generalized failure mechanism.

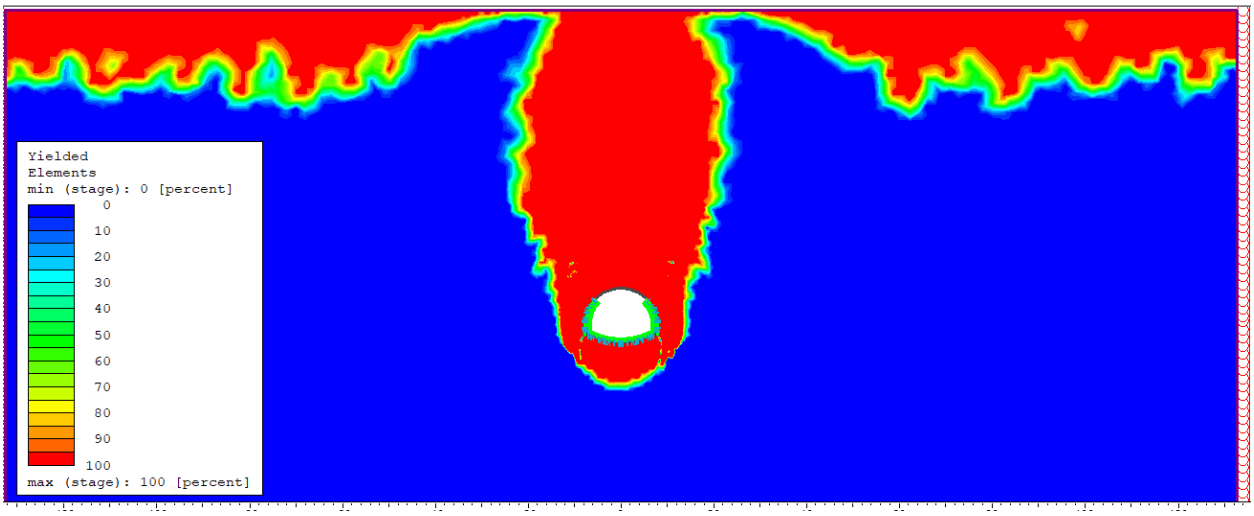

Figure 85 Yielded elements (%) around the tunnel for PQ-5D

After the removal of the tunnel crown (Stage 15), the yielded elements increase significantly and propagate from the tunnel towards the ground surface in all depths of poor quality rock mass, indicating a loss of confinement and the development of a larger plastic failure zone compared to Stage 14.

For the average-quality (AQ) and strong-quality (GQ) rock masses, no yielded elements were detected in the numerical analyses after crown degradation (Figure 86). Consequently, no plastic zone figures are reported for these cases. This confirms that the strength and stiffness of these rock masses are sufficient to prevent yielding, even under severe damage conditions.

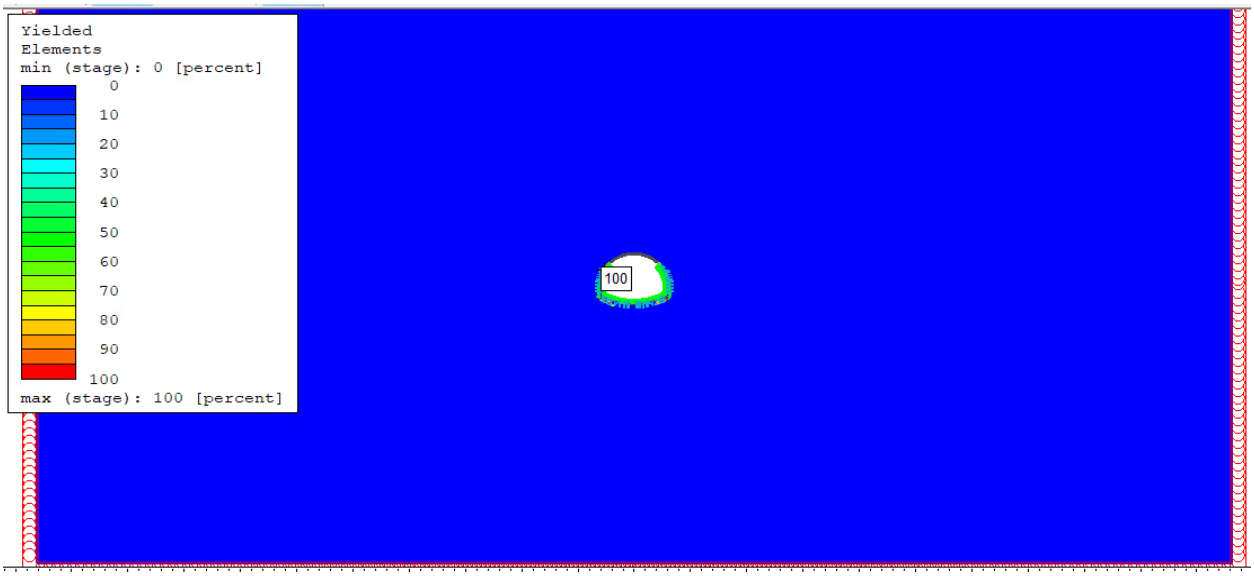

Figure 86 Plastic zone AQ-5D

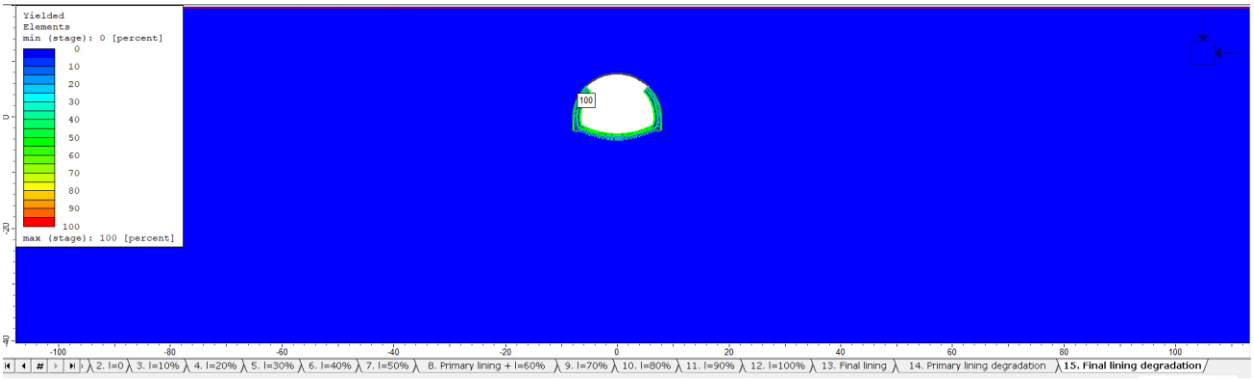

Figure 87 GQ rock mass plastic zone (no yielding)

4.4.3 Maximum shear plastic strain

The maximum shear plastic strain observed in all models of poor quality rock mass at depths of 1D, 2D and 5D, after the removal of the tunnel crown represents zones where the rock mass has undergone shear failure due to stress redistribution due to the removal of a tunnel crown. Removing the crown eliminates confinement and breaks the natural stress arch above the tunnel, causing vertical loads to transfer to the sidewalls and shoulders. This results in concentrated shear stresses at the crown sidewall transition and the formation of a plastic zone propagating upward above the tunnel, as visible in the green–yellow regions.

From 1D to 2D and 5D, increasing depth leads to higher vertical stress, which build up shear plastic strain above the tunnel after crown removal. As a result, the plastic zone becomes more concentrated and extends upward more clearly at 5D.

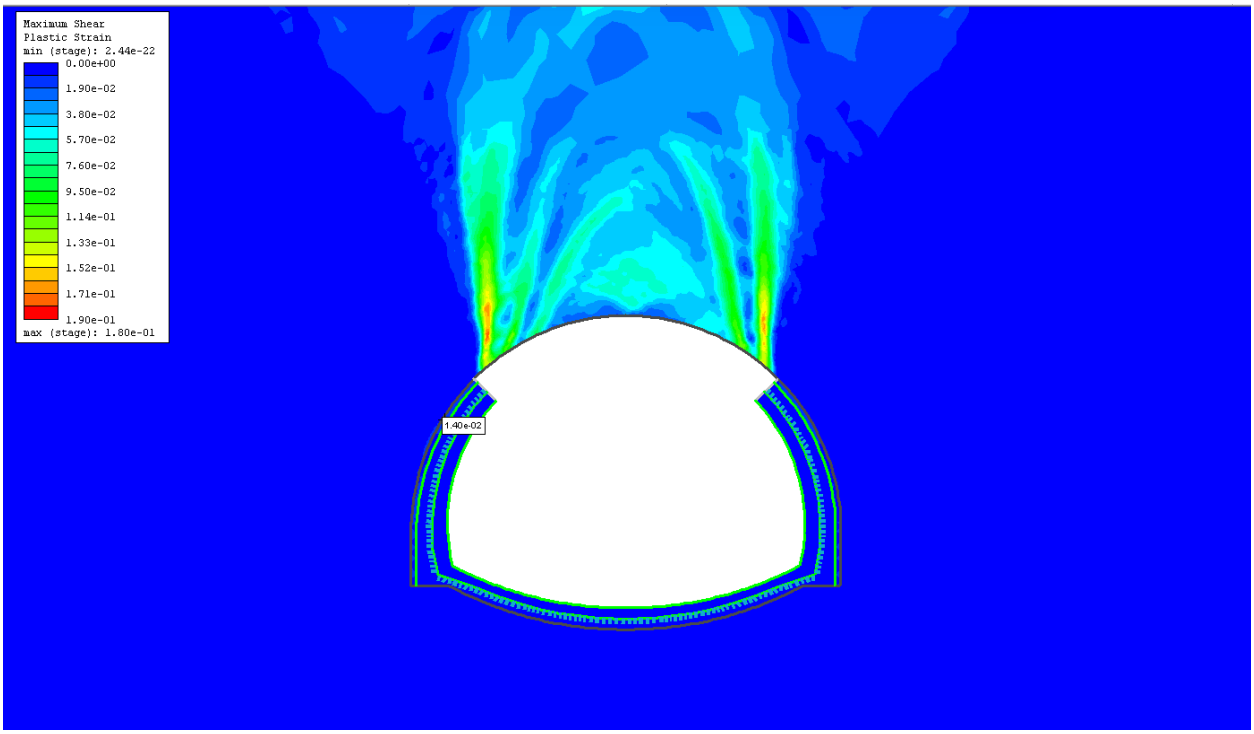

Figure 88 Maximum shear plastic strain PQ-1D

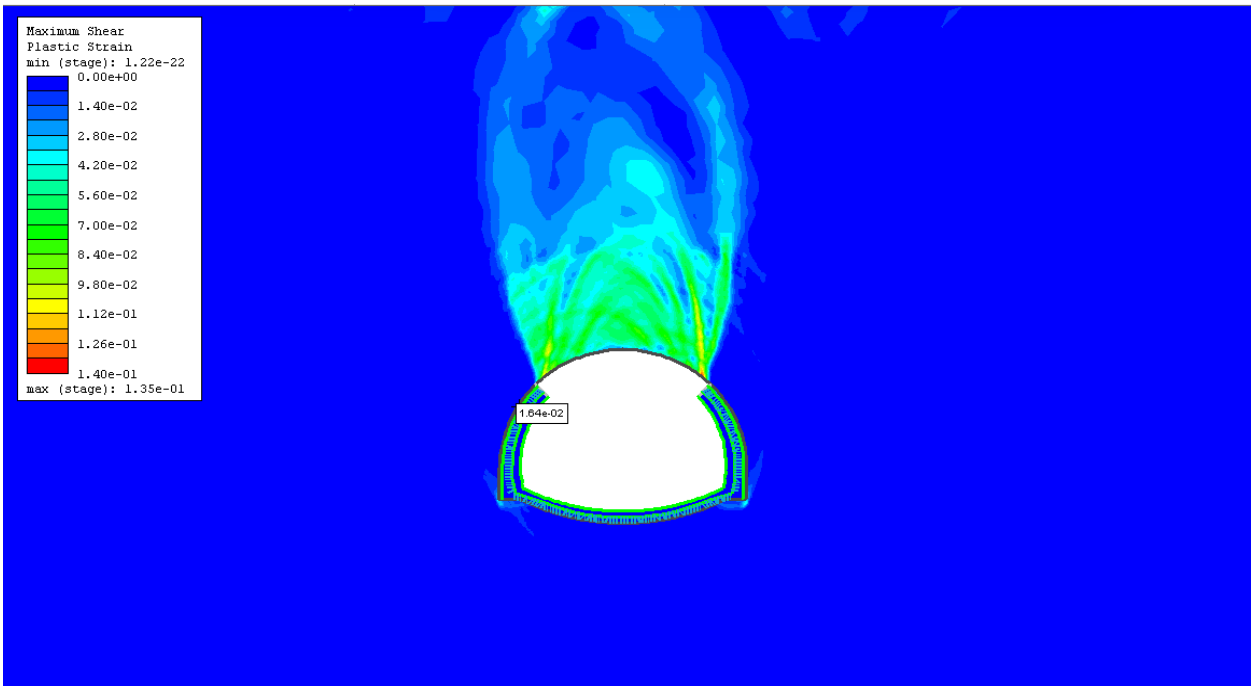

Figure 89 Maximum shear plastic strain PQ-2D

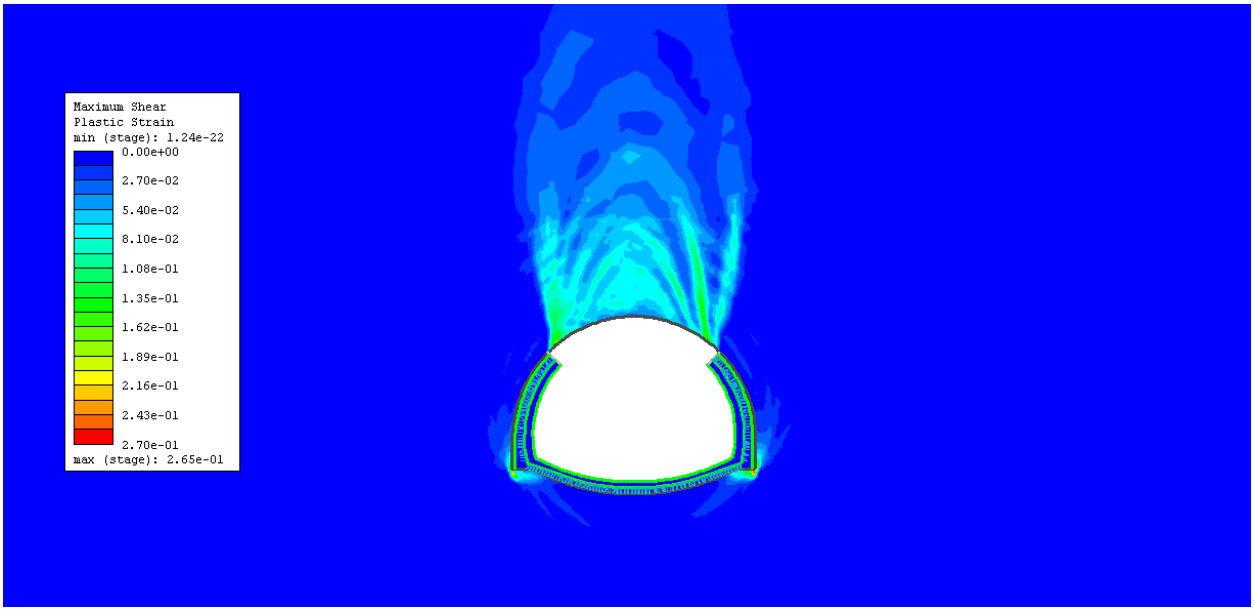

Figure 90 Maximum shear plastic strain PQ-5D

Figure 91 revealed that the maximum shear plastic strain for the average quality rock mass case and a 1D depth was negligible. This trend was consistently observed for all the investigated depths for rock masses of both average and good quality.

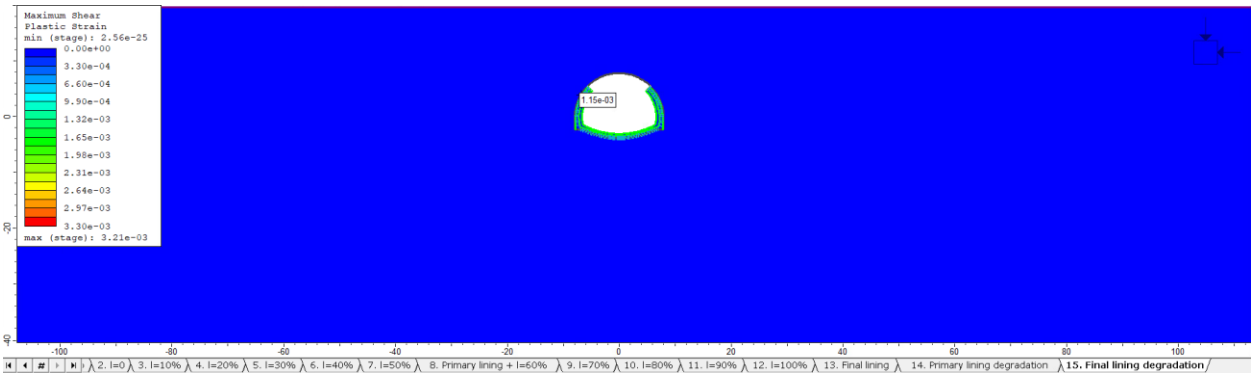

Figure 91 Maximum plastic shear Plastic strain AQ-1D

Moreover, as already seen in section 4.4.2, no yielded elements were shown as well assuring and confirming that, under tunnel crown removal, higher rock mass quality effectively limits the development of plastic deformation, preserving the overall stability of the tunnel.

4.4.4 Stability Threshold Analysis after Crown Removal

Following the previous numerical analyses, a further set of RS2 simulations was carried out to identify the stability threshold of the tunnel after crown removal. An iterative procedure was adopted starting from the poor-quality rock mass parameters, representing a more conservative approach than starting from better rock mass conditions.

In this phase, the intact rock properties were kept unchanged $\left(\sigma_c = 7.5\,\text{MPa},\ m_i = 9.6,\ \gamma = 23\,\text{kN/m}^3\right)$, while only the GSI value was progressively varied in order to evaluate its influence on model convergence. The first analyses were performed for GSI values of 30, 40, and 50 for the three considered tunnel depths, namely 1D, 2D, and 5D. The results showed that only the models with GSI = 50 converged after crown removal, whereas the models with GSI = 30 and GSI = 40 did not converge.

Since the transition between instability and stability was found to lie between GSI = 40 and GSI = 50, additional analyses were carried out within this interval in order to refine the threshold value. For this reason, three further sets of models, named limit 44, limit 45, and limit 46 were analysed for GSI values of 44, 45, and 46, respectively, while maintaining the same intact rock parameters. These refined analyses made it possible to identify more accurately the minimum rock mass quality required for convergence after crown removal. The results showed that the first fully stable condition was obtained at GSI = 46, for which convergence was achieved for all analysed depths. Therefore, this condition can be considered the threshold at which the rock mass is able to sustain tunnel crown removal.

The Hoek–Brown failure criterion was then used only to provide a graphical representation of the stress conditions associated with the analysed cases.

The models were illustrated in a theoretical point of view and hoek-brown criterion graphical representation were plotted to better understand results coming from software models.

Table 51 Limit model rock mass properties in comparison to other rock masses

Parameter	Poor Rock (Flysch)	Limit 30	Limit 40	Limit 50	Average Rock (Quartz–Mica Schist)	Good Rock (Gneiss)
Young's Modulus (E) [MPa]	480	866,0	1540,0	2738,6	13,000	43,000
Poisson's Ratio (ν) [-]	0,3	0,3	0,3	0,3	0,3	0,3
Unit Weight (γ) [-]	22	23	23	23	25	27
Intact rock strength (σci) [MPa]	7,5	7,5	7,5	7,5	30	110
GSI[-]	20	30	40	50	65	75
Hoek-brown constant (mb)	0,55	0,788	1,525	2,616	4,5	7,25
Hoek-brown constant (s)	0	0,0004	0,0013	0,0039	0,02	0,062
constant (a)	0,5	0,5	0,5	0,5	0,5	0,5

Starting from the limit 30 model, the strength properties refer to a GSI of 30, slightly above the poor-quality rock mass characterized by a GSI of 20. According to RS2 computation for the 1D case, the model did not converge at stage 15 revealing failure. As shown in Figure 103, there is significant displacement above tunnel crown which propagates towards the ground surface.

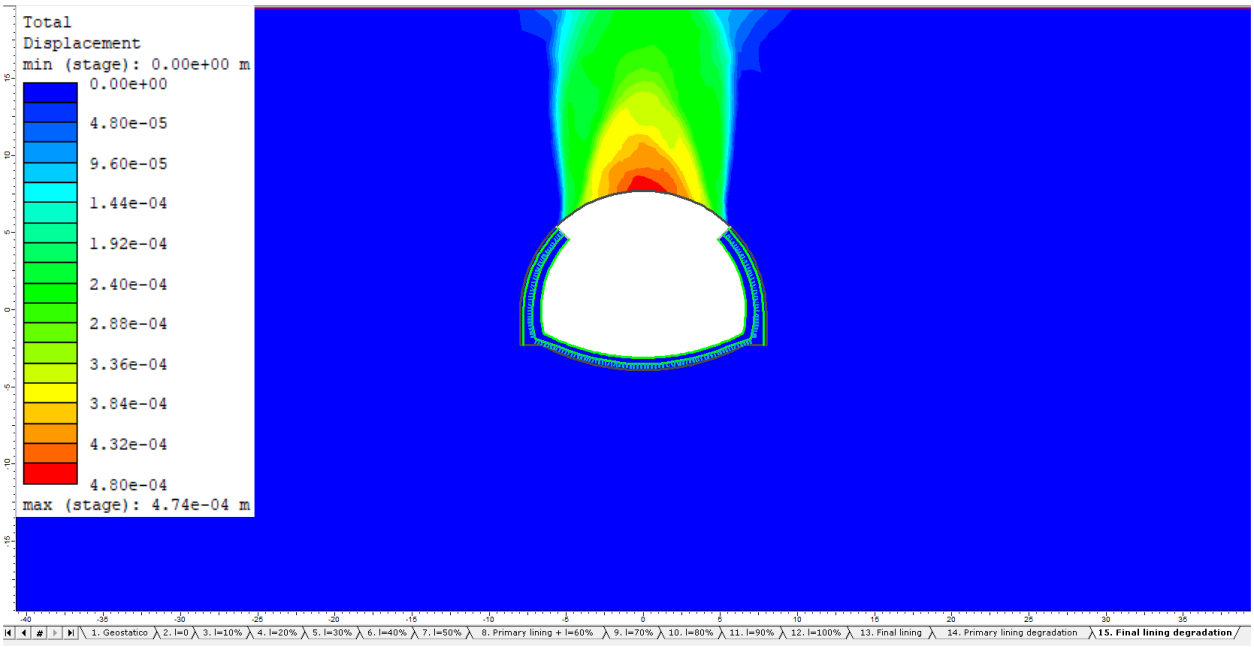

Figure 92 Total displacement 1D_limit_30

The maximum shear strain distribution around the tunnel (Figure 93) shows that high shear strains concentrate along the tunnel boundary, especially at the tunnel crown, indicating zones of yielding after fire-induced damage at the tunnel crown. The strain contours propagate upward, forming a shear band above the tunnel, which suggests ground loosening and possible instability in the crown area.

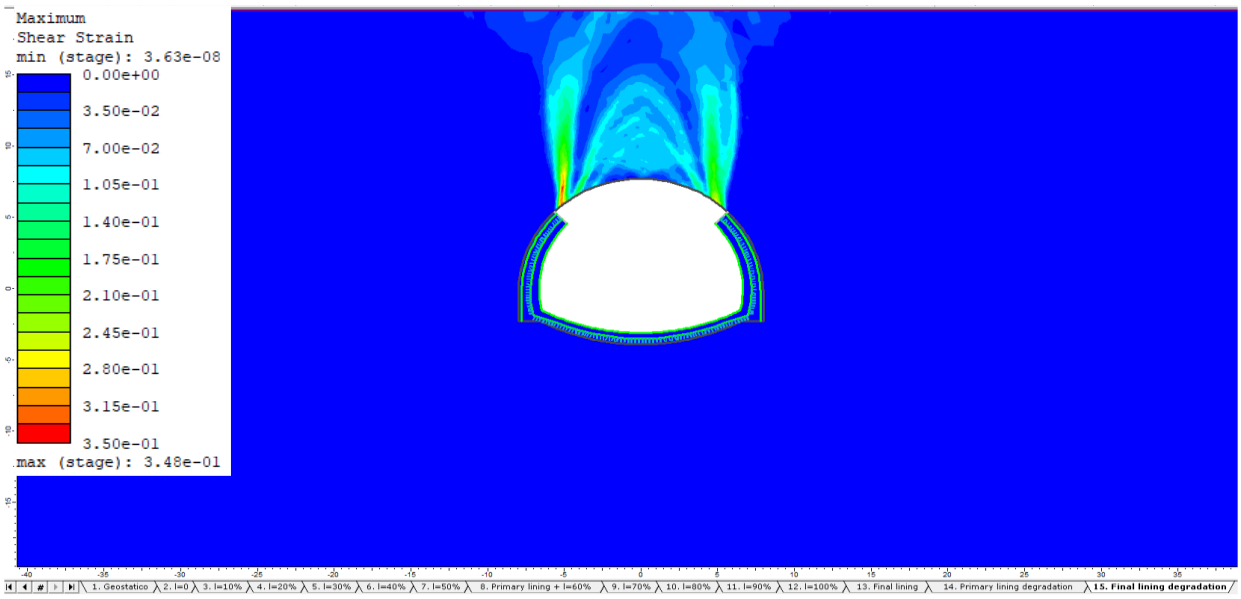

Figure 93 Maximum shear strain 1D_limit_30

Yielding is concentrated immediately around the excavation boundary, propagating from the crown and sidewalls. The yielded zone extends continuously upward toward the ground surface,

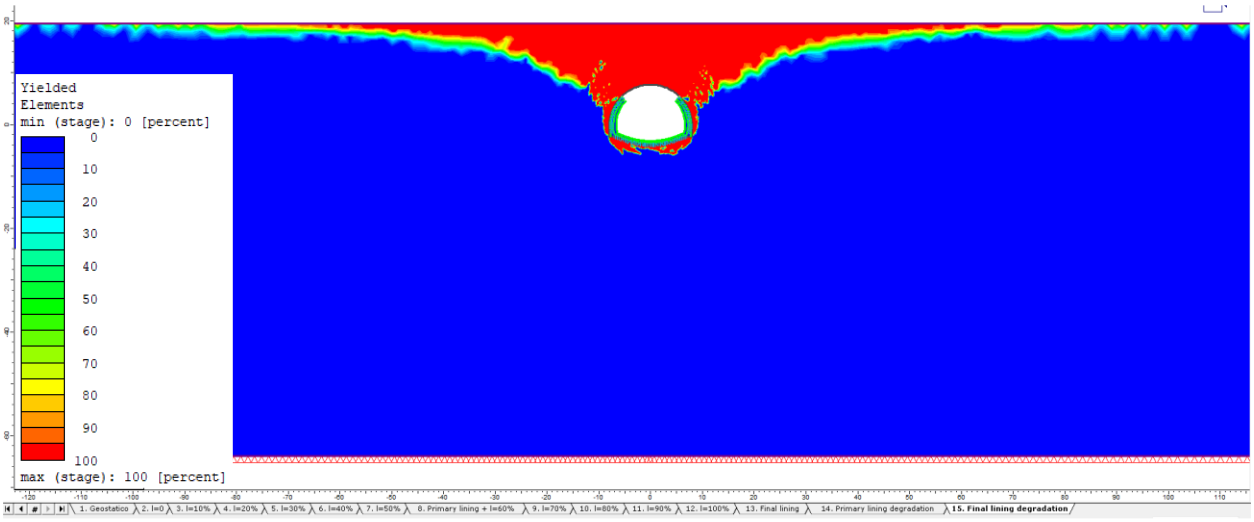

Figure 94 plastic zone 1D_limit_30 model

At depth of 2 times the tunnel diameter having same properties, the displacement still exists, however it does not reach completely the ground surface (Figure 95).

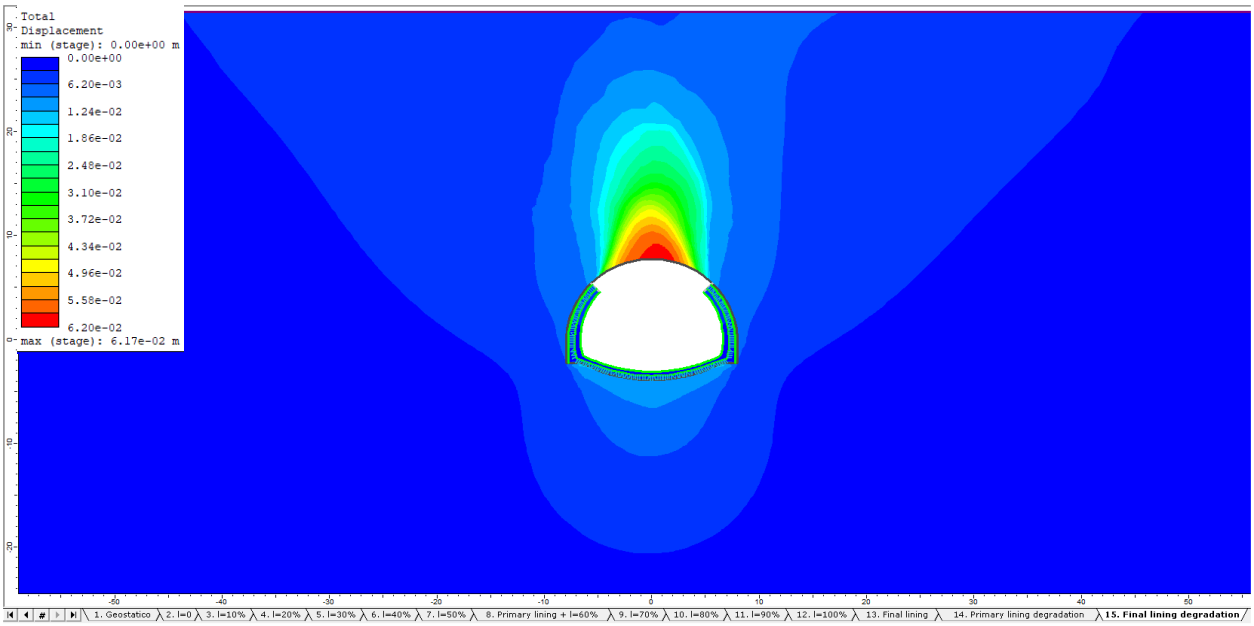

Figure 95 Total displacement at stage 15 of '2D_Limit_30 model'

We can also still visualise the yielded elements propagating from tunnel crown reaching surface but not in a continuous manner like in 1D situation.

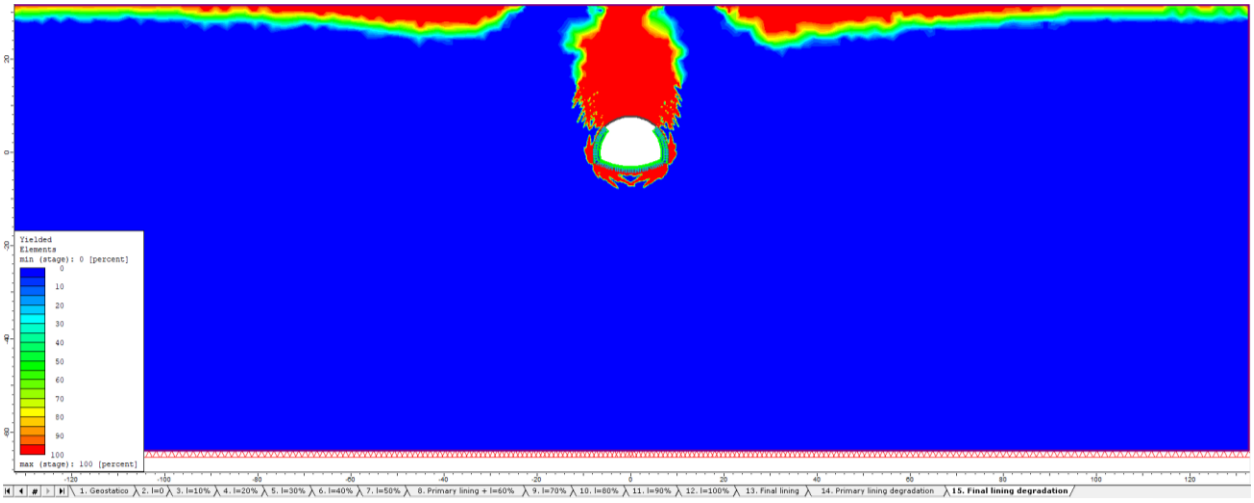

Figure 96 Plastic zone showing failure in 2D_limit_30 model

Maximum plastics shear strain for 2D-limit shows high shear plastic strains that develop at the crown shoulders and propagate upward, forming an arch shape plastic zone. This indicates progressive yielding towards the surface, which reflects shear deformation and as a result failure occurs (Figure 97).

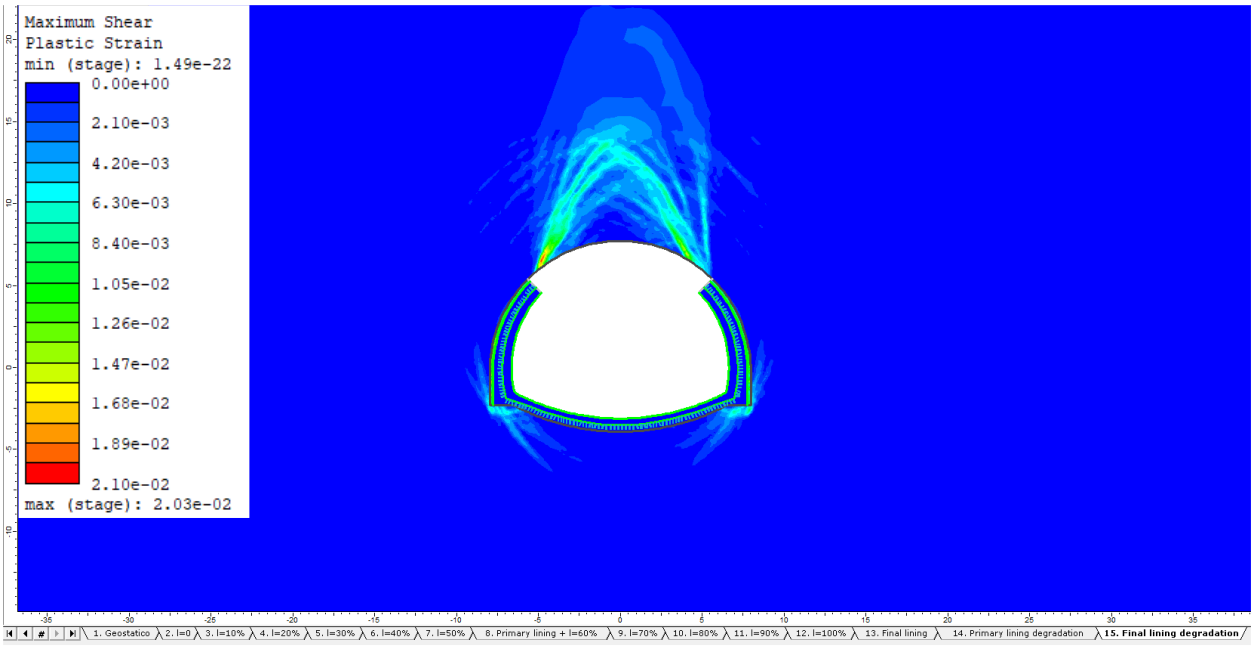

Figure 97 Maximum plastic shear strain for 2D_limit_30 model

Going to the limit 40 models, we are simulating a better type of rock mass having GSI=40. This model still shows non convergence at stage 15 revealing the failure occurring upon crown damage in all depths.

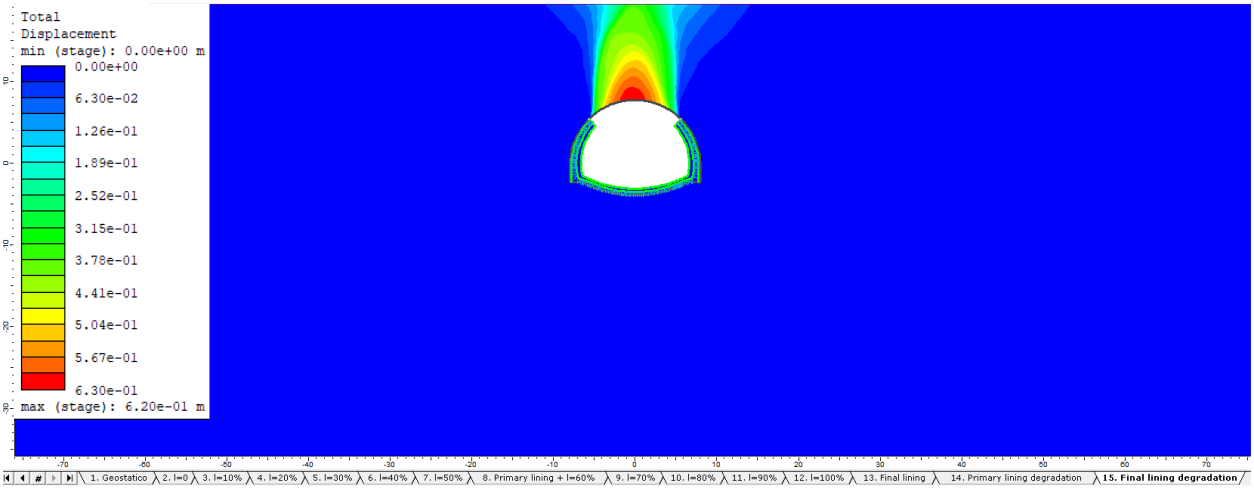

Figure 98 Total displacement for 1D_limit_40 model

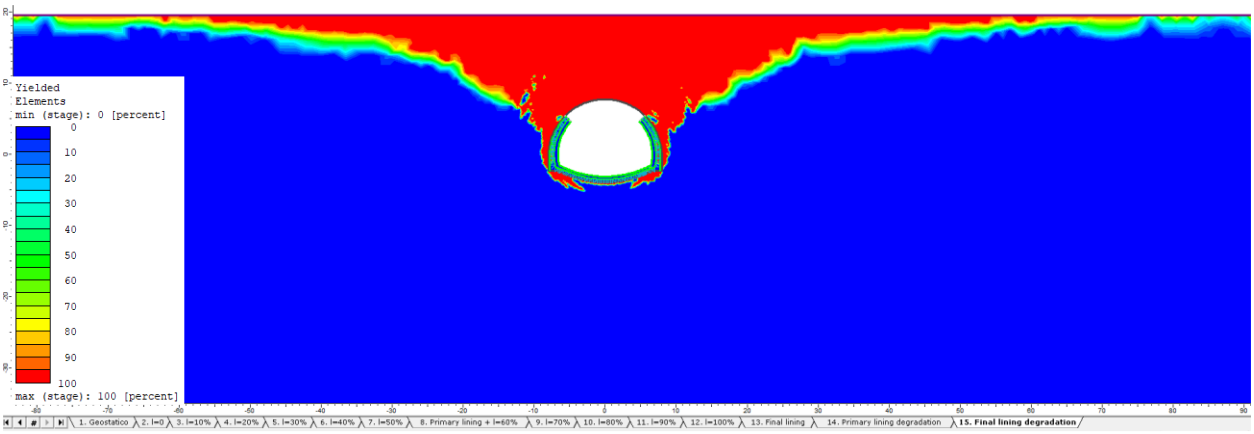

Figure 99 Plastic zone of 1_D limit_40 model

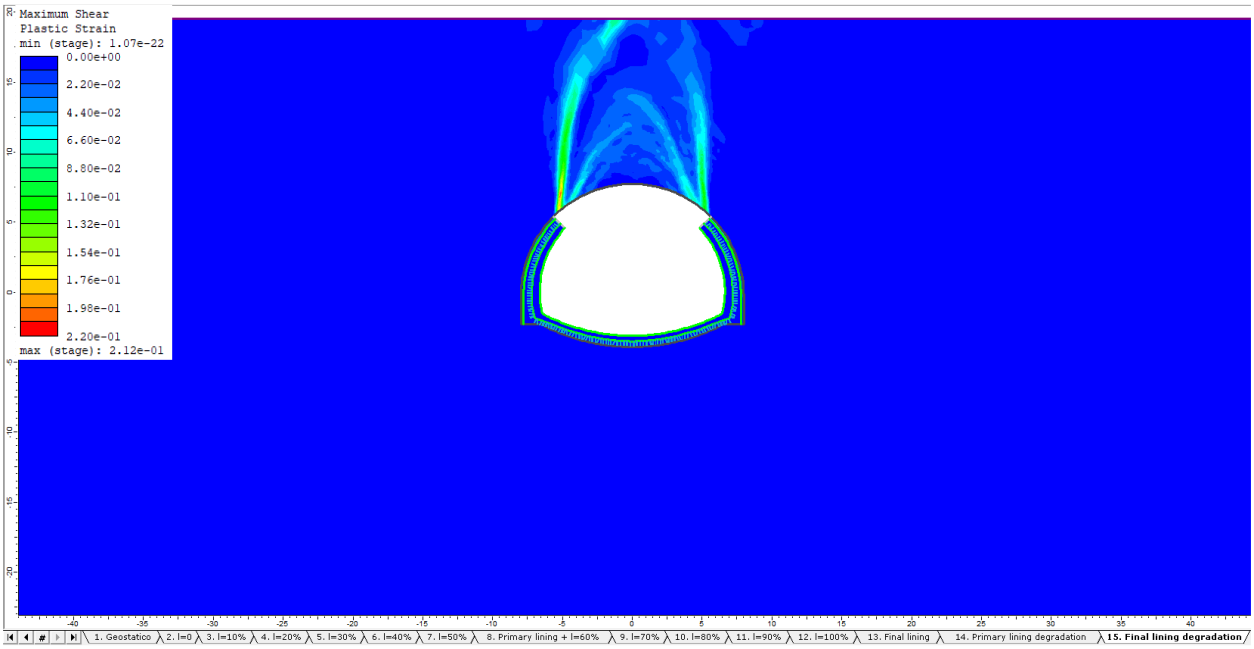

Figure 100 Plastic shear strain 1D_limit_40 model

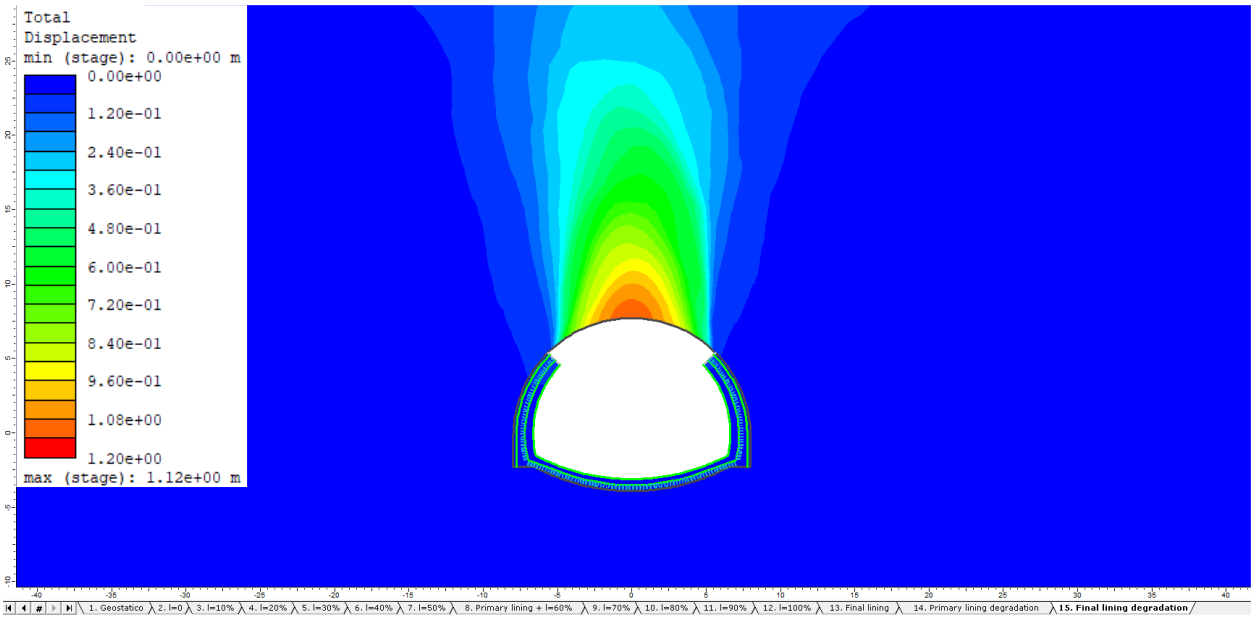

Figure 101 Total displacement of 2D_Limit_40 model showing failure above tunnel crown reaching the ground surface

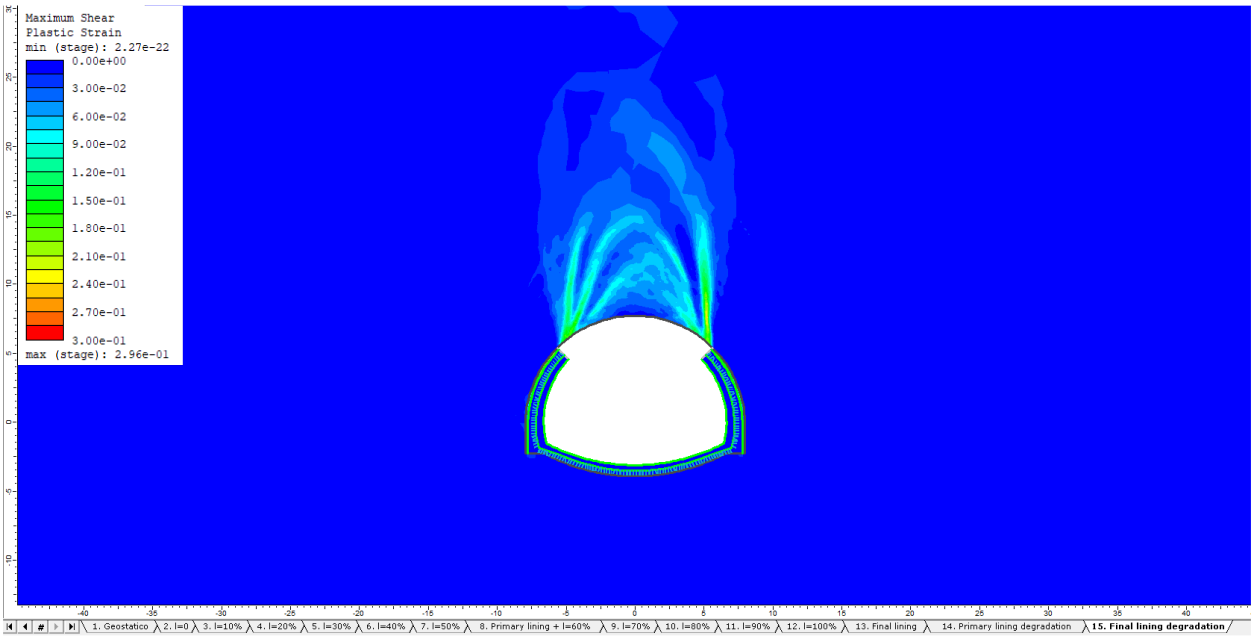

Figure 102 Maximum shear strain 2D_Limit_40 model

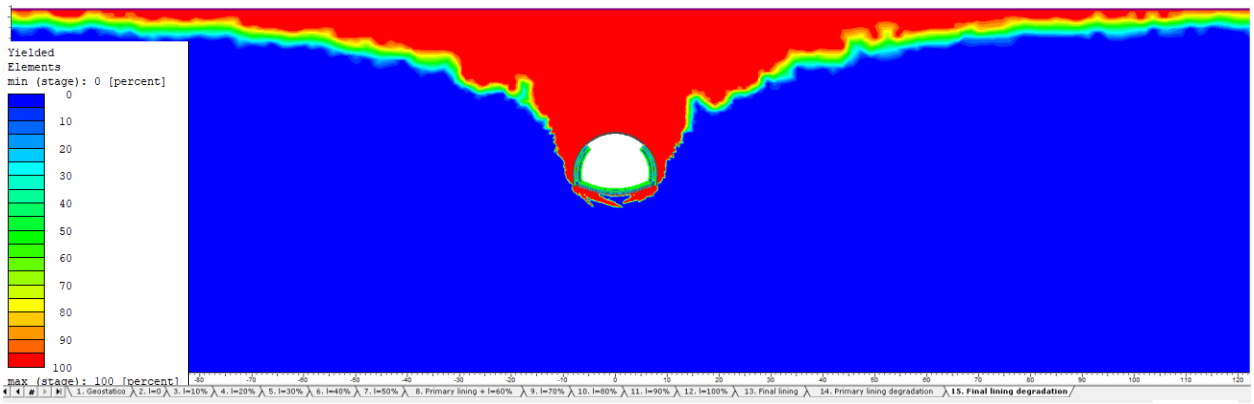

Figure 103 Plastic strain of 2D_Limit_40 model

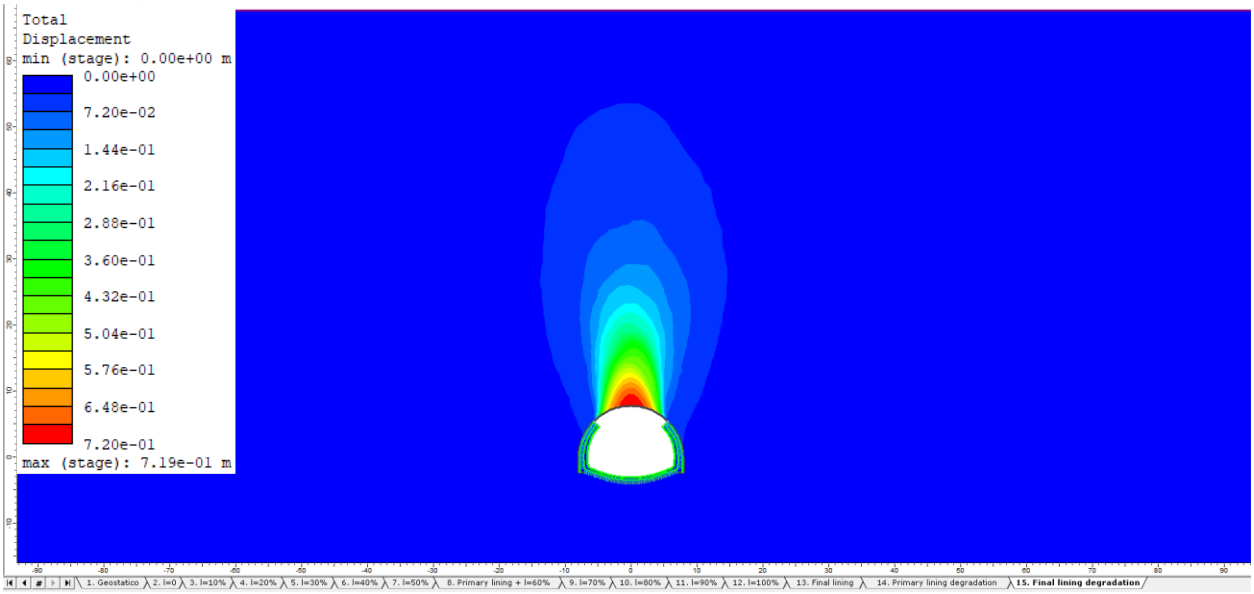

Figure 104 Total displacement of 5D_Limit_40 model showing failure above tunnel crown not reaching the ground surface

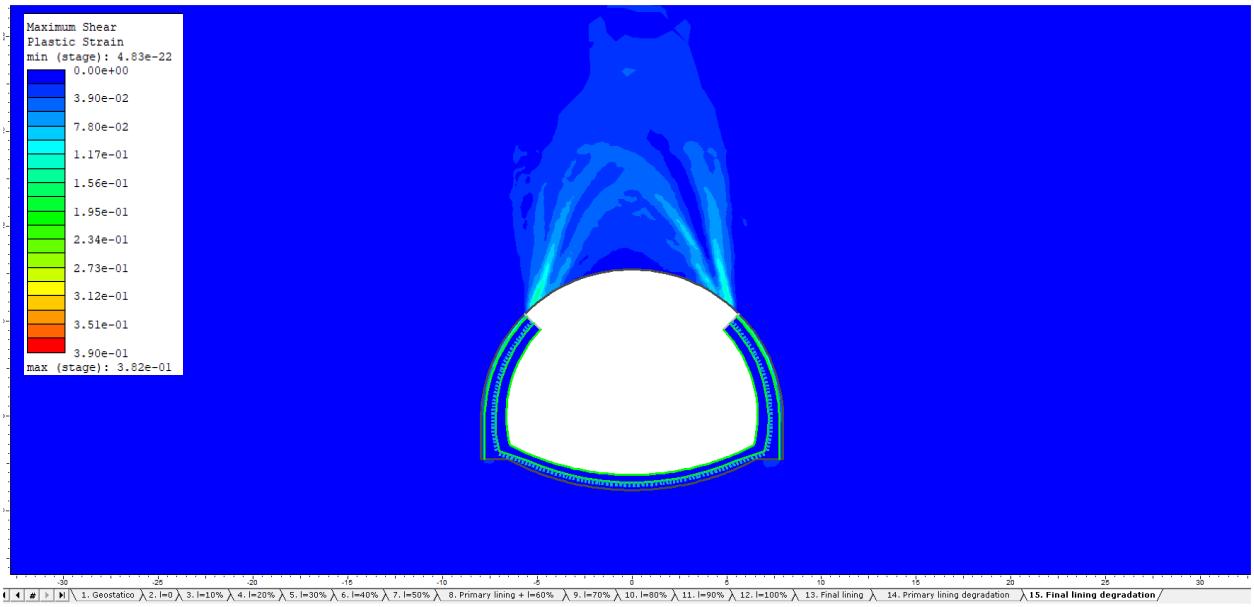

Figure 105 Maximum shear strain for 5D_limit_40 model

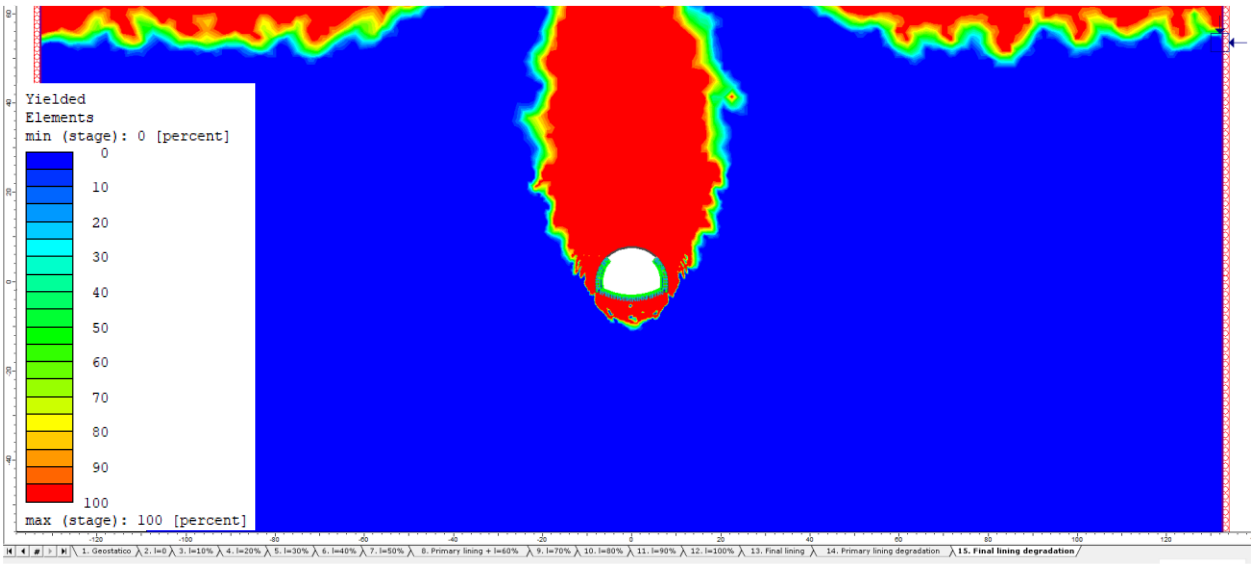

Figure 106 Plastic zone for 5D_limit_40 model

In the third numerical model limit 50 of GSI=50, slightly below the average quality properties where we had no failure, the analysis converged after the removal of the tunnel crown, indicating

that the system was able to reach a stable equilibrium condition despite the simulated fire-induced damage.

The displacement pattern suggests that the overall stability of the tunnel is preserved in all depths.

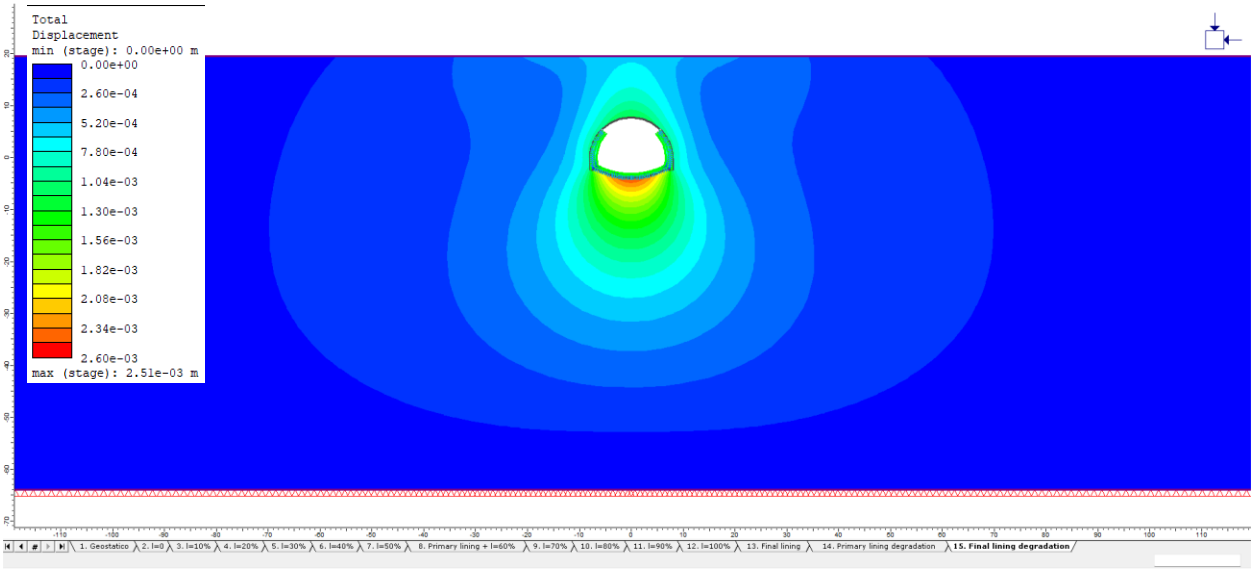

Figure 107 Total displacement of 1D_limit_50 model showing no failure

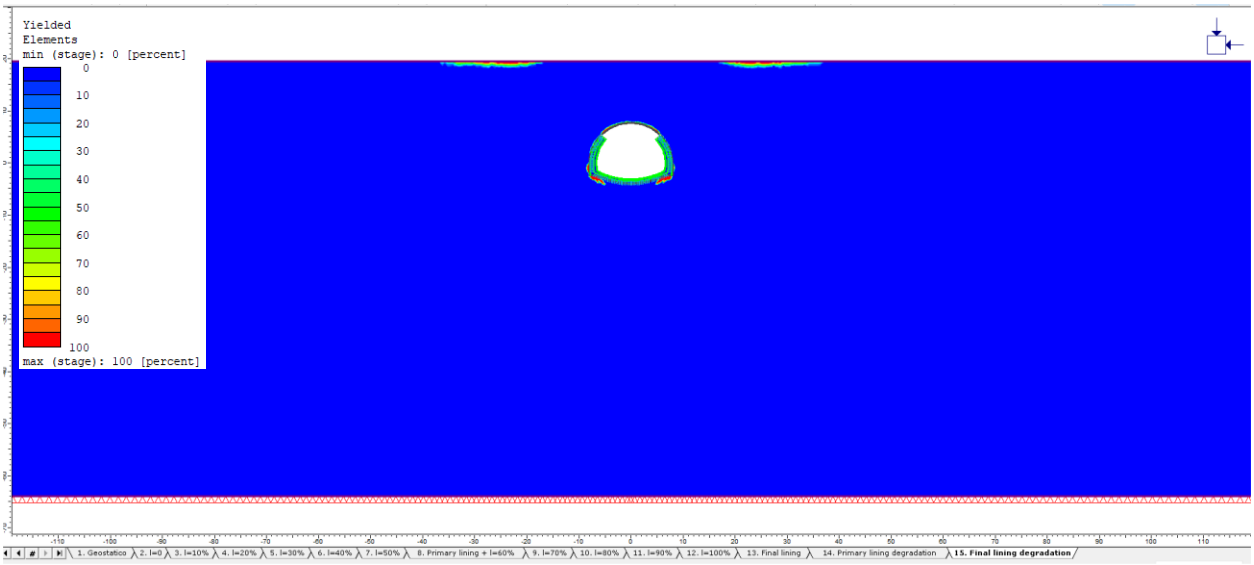

Figure 108 Plastic zone for model 1D_limit_50

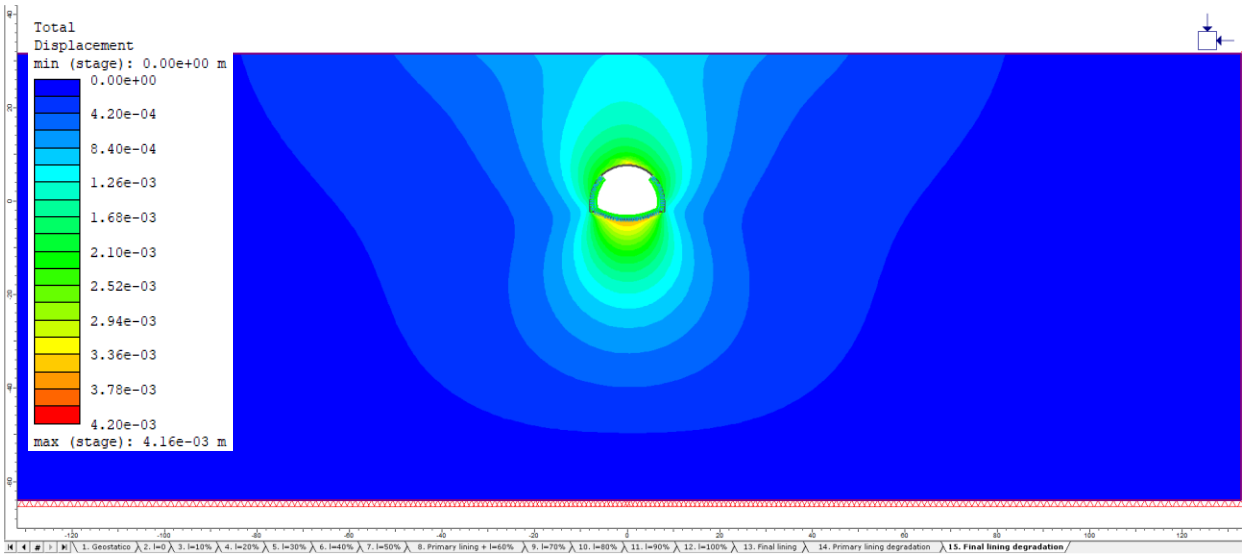

Figure 109 Total displacement of 2D_Limit_50 model

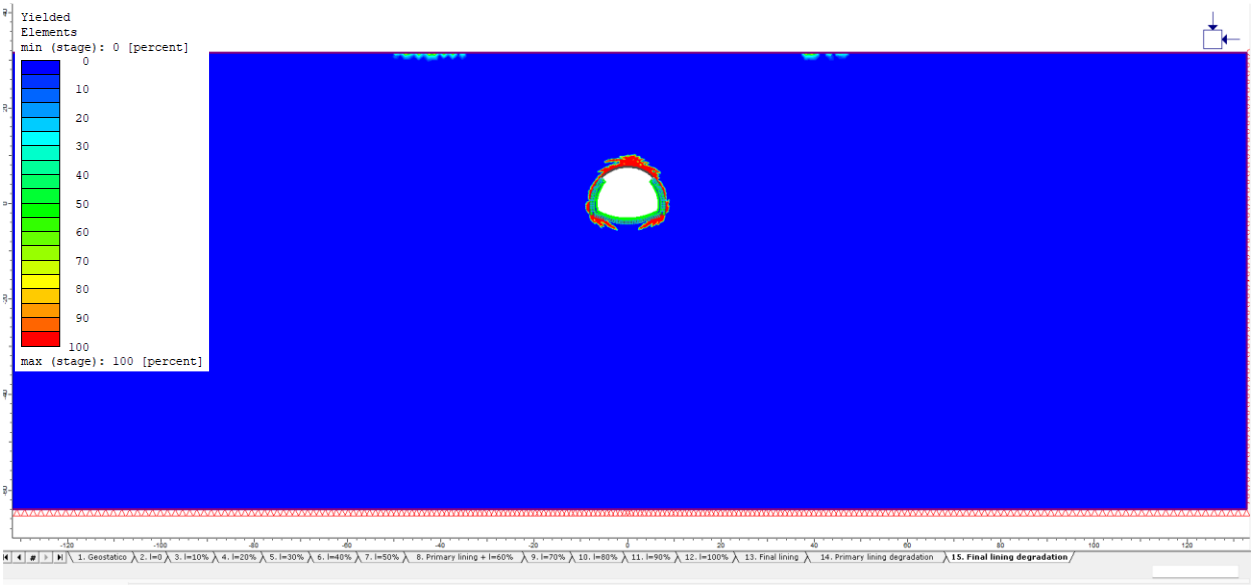

Figure 110 Plastic zone of model 2D_Limit_50

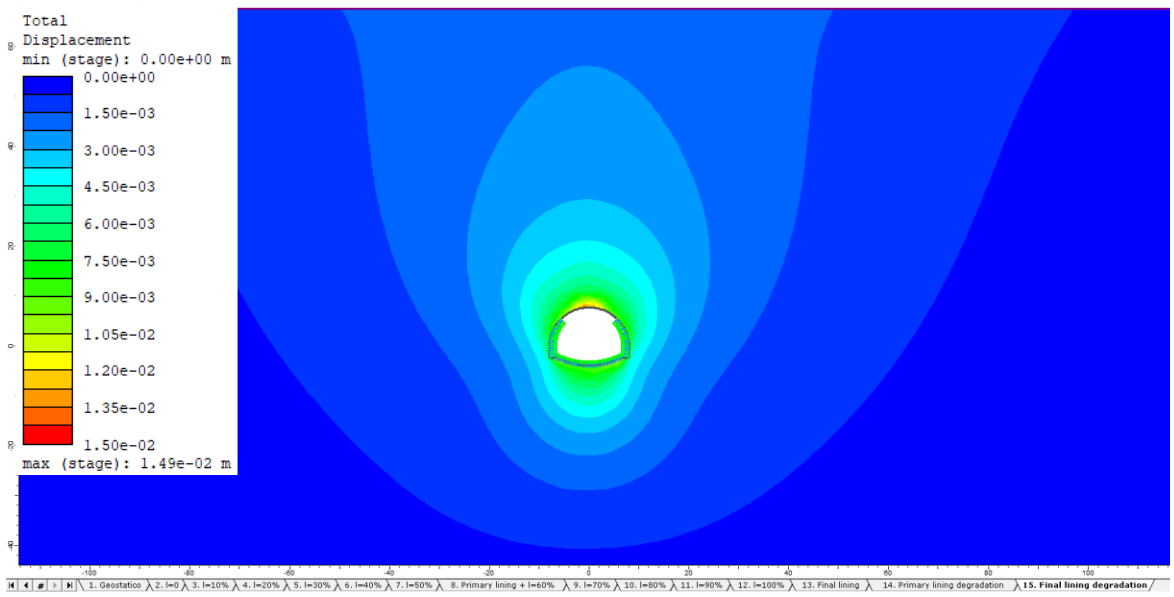

Figure 111 Total displacement at stage 15 of 'Limit_50 model' At 5D depth

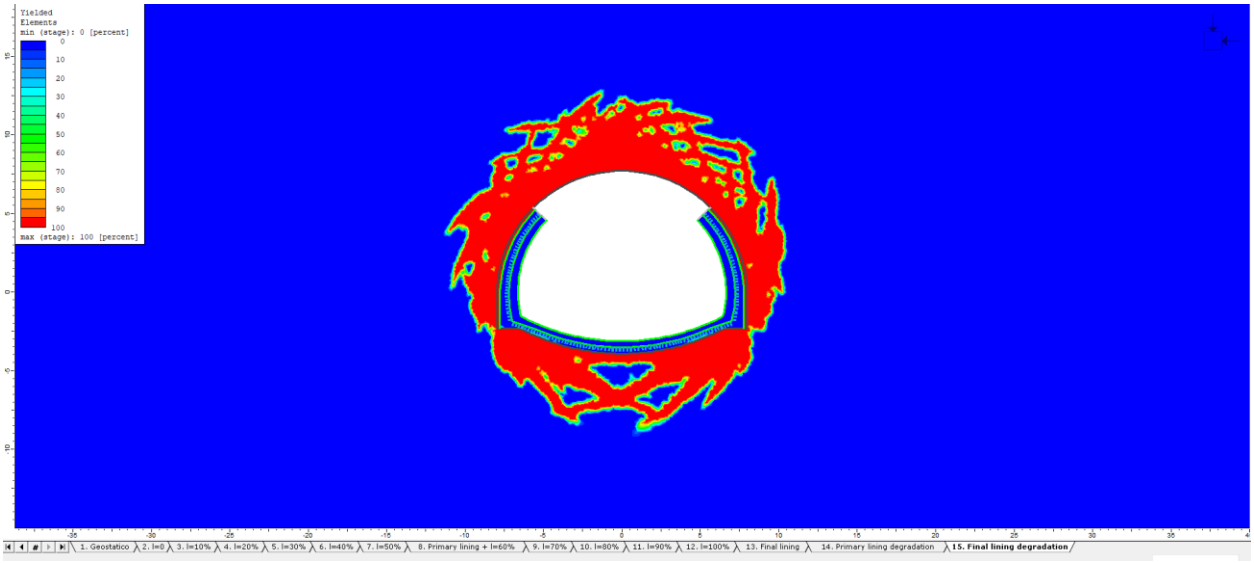

Figure 112 Plastic zone forming around tunnel of model 5D_limit _50

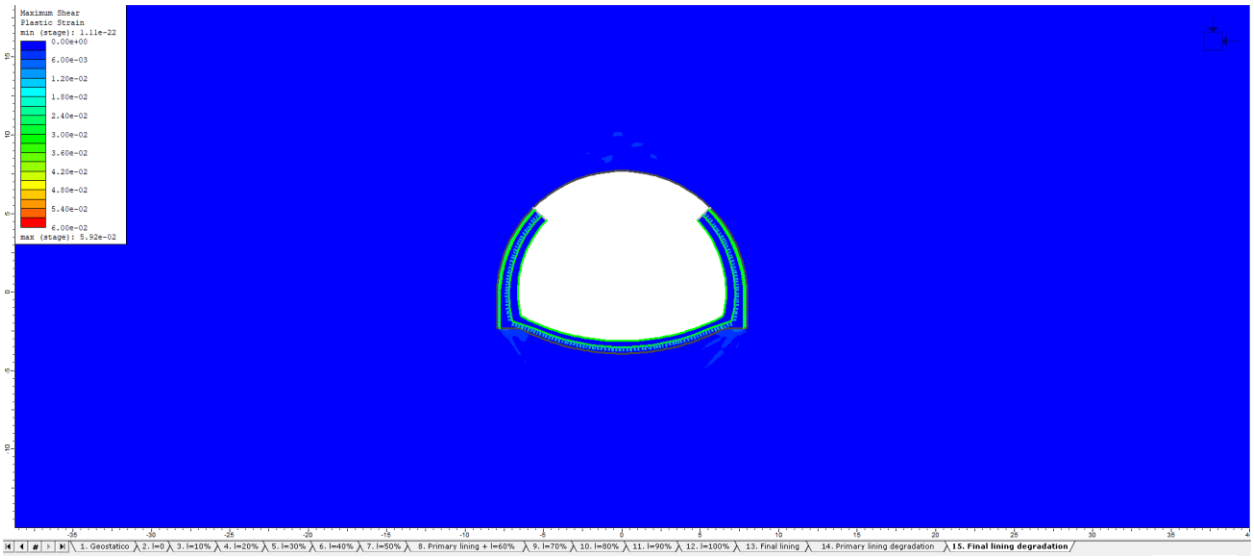

Figure 113 Maximum plastic shear strain for 5D_limit_50 model

After the initial analyses carried out for GSI = 30, 40, and 50, additional models were introduced to refine the stability assessment more accurately. Since the results indicated that the transition between non-convergence and convergence occurred between GSI = 40 and GSI = 50, further analyses were performed for GSI = 44, 45, and 46 in order to identify the threshold condition with greater precision.

For the 1D, GSI = 44 model, the results indicate unstable behavior after crown removal. The total displacement is concentrated above the tunnel crown, while the yielded elements and maximum shear plastic strain show the development of an extended damaged zone propagating from the crown toward the ground surface. This response indicates that the surrounding rock mass is unable to provide sufficient confinement after crown loss, leading to non-convergence of the numerical model.

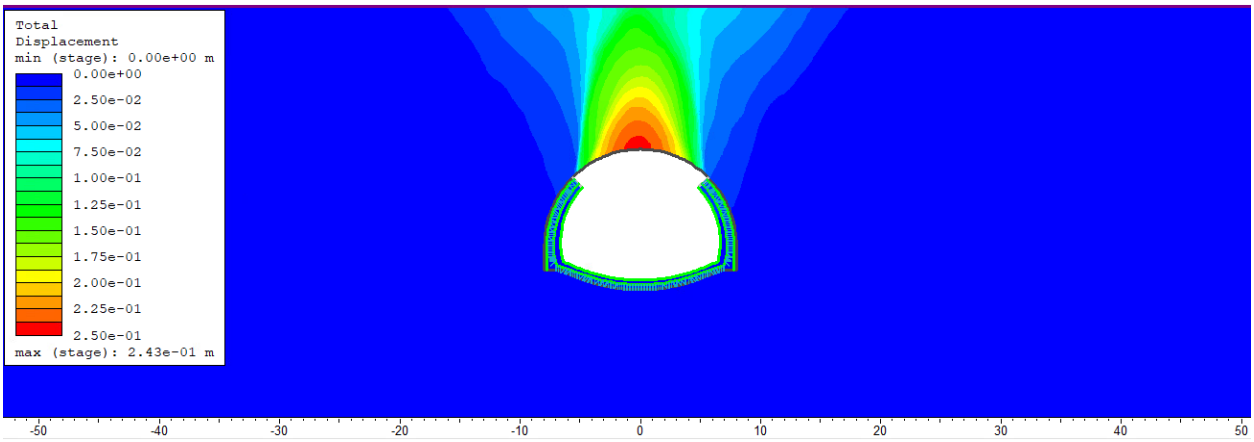

Figure 114 Total displacement at stage 15 of 'Limit_44 model' At 1D depth

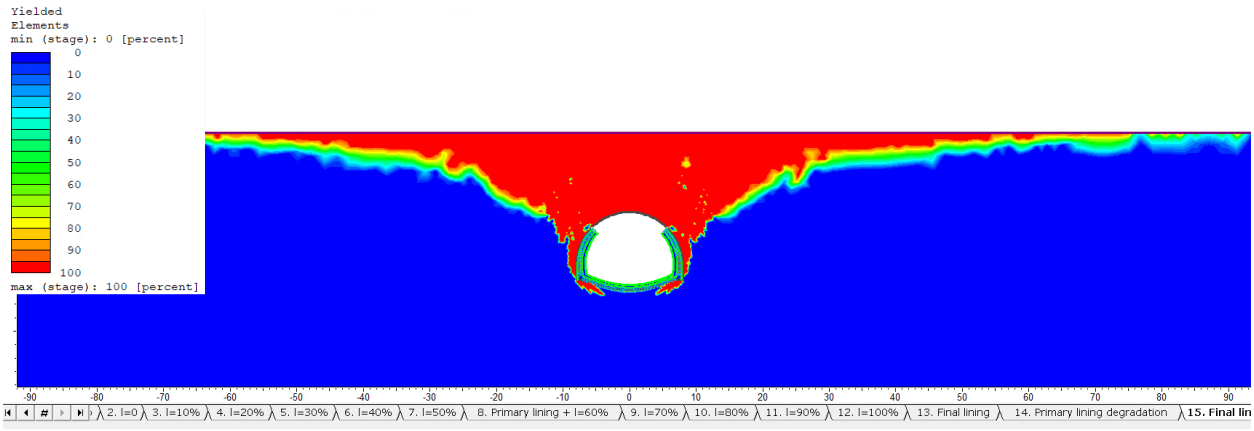

Figure 115 Plastic zone for model Limit 44-1D at stage 15

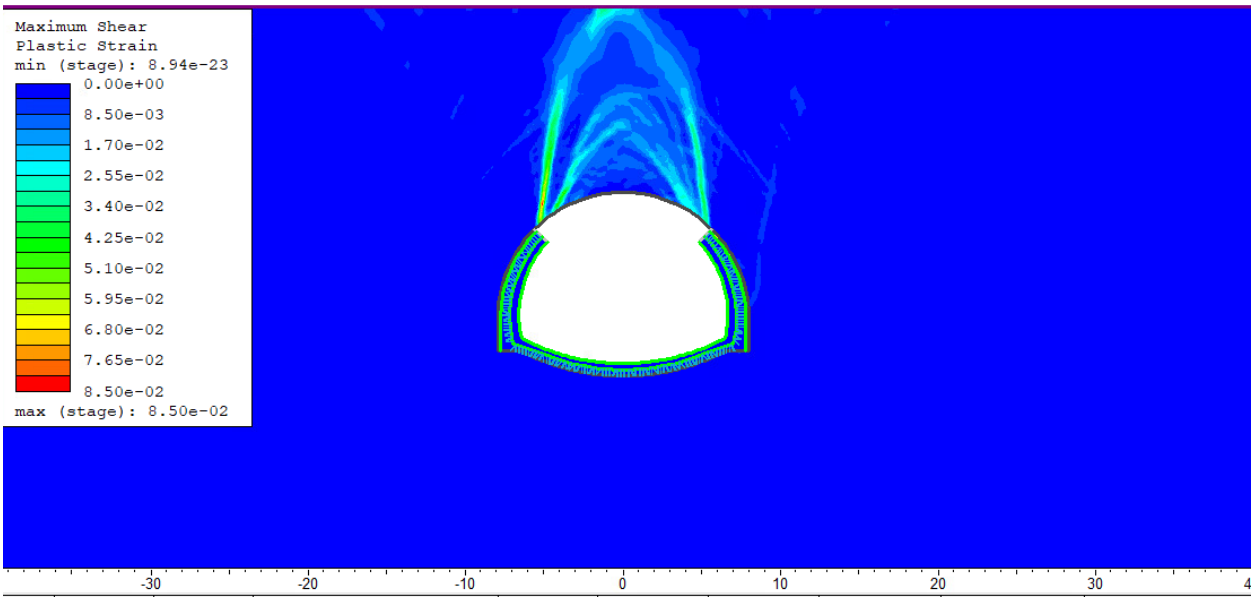

Figure 116 maximum shear plastic strac Limit44-1D at stage 15

For the 5D, GSI = 44 model, the yielded elements confirm a clearly unstable response after crown removal. A continuous failure zone develops from the tunnel crown toward the ground surface, indicating that the rock mass cannot provide sufficient confinement under deeper cover conditions.

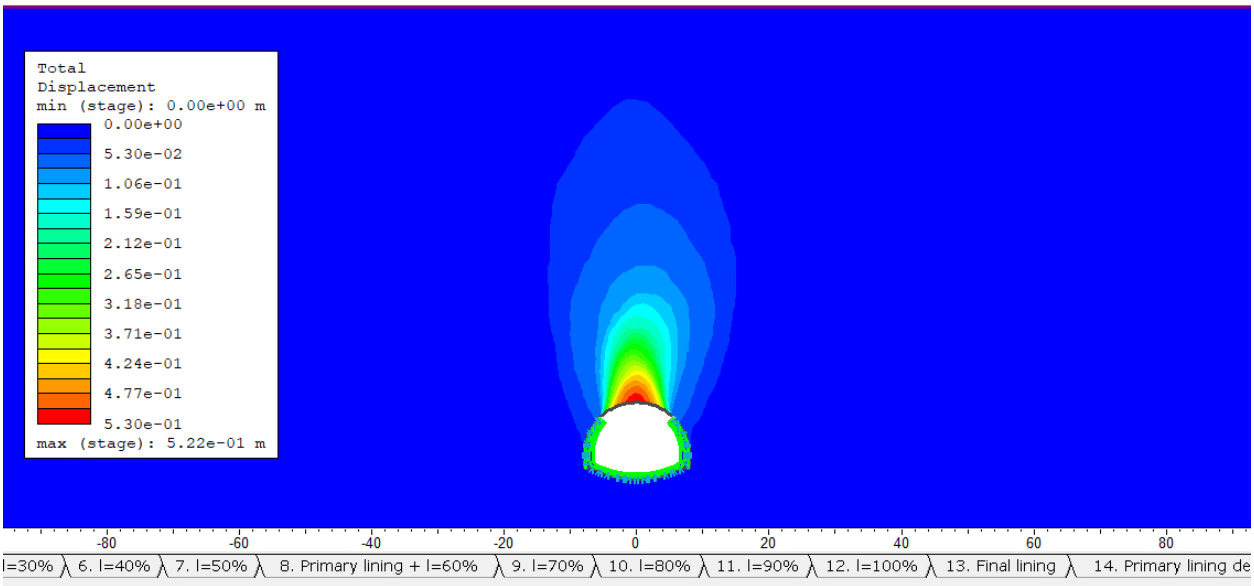

Figure 117 Total displacement at stage 15 of 'Limit_45 model' At 5D depth

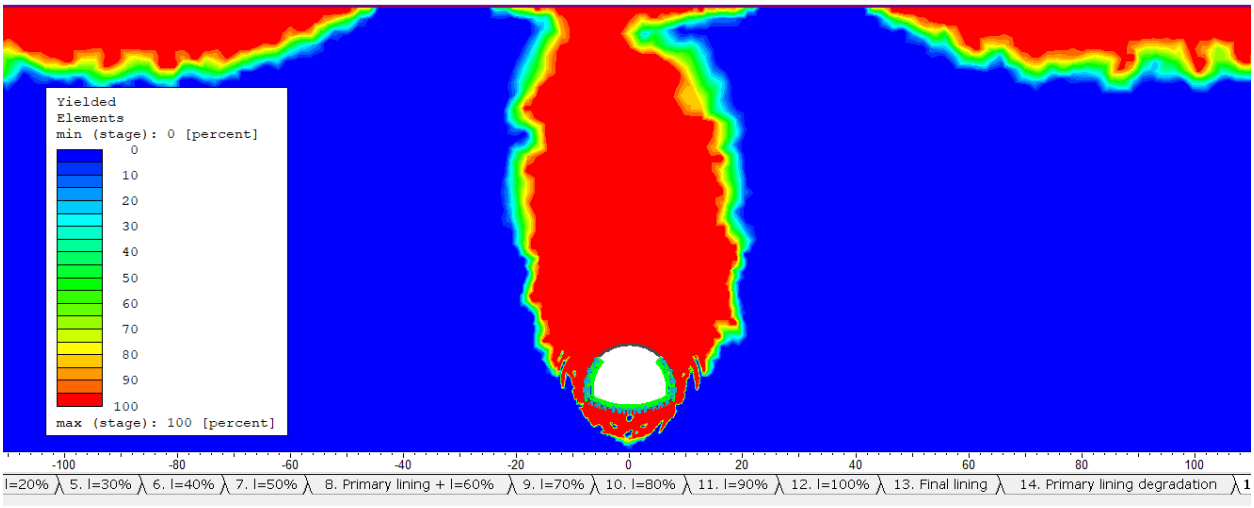

Figure 118 plastic zone for limit 44-5D (stage 15)

For the 1D, GSI = 45 model, the total displacement remains mainly concentrated above the tunnel crown, but with a much lower magnitude compared to the GSI = 44 case.

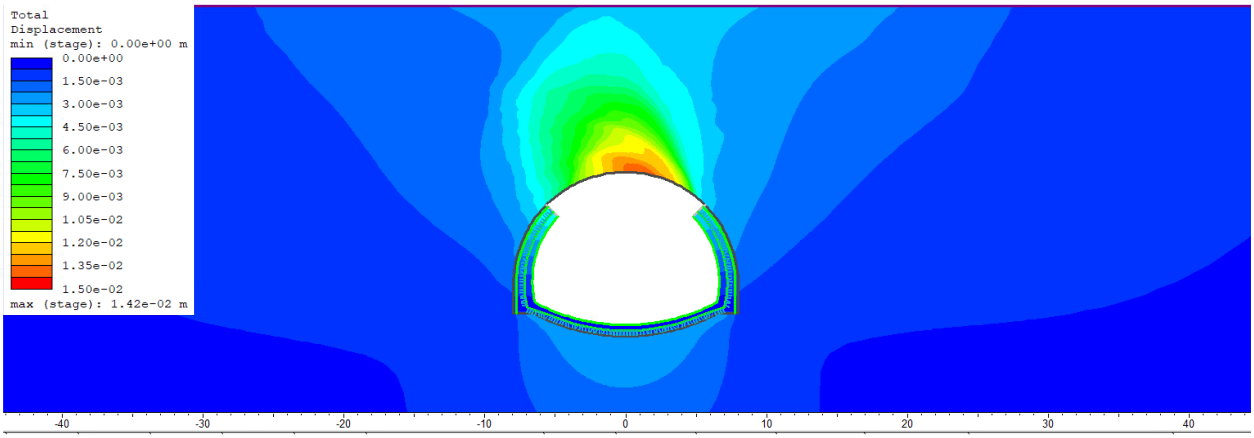

Figure 119 Total displacement at stage 15 of 'Limit_45 model' At 1D depth

For the 2D, GSI = 45 model, the model did not converge, and the yielded zone extends from the crown toward the ground surface, indicating unstable behavior

The failure envelopes are represented in the σ_1–σ_3 space, with the major principal stress σ_1 on the y-axis and the minor principal stress σ_3 on the x-axis (Figure 120).

The stress conditions leading to failure after tunnel crown removal were further illustrated in the Hoek–Brown failure criterion. For rock masses, the criterion is expressed as:

$$\sigma_1 = \sigma_3 + \left(m\,\sigma_{\{ci\}\sigma_3} + s\,\sigma_{\{ci\}}^2 \right)^{\{\alpha\}}$$

The parameter $m_b$represents the reduced Hoek–Brown constant for the rock mass and is obtained from the intact rock parameter $m_i$as a function of the Geological Strength Index (GSI):

$$m_b = m_i \exp\left(\frac{GSI - 100}{28}\right)$$

This reduction reflects the loss of strength due to jointing and fracturing within the rock mass.

The parameter s accounts for the degree of interlocking and disturbance of the rock mass structure and is defined as:

$$s = \exp\left(\frac{GSI - 100}{9}\right)$$

Lower values of GSI lead to a rapid decrease in s, indicating reduced rock mass strength.

The exponent α controls the curvature of the Hoek–Brown failure envelope and is assumed constant in this study:$\alpha = 0.55$

This value is commonly adopted for rock mass applications in numerical analyses.

The deformation modulus of the rock mass, E_d, is estimated using an empirical relationship proposed by Hoek and Brown (1997):

$$E_d = \sqrt{\frac{\sigma_{ci}}{100}} \cdot 10^{\frac{GSI-10}{40}} \text{for } \sigma_{ci} < 100 \text{ MPa}$$

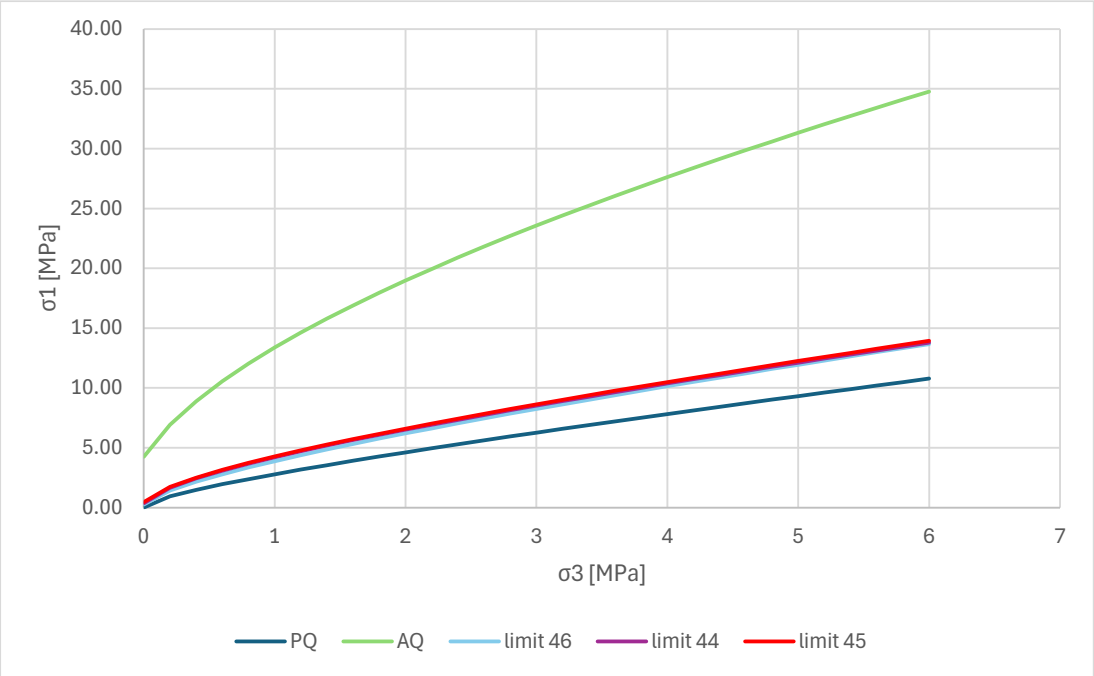

Figure 120 Hoek-Brown curve

The Hoek–Brown curves were used only as a graphical representation of the analysed rock mass conditions. According to the RS2 results, the stability threshold after crown removal lies between GSI = 44 and GSI = 46, with full convergence reached at GSI = 46. This result confirms that rock masses with mechanical properties close to this threshold are sensitive to loss of confinement.

This result confirms that rock masses with mechanical properties close to this threshold are particularly sensitive to the loss of confinement induced by crown damage. Small variations in GSI within this range produce significant changes in the numerical response, showing that tunnel stability is strongly controlled by rock mass quality.

This numerical investigation was carried out to evaluate the structural response of tunnels subjected to localized crown removal, representing severe damage conditions such as those that may occur during fire events. The analysis focused on identifying the minimum rock mass quality required to maintain tunnel stability after the loss of crown support. The results showed a clear difference in behaviour among the analysed rock mass conditions. The numerical analyses for GSI = 44 did not converge after crown removal at any of the considered depths, indicating unstable conditions. Similarly, the model with GSI = 45 converged only at 1D, while it remained non-

convergent at 2D and 5D, showing insufficiency to ensure full stability. In contrast, the model with GSI = 46 successfully converged for all considered depth conditions.

For the threshold condition, the results showed damage concentrated at the tunnel crown, with limited displacement, confined yielding, and no evidence of continuous failure surfaces or instability. Under these conditions, the surrounding rock mass was able to redistribute stresses and maintain the overall structural stability of the tunnel despite the loss of crown support.

By progressively varying the GSI while keeping the intact rock parameters unchanged, it was possible to identify a threshold condition separating unstable and stable tunnel responses. The GSI = 46 model represents the minimum rock mass condition capable of maintaining global stability after crown removal. Rock masses with properties equal to or better than this threshold are expected to provide sufficient confinement and stress redistribution to prevent collapse, even in the presence of significant localized damage.

Table 52 summarizes the convergence results for all analysed models after crown removal. The results confirm that only the models with sufficient rock mass strength and stiffness were able to reach equilibrium, whereas weaker rock mass conditions resulted in non-convergent solutions.

Table 52 RS2 models' outcomes after simulation of fire-induced damage (stage 15) based on rock mass condition and GSI.

Model	Rock mass condition	GSI	1D	2D	5D
GQ	Good quality	75	Converged	Converged	Converged
AQ	Average quality	65	Converged	Converged	Converged
Limit 50	Poor quality	50	Converged	Converged	Converged
Limit 46	Stability threshold PQ	46	Converged	Converged	Converged
Limit 45	Poor quality	45	Converged	Not conv.	Not conv.
Limit 44	Poor quality	44	Not conv.	Not conv.	Not conv.
Limit 40	Poor quality	40	Not conv.	Not conv.	Not conv.
Limit 30	Poor quality	30	Not conv.	Not conv.	Not conv.
PQ	Poor quality	20	Not conv.	Not conv.	Not conv.

Chapter 5

Conclusion

This study is articulated around two main topics. First, it examines the assessment of tunnel segmental linings by addressing inspection techniques, defect recognition, and structural response under severe damage conditions. The main objective is to identify the defects affecting segmental linings by investigating different guidelines and highlighting defects that are not currently considered in the Italian guidelines for existing tunnels. To ensure the safety and long-term performance of tunnel linings, regular inspections are essential for identifying different types of defects and supporting the selection of appropriate maintenance strategies. In addition, the study investigates fire-induced damage in tunnels by simulating damage occurring at the tunnel crown and analyzing the resulting structural response in three different rock mass types using a Finite Element software. The analysis ultimately aims to provide tunnel owners with useful guidance to distinguish between situations that require detailed verification and those that are clearly not a cause for concern. The analyses carried out determine limit rock mass in terms of strength and GSI required to withstand fire-induced damage and avoid consequences for the buildings above. This numerical investigation was conducted to evaluate the structural response of tunnels subjected to localized crown removal, representing severe damage conditions such as those that may occur during fire events.

Inspection techniques used for the assessment of tunnel segmental linings begins with conventional inspection approaches based on the guidelines developed by the ITA tech SIG Working Group 2, particularly those presented in the publication *"Damage of Segmental Lining Tunnels"*, which provide a framework for identifying and classifying common defects. The study then reviews recent developments involving the use of artificial intelligence in tunnel inspection.

Artificial intelligence is becoming a valuable tool for tunnel lining inspections, enabling faster and more consistent detection of defects through advanced image analysis. However, its effectiveness can still be influenced by varying tunnel conditions and imaging environments. These approaches demonstrate how automated image analysis and data processing can support defect detection and monitoring. In addition, non-destructive testing (NDT) methods are discussed as valuable inspection tools that enable engineers to assess the internal condition of tunnel linings without causing damage to the structure. Techniques such as ground-penetrating radar, ultrasonic testing, impact-echo, infrared thermography, and tomography provide important information on defects including cracks, voids, delamination, and material deterioration. Together, these methods support better evaluation of tunnel linings and contribute to earlier defect detection, better maintenance planning, and improved structural safety.

Defect classification in tunnel segmental linings was examined through three main sources: the SIG Working Group publication *Damages of Segmental Lining Tunnels*, the *Italian Guidelines for Existing Tunnels*, and a private defect catalogue developed by a motorway concessionaire. The comparison showed that all three sources include the most common defects, such as cracks, water infiltration, and surface deterioration, while also revealing differences in the way defects are classified and interpreted. The SIG publication provides a more detailed and technical approach specific to segmental lining tunnels, whereas the Italian Guidelines address these defects within the broader category of existing tunnels and assess them mainly according to intensity and extent. The private defect catalogue adds practical observations, particularly regarding defect location and recording. Overall, this study highlighted the defects that are mentioned in some references but omitted in others, showing through comparison that it would be useful to include these missing defects in order to support a more complete and safe assessment of tunnel segmental linings.

The numerical modelling demonstrates that tunnel stability under severe crown damage is governed primarily by rock mass quality, with tunnel depth influencing the extent of the response. Poor-quality rock masses of (σci = 7.5MPa, GSI=20), showed the most critical behavior, with large displacements, extensive plastic zone development, and non-convergent solutions at all analyzed depths after crown removal, indicating an inability of the surrounding ground to maintain equilibrium once confinement was lost. In contrast, average (σci=30MPa and GSI=65) and good-quality rock masses (σci=110MPa and GSI=75 exhibited a much more stable response,

characterized by limited deformation, negligible plastic strain, and no significant yielding even under the simulated severe damage conditions. A further series of analyses, stemming from the poor quality rock mass case and based on progressively increasing the GSI while keeping the intact rock properties unchanged, made it possible to identify a clear stability threshold. The results demonstrate that rock mass quality is the controlling factor in maintaining tunnel stability after severe crown damage, with a threshold condition identified at GSI = 46, below which the surrounding ground is no longer able to provide sufficient confinement and stress redistribution to prevent failure. This threshold therefore defines the transition between unstable and stable tunnel behaviour under crown deterioration and provides a useful basis for evaluating minimum ground quality requirements in the design of tunnels exposed to severe local damage like fire induced damage.

References

Barton, N., Lien, R., & Lunde, J. (1974). Engineering classification of rock masses for the design of tunnel support. Rock Mechanics, 6(4), 189–236.

Beard, A., & Carvel, R. (2005). The handbook of tunnel fire safety. Thomas Telford Publishing, London.

Beck, J. S., & Yuan, X. (2005). Non-destructive testing methods for tunnel linings. Tunnelling and Underground Space Technology, 20(6), 673–685.

Brady, B. H. G., & Brown, E. T. (2006). Rock mechanics for underground mining (3rd ed.). Springer, Dordrecht.

Carvel, R., & Beard, A. (2005). The influence of tunnel fire safety measures on structural performance. Fire Safety Journal, 40(5), 481–493.

Cha, Y. J., Choi, W., & Büyüköztürk, O. (2017). Deep learning-based crack damage detection using convolutional neural networks. Computer-Aided Civil and Infrastructure Engineering, 32(5), 361–378.

Chakeri, H. (2021). Analysis of segmental tunnel lining behaviour under construction and operational loads. Tunnelling and Underground Space Technology, 110, 103827.

Flath, T. (2009). Installation processes of precast tunnel lining segments. Proceedings of the ITA World Tunnel Congress.

Grosse, C., & Ohtsu, M. (2008). Acoustic emission testing. Springer.

Guo, Z., Li, H., & Chen, Y. (2021). Deep learning-based defect detection for civil infrastructure inspection: A review. Automation in Construction, 125, 103607.

Hoek, E., Carranza-Torres, C., & Corkum, B. (2002). Hoek–Brown failure criterion – 2002 edition. Proceedings of NARMS-TAC Conference, Toronto.

International Tunnelling Association (ITA). (2019). Guidelines for inspection and maintenance of tunnel lining.

Jiang, N., et al. (2023). Application of ultrasonic and radar methods for tunnel lining inspection. Construction and Building Materials, 362.

Kalifa, P., Menneteau, F. D., & Quenard, D. (2000). Spalling and pore pressure in HPC at high temperatures. Cement and Concrete Research, 30(12), 1915–1927.

Khoury, G. A. (2000). Effect of fire on concrete and concrete structures. Progress in Structural Engineering and Materials, 2(4), 429–447.

Liu, X., et al. (2015). Mechanical behaviour of rock mass surrounding tunnels under damage conditions. Tunnelling and Underground Space Technology, 47, 150–160.

Marini, P. (2023). Inspection and quality control of segmental tunnel linings: Brenner Base Tunnel case study. Tunnelling and Underground Space Technology.

Mindeguia, J. C. (2009). Contribution to the understanding of concrete behaviour at high temperature. PhD thesis, École Centrale Paris.

Ministero delle Infrastrutture e della Mobilità Sostenibili (MIMS). (2022). Linee guida per la classificazione e gestione del rischio, la valutazione della sicurezza ed il monitoraggio delle gallerie esistenti. Rome, Italy.

Palmström, A. (2001). Rock engineering: Concepts and design principles. Balkema Publishers.

Peng, Y., et al. (2021). Ground penetrating radar applications in tunnel inspection. Automation in Construction, 125.

Rocscience Inc. (2023). RS2 – 2D finite element analysis for geotechnical engineering. Rocscience, Toronto.

Rocscience Inc. (2024). RS2 – 2D finite element analysis for geotechnical engineering. Rocscience, Toronto, Canada.

SIG Working Group 2. (2019). Inspection and maintenance of precast tunnel segmental linings. International Tunnelling Association.

Sjölander, J., Johansson, A., & Spross, J. (2023). Towards automated tunnel inspections using computer vision and machine learning. Automation in Construction, 147, 104728.

Valentini, L., & Faini, A. (2024). Artificial intelligence for defect detection in tunnel segmental linings. Automation in Construction, 158.

Yeum, C. M., & Dyke, S. J. (2015). Vision-based automated crack detection for infrastructure inspection. Computer-Aided Civil and Infrastructure Engineering, 30(10), 759–770.

Zhang, L., Yang, F., Zhang, Y. D., & Zhu, Y. J. (2016). Road crack detection using deep convolutional neural networks. IEEE International Conference on Image Processing, 3708–3712.

Zhou, Y., & Wu, B. (2023). Structural response of tunnel linings subjected to fire-induced damage. Tunnelling and Underground Space Technology, 137, 105018.